A Performance Enhanced 1-bit Bandpass Sturdy-MASH Delta-Sigma Modulator for Radio-over-Fiber Fronthaul Transmission Systems

Jianzhao Gou

A Thesis

in the Department of

Electrical and Computer Engineering

Presented in Partial Fulfillment of the Requirements

For the Degree of

Master of Applied Science (Electrical and Computer Engineering)

at Concordia University

Montreal, Quebec, Canada

October 2024

CONCORDIA UNIVERSITY
SCHOOL OF GRADUATE STUDIES

This is to certify that the thesis prepared

By: Jianzhao Gou

Entitled: A Performance Enhanced1-bit Bandpass Sturdy-MASH Delta-Sigma Modulator for Radio-over-Fiber Fronthaul Transmission Systems

and submitted in partial fulfillment of the requirements for the degree of

Master of Applied Science (Electrical and Computer Engineering)

complies with the regulations of this university and meets the accepted standards with respect to originality and quality.

Signed by the final examining committee:

______________________________________Chair
Dr. Glenn Cowan

______________________________________Examiner
Dr. Glenn Cowan

______________________________________Examiner
Dr. Chadi Assi (CIISE)

______________________________________Thesis Supervisor(s)
Dr. John Xiupu Zhang

Approved by: ____
Dr. Wei-Ping Zhu, Associate Chair, Graduate Studies, ECE
Chair of Department or Graduate Program Director

October 2024

____
Dr. Mourad Debabbi
Dean of Gina Cody School of Engineering and Computer Science

ABSTRACT

A Performance Enhanced 1-bit Bandpass Sturdy-MASH Delta-Sigma Modulator for Radio-over-Fiber Fronthaul Transmission Systems

Jianzhao Gou

Currently, in fronthaul transmission systems of radio access network (RAN), the digitized common public radio interface (CPRI) are being widely used. However, with the development of 5G technology, there are higher demands on signal bandwidth, transmission rate, energy consumption, and other aspects in the fronthaul system. Due to its limited spectrum utilization, high complexity, and large power consumption of the remote radio head (RRH), the digitized CPRI is difficult to satisfy the new requirements of 5G for fronthaul. As an efficient and concise modulation scheme, delta sigma modulator (DSM) can replace multi-bit analog to digital converters (ADCs) with the passive filters at the receiver side of the fronthaul, significantly reducing the complexity of RRHs while meeting the requirements for transmission rate and efficiency. Therefore, DSM has received widespread attention in recent years, and there have been significant developments in new technologies and various structures related to DSM.

In this thesis, an in-depth analysis and comparison of several different structures of 1-bit DSMs are conducted, and an enhanced 1-bit sturdy multi-stage noise-shaping (SMASH) structure for digital fronthaul systems is proposed. The proposed SMASH DSM is based on the traditional SMASH structure, with some structural changes and simplifications made to enhance the modulator's noise shaping capability. In the thesis, a 100-MHz bandwidth 64 quadrature amplitude modulation (64-QAM) orthogonal frequency division multiplexing (OFDM) signal is used as a digital baseband signal and then modulated onto RF carriers with a center frequency of 2.5 GHz. Finally, the bandpass 1-bit DSM modulation is performed. The process is simulated and experimentally verified.

The detailed comparison among the traditional single-stage delta-sigma modulator (SDSM), the traditional MASH and SMASH, and the proposed SMASH is presented in the fronthaul transmission system. The OFDM signal at radio frequency (RF) is quantized to two bits by SDSM/MASH/SMASH ADC, and this digitized signal is transmitted over 20-km single mode fiber (SMF) in a 2-level amplitude non-return-to-zero (NRZ) or 4-level pulse amplitude modulation (PAM4) intensity modulation direct detection (IM-DD) system.

Firstly, it is found that the proposed SMASH DSM has the widest input dynamic range (DR), which means it has better stability, followed by traditional SMASH and MASH, while SDSM performs the worst in terms of input DR.

Then, in the case of fiber transmission systems, the proposed SMASH has better noise suppression performance than the traditional MASH and SMASH schemes. In the directly received system, also known as the electric back-to-back (EBTB) system, the error vector magnitude (EVM) of the proposed SMASH, traditional MASH, and SMASH are -32.56 dB, -29.03 dB, and -29.31 dB, respectively. The proposed one has an around 3.2 dB EVM improvement. And in the IM-DD fiber transmission over 20-km SMF, the EVM are -24.71 dB, -23.93 dB, and -22.36 dB, respectively. The proposed scheme also has an around 2.4 dB EVM improvement compared to the traditional SMASH.

Finally, the comparison result of the two SMASH DSMs is verified in the experiment. In the case of EBTB and optical back-to-back (OBTB) systems, the proposed SMASH has an over 3 dB EVM improvement compared with the traditional SMASH. And in the case of the fiber link, the EVM for proposed SMASH is increased by 2.76 dB and 2.94 dB compared to the traditional one over the 8 km and 20 km fiber, respectively.

ACKNOWLEDGEMENTS

As I complete this thesis, I would like to take this opportunity to express my deepest gratitude to all those who have supported and helped me throughout this long journey.

First and foremost, my deepest thanks go to my family, especially my parents, for their unconditional love and support. Their belief and encouragement have been a constant source of strength, enabling me to persevere through difficult moments.

Next and the most important, I am profoundly grateful to my supervisor, Professor John Xiupu Zhang, for his invaluable guidance, unwavering support, and insightful feedback throughout the entire research process. His expertise and patience have been instrumental in helping me overcome challenges and develop a deeper passion for academic research.

I would also like to extend my thanks to my lab members, Xiaoran Xie and Gaowen Chen, who generously shared their knowledge, resources, and offered valuable feedback during our discussions. Their collaboration has been a vital source of motivation and inspiration.

Moreover, I owe a great deal of appreciation to my lab members, Saeed Haydhah, Zijian Cheng, Fujuan Huang, and Qazi Tareq, whose support and encouragement also have helped me stay grounded and focused during the research.

Finally, I would like to express my gratitude to all the staff of the ECE department of Concordia, for providing me with the academic environment, resources necessary, and patience to complete this research. Without their support, this thesis would not have been possible.

Once again, my sincerest thanks to everyone who has contributed to this work.

Contents

List of Figures

List of Tables

List of Acronyms

AMPS	advanced mobile phone system
AM	amplitude modulation
ADC	analog to digital converter
AWG	arbitrary waveform generator
AR	augmented reality
ARoF	analog radio over fiber
ASK	amplitude shift keying
BBU	baseband unit
BS	base station
BER	bit error rate
CS	circuit switching
CP	cyclic prefix
CDMA	code-division multiple access
CIFB	cascade integrators with feedback
CIFF	cascade integrators with feedforward
CPRI	common public radio interface
CMOS	complementary metal-oxide-semiconductor
C-RAN	cloud radio access network
CRFB	cascade resonators with feedback
CRFF	cascade resonators with feedforward
DSM	delta sigma modulation
ΔΣ modulator	delta sigma modulator
DSM	delta-sigma modulator
DR	dynamic range
DRoF	digital radio over fiber
DSP	digital signal processing
DSL	digital subscriber line
DAC	digital to analog converter
DC	direct current
DFB laser	distributed-feedback laser
EBTB	electrical back-to-back
E/O	electric/optic
EDFA	erbium doped fiber amplifier
EVM	error vector magnitude
FFT	fast Fourier transformation
FPGA	field-programmable gate array
FSK	frequency shift keying
5G	fifth generation
FIR	finite impulse response
1G	first generation

4G	fourth generation
FDM	frequency division multiplexing
FSK	frequency shift keying
FDMA	frequency-division multiple access
FMT	filtered multi-tone
GSM	global system for mobile communications
GVD	group-velocity dispersion
HD	high-definition
IBN	in-band quantization
IIR	infinite impulse response
I/Q	in-phase and quadrature
IC	integrated circuit
IM-DD	intensity modulation direct-detection
ICI	inter-channel interference
IoT	Internet of things
IFFT	inverse fast Fourier transformation
ITU	International Telecommunication Union
LAN	local area network
LSCP	large-scale collaborative processing
LTE	long-term evolution
MASH	multi-stage noise-shaping
MIMO	multiple-input multiple-output
MSA	maximum stable amplitude
NTF	noise transfer function
NR	new radio
NRZ	non-return to zero
OBSAI	open base station architecture initiative
OBTB	optical back-to-back
OBG	out-of-band gain
O/E	optic/electric
OTx	optical transmitter
OFDM	orthogonal frequency-division multiplexing
OSR	oversampling ratio
PAM	pulse amplitude modulation
PD	photodiode
PM	phase modulation
PN	pseudo-random noise
PA	power amplifier
PS	packet switching
PSD	power spectral density
PDM	pulse density modulation
QAM	quadrature amplitude modulation
QPSK	quadrature phase-shift keying

RAN	radio access network
RF	radio frequency
RoF	radio over fiber
ROP	received optical power
RIN	relative intensity noise
RRH	remote radio head
RMS	root mean square
2G	second generation
SDSM	single stage delta sigma modulator
SNR	signal to noise ratio
STF	signal transfer function
SMASH	sturdy multi-stage noise-shaping
SMF	single mode fiber
SMS	short messaging service
SISO	single-input single-output
SQNR	signal to quantization noise ratio
3G	third generation
TDMA	time-division multiple access
USTF	unity signal transfer function
VR	virtual reality
WAN	wide area networks

Chapter 1 Introduction

1.1 Development of communication systems and C-RANs

Over the past few decades, the growing number of users and the expansion of application scenarios had led to increased demands for bandwidth, data rate, spectrum efficiency, and coverage in communication systems, which had significantly accelerated the development of cellular communications [1].

Before the 2000s, the first generation (1G) and the second generation (2G) of mobile communication technology were gradually introduced and developed in the 1980s and 1990s, respectively. 1G enabled voice calls with analog signals, and 2G provided voice services as well as the use of short messaging service (SMS), with digital signals with a set of protocols named Global System for Mobile Communications (GSM) [2]. Plus, with the advent of 2.5G technology, the ability to send and receive emails and browse the internet became possible [3].

During the 2000s, the introduction of 3G technology brought to advancements in several fields, such as mobile TV and video telephony, where the emergence of smartphones and various mobile applications is occurring [3]. 3G was built upon the standards developed by the International Telecommunication Union (ITU) and was a component of the IMT-2000 International Mobile Telecommunications effort. The technologies about 3G enabled network operators to offer a wider range of advanced services to their clients while also improving network capacity by enhancing spectral efficiency [4]. For 1G and 2G, circuit switching (CS) was employed, but initially, both circuit and packet switching (PS) were utilized in 3G. The integration of 3G technology, along with other factors, had the ability to unify and combine existing cellular standards. The standards mentioned included GSM (Global System for Mobile), TDMA (Time-Division Multiple Access), and CDMA (Code-Division Multiple Access) [5]. The multiple access (MA) technology transitioned from TDMA and CDMA to CDMA as the prevailing standard. GSM/IS-136 was evolved into Wideband CDMA (WCDMA), whereas CDMA-One transformed into CDMA2000. CDMA utilized pseudo-random noise (PN) codes to separate many customers and transmitted them simultaneously across the entire available bandwidth [3].

Due to the increase and development of several mobile internet and video applications, customers had greater demands for system capacity and data rate during the 2010s, which drives the development of fourth-generation (4G) digital cellular technology. To support mobile internet and video applications, it is crucial to significantly improve data transmission speeds. Long-term evolution (LTE), often known as 4G, is a technology designed to explicitly enable packet-switched networking. OFDMA (Orthogonal Frequency-Division Multiple Access), which employs IFFT (inverse fast Fourier transform) and FFT (fast Fourier transform) procedures, was selected to effectively handle FDMA multiple access [3]. This approach partitions the spectrum into subchannels, each separated by a distance of 15 kHz, greatly improving the efficiency of spectrum utilization. Multiple-Input Multiple-Output (MIMO) systems have emerged as one of the most promising approaches for achieving high data rates and more reliable wireless communication systems in recent years. Multiple antennas are installed at both the transmitters and the receivers. The capacity of the MIMO system is positively correlated with the number of transmit and receive antennas. MIMO systems offer higher multiplexing gain (data throughput), diversity gain, and coding gain (link dependability) compared to conventional Single-Input Single-Output (SISO) systems [6].

However, during the 2020s, the growing popularity and high demand for new applications like virtual reality (VR), augmented reality (AR), high-definition (HD) screening, video conferencing, the Internet of Things (IoT), the Internet of Vehicles, and autonomous driving have posed various significant challenges to 4G networks in terms of data rate, connectivity, and latency [1]. The 5G New Radio (NR) network was born under such demands. Compared to 4G cellular networks, 5G is expected to offer increased system capacity, faster data rates for users, much more connections, higher band utilization rate, reduced latency, more adaptable bandwidth deployment, and a wider range of services. Furthermore, 5G communication systems prioritize enhanced security, improved quality of service, and energy-efficient communication solutions. The aforementioned requirements are continuously propelling the advancement of 5G, and several nascent technologies related to 5G communications have been developed and implemented, such as massive MIMO, software-defined networking, Millimeter-Wave, spectrum sharing, Ultra-Dense Network, and cloud radio access network (C-RAN), etc. [1], [3], [4], [5], [7], [8], [9].

Table 1-1 illustrates the evolution of communication networks from the 1G to the 5G [1]-[9]. Evidently, communication networks are developing towards wider bandwidth, higher capacity, and faster transmission speeds, while also supporting more intelligent user services.

Table 1- 1 Evolution of communication networks from 1G to 5G [1]-[9]

Generations	1G	2G	3G	4G	5G
Year	Before 1980s	1990s	2000s	2010s	2020s
Multiplexing	FDMA	FDMA, TDMA	CDMA	CDMA, OFDM	CDMA, OFDM
Switching	Circuit	Circuit	circuit and packet	packet	packet
Speed	2 Kbps	14.4-64 Kbps	2 Mbps	200 Mbps to 1Gbps	Up to 100 Gbps
Maximum Bandwidth	30 kHz	200 kHz	1.25 MHz	20 MHz	Up to 400 MHz
Technology	AMPS, NMT	GSM	WCDMA, CDMA2000	LTE MIMO	New Radio
Service/ Applications	Voice	Voice and SMS	Voice, SMS, Mobile Internet	High data rate Mobile Internet, Video streams, Wearable Device	Very high data rate Internet, HD Video, Wearable Device, VR, AR, IoT

Among them, C-RAN is a core technology in 5G network architecture. The growing demand for processing power, along with the emergence of diverse small cell traffic patterns, both in terms of space and time, make the concept of the C-RAN quite appealing [8]. In the 4G and the previous communication networks, the cellular radio station, which is also called evolved Node B (eNB), has a variety of functions, including baseband modulation, digital-to-analog conversion (DAC), analog-to-digital conversion (ADC), up-conversion, and RF signal transmission, etc. However, in 5G C-RAN networks, the conventional eNB is divided into two parts. One is the baseband unit (BBU), which is migrated and clustered into a BBU pool, providing large-scale collaborative processing (LSCP), while the other part only retains the radio frequency functions and is closer to users, referred to as the remote radio head (RRH) [8], [10].

Figure 1-1 shows the architecture of C-RAN, in which the BBU pool commonly communicates with the RRHs via the Common Public Radio Interface (CPRI) protocol [10]. The network connecting the BBUs and RRHs is the fronthaul network, while the network connecting the BBU pool, the eNB, and the core network is the backhaul network. Nowadays, CPRI has been the main protocol used in fronthaul networks; however, it is not expected to be the optimal resolution due to the increasing bandwidth demands of future fronthaul systems [11]. More and more efficient and economical technologies are introduced to satisfy the communication requirement of radio-over-fiber (RoF) that is applied to fronthaul systems, such as 1-bit Delta Sigma Modulation (DSM), which achieves high sampling rates, reduces the impact of nonlinearity, and reduces energy consumption by replacing traditional DACs. DSM has become an important research direction for future fronthaul technology.

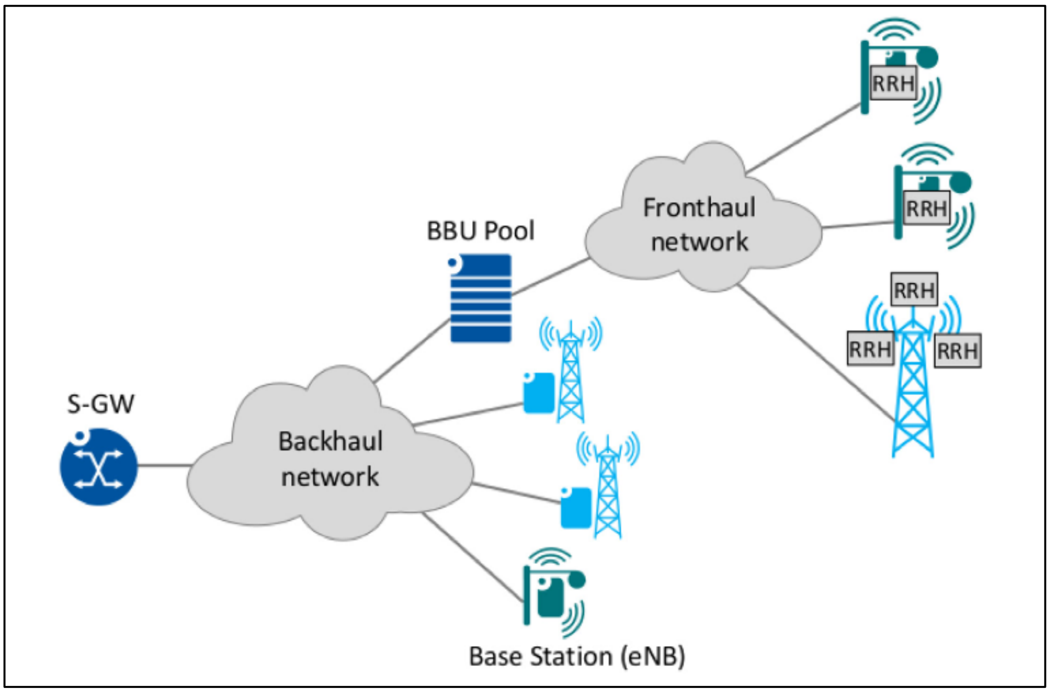

Figure 1- 1 Mobile backhaul and fronthaul network architecture [12]

1.2 Introduction to fronthaul and radio-over-fiber systems

The rapid growth of mobile users, along with the need for large data capacity, quicker data speed, minimal delay, and dependable services, have fueled the development of 5G networks, and C-RAN has been applied as a highly promising architecture for meeting the above demands [11]. In C-RANs, as the link between BBUs and RRHs, fronthaul is one of the most necessary parts, which can be implemented using several technologies, including optical fiber transmission, ordinary wireless communication, or even millimeter wave communication [13]. Due to various considerations such as operating costs and transmission efficiency, one of the current development trends of 5G technology in fronthaul networks is to allow RRHs to assume fewer processing units and hand over a large number of digital-to-analog conversion and information processing functions to the BBUs. It is with these factors in mind that the RoF system is widely regarded as a cost-effective and dependable solution for future access networks. It achieves this by utilizing optical fiber, which has a large transmission bandwidth capacity [14].

RoF is a technique that modulates the radio frequency (RF) subcarrier onto an optical carrier in order to distribute it over a fiber network. In C-RAN networks, due to the increasing demands for transmission rates, bandwidth, and capacity for fronthaul, traditional transmission media are struggling to meet these requirements. As a result, RoF systems are becoming an increasingly popular solution for fronthaul.

Typically, in the RoF structure, a RF signal, usually exceeding 10 GHz, is modulated onto a light-wave signal and then sent across the optical link. Hence, wireless signals are transmitted on fiber to RRH at high frequencies and then converted from the optical to electrical domain there. Subsequently, the signals are amplified and emitted by an antenna. Consequently, there is no need for frequency up/down conversion at the different RRHs, which allows for a straightforward and cost-effective installation at these stations. Figure 1-2 shows the architecture of the RoF system.

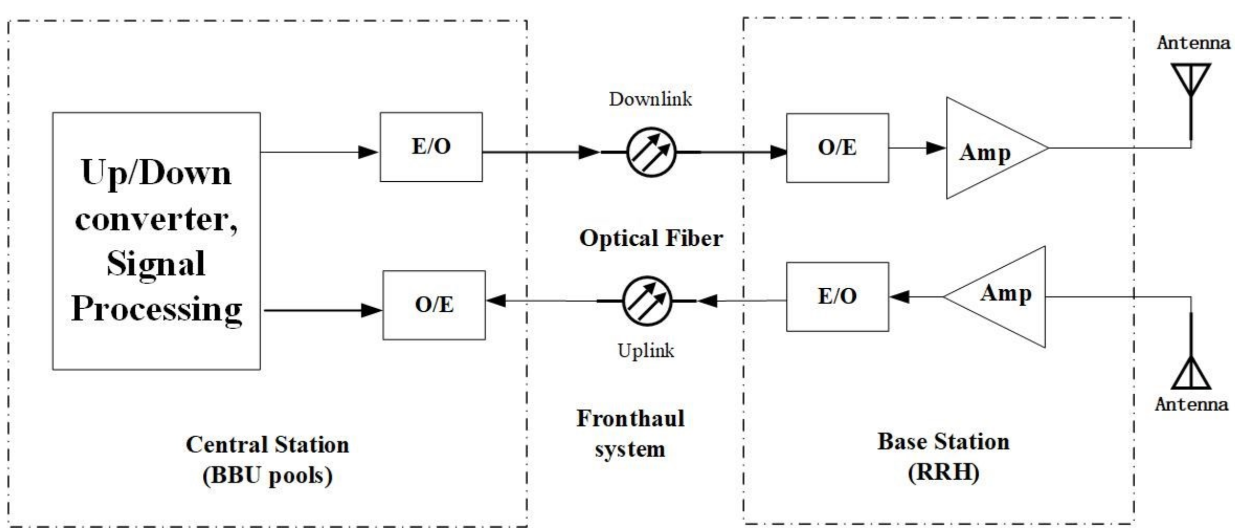

Figure 1- 2 Typical RoF architecture in fronthaul system

RoF systems are generally divided into two main categories: analog and digital RoF. Analog RoF (ARoF) modulates the optical carrier by analog radio signal, which is a cost-effective fronthaul network. However, due to the direct modulation by the optical transmitter, analog RoF is easily affected by nonlinear distortion that is introduced with power amplifiers (PAs), memory effects, and other transmission nonlinearities. Figure 1-2 also can be shown as the architecture of an analog RoF system.

Compared with analog RoF system, digital RoF (DRoF) has the ability to overcome the issue above because of its resistance to nonlinearity [15]. After the process of up-sampling, the RF signal is quantized by ADC and DAC and finally becomes the digitized RF signal. Since the generated digital signal only has limited voltage levels, usually 2 levels or 4 levels, the impact of nonlinear devices in transmission systems has been greatly reduced. Therefore, digital RoF has become one of the most popular solutions used in CPRI. The structure of digital RoF systems is illustrated in Figure 1-3.

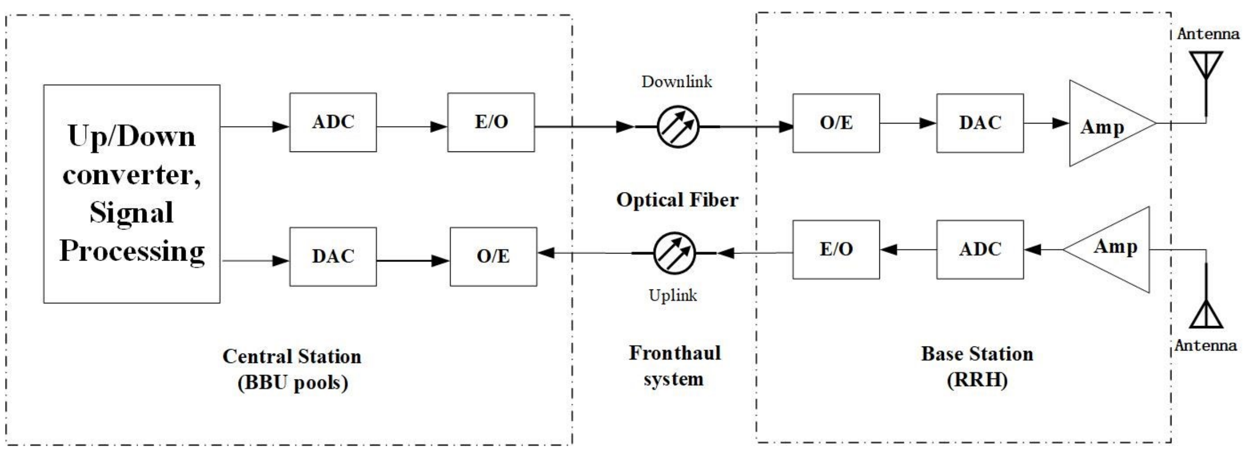

Figure 1- 3 Digital RoF architecture in fronthaul system

1.3 Introduction to delta-sigma modulation system

With the further development of 5G technology, the fronthaul system's requirements for bit rates are becoming increasingly demanding. Although DRoF overcomes the nonlinear issue, the increasing transmission speeds require ADC/DAC to have higher sampling rates to ensure data conversion performance in 5G networks. On the one hand, the additions of ADC/DACs at the base station (RRH) bring larger power consumption and compatibility issues; on the other hand, to decrease the quantization noise, the ADC/DACs are required more quantization bits, which also increases the complexity and design costs of the base stations. As a result, the DSM system is introduced and adapted to deal with the above issues, and more work can be done to improve the modulation performance based on the DSM technique.

A typical RoF transmission system with DSM is illustrated in Figure 1-4. Compared to the traditional digital RoF, a bandpass filter replaces the DAC in the base station, which greatly decreases the complexity and costs because the filter could be realized with an analog device. Moreover, the delta-sigma modulator processes the digital signal in BBU pool or the central station, and the ADC/DAC part could apply a 1-bit quantization level to complete the modulation (1-bit DSM). As long as the sampling rate is reasonably increased in the DSM system and appropriate structures are adopted, it is easy to meet the requirements of 5G transmission while significantly reducing costs. The basic principle and the detailed structures of the DSM will be discussed in detail in the following chapters.

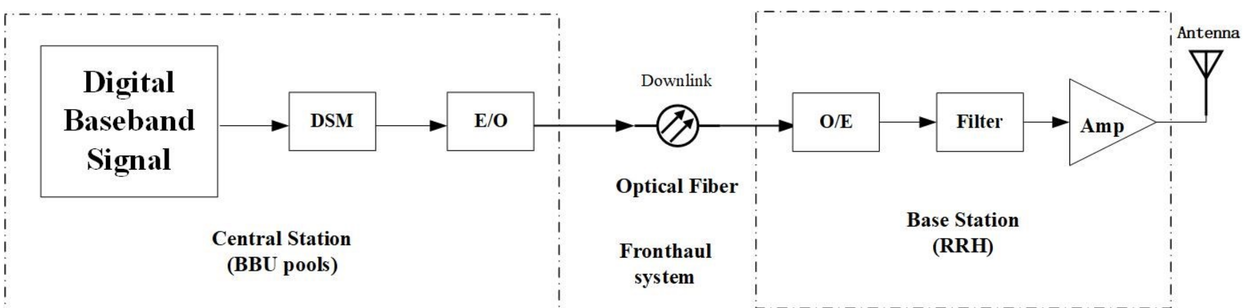

Figure 1- 4 A DSM-based RoF transmission system (downlink)

1.4 Thesis outline

The thesis will go through the usage and performance of 1-bit DSM technique in a discrete-time radio-over-fiber fronthaul transmission system. It shall consist of a literature review, theory, simulation, experiments confirmation. The rest of the thesis is organized as below:

Chapter 2 is the literature review about the RoF systems and delta-sigma modulations. This part will mainly introduce the basic DSM, high order DSM, and the current development.

Chapter 3 presents the theoretical principles of delta-sigma modulations, including the bandpass delta-sigma modulator, the stability of DSM, and the typical types of multi-stage delta-sigma modulations, as well as the proposed work.

Chapter 4 shows the simulation results and the comparisons of current multi-stage DSM and the proposed multi-stage DSM in a RoF transmission system.

Chapter 5 exhibits the experiment setup and procedures. A comparison of the results verifies the structures's performance.

Chapter 6 makes the conclusion of this thesis and provides possible improvement for future work to achieve better performance in the DSM-based RoF system.

Chapter 2 Background and literature review

In chapter 2, Firstly, the RoF system is introduced, highlighting its important position and development needs in fronthaul based on DSM, and the key aspects and technologies are also involved in its specific implementation, as well as the current application status, which is the main content of section 2.1. In section 2.2, the main principles of DSM are discussed, along with its primary types and several common implementations of DSM in RoF systems. Plus, N-bit and 1-bit delta-sigma modulators are described and compared, and the applications mainly consist of lowpass and bandpass, each suited for different scenarios. Finally, section 2.3 discusses methods to improve DSM performance, including increasing the order and applying cascading schemes, as well as their common structures.

2.1 Radio over fiber system

2.1.1 Delta-sigma modulation in RoF system for fronthaul interface

In the 4G era, a proposal was made to improve the capacity, coverage, and flexibility of mobile data networks by implementing C-RAN. This involves separating the baseband processing functions from the base stations (BS) at cell sites and consolidating them in a centralized BBU pool. This simplifies each BS to a RRH and allows for radio coordination among multiple cells [16], [17]. Like mentioned in Chapter 1, C-RAN has two parts: one is the backhaul network that connects BBU pools to central/base stations, and the other is the fronthaul network from BBUs to RRHs, where CPRI is the most used fronthaul interface in 4G. Besides, open base station architecture initiative (OBSAI) specifications are also applied as the internal interface by RAN vendors [17].

The initial version of the CPRI standard was proposed in late 2003 by five producers of radio equipment, and the following version was released in 2013 [17]. CPRI addresses the physical layer and layer 2 by establishing a frame that encompasses I and Q samples generated from digitizing a radio signal, synchronization data, and various control and management information. According to that mentioned before, a digital RoF system has a better ability to overcome the nonlinear distortion that is introduced by fiber and other nonlinear devices. As a digitization interface, CPRI samples and quantizes each LTE signal using a Nyquist ADC with a sampling rate of 30.72 MSa/s and 15 quantization bits and transports the streams with optical intensity modulation-direct detection (IM-DD) links [18], [19]. It is advisable to use enhanced CPRI (eCPRI) with a divided physical layer to reduce fiber traffic and strengthen the efficiency of the fiber link, although it increases the complexity of RRH that consists of analog devices in a low physical layer [20]. Figure 2-1 shows the basic operation principle of a Nyquist ADC.

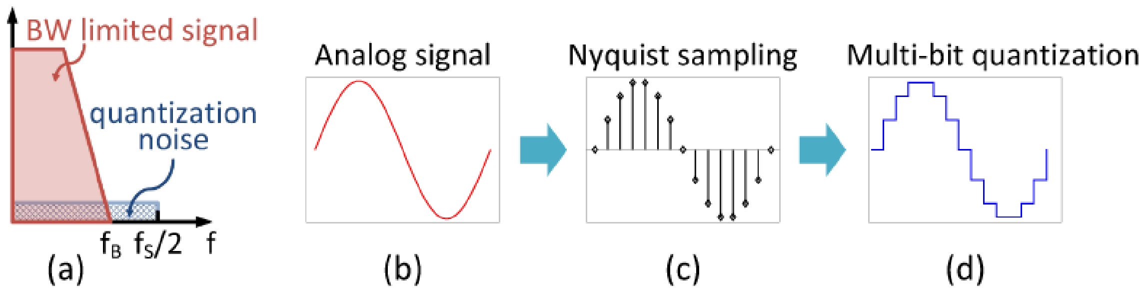

Figure 2- 1 Principle of Nyquist ADC. (a) Digital baseband signal in frequency domain with quantization noise distributed in the Nyquist zone. (b) Input analog signal. (c) Nyquist sampling. (d) Quantization result. [21]

However, the utilization of the Nyquist ADC in the CPRI results in the production of significant quantization noise that is evenly spread throughout the Nyquist frequency spectrum. To reduce quantization noise, a high number of quantization bits are used in each sample, leading to low spectral efficiency and the requirement for a wider data bandwidth [20]. As a result, the CPRI technique struggles to meet the demands of future fronthaul interfaces. Therefore, in order to ensure efficient spectrum utilization while meeting the demand for reducing quantization noise in ADCs, the delta-sigma modulation-based interface has emerged and is receiving more and more attention.

Compared with the CPRI-based interface, the DSM-based fronthaul interface utilizes a larger sampling rate rather than Nyquist frequency to decrease the quantization noise without more quantization bits. The higher sampling rate widens the Nyquist frequency domain and puts the quantization noise on a wider frequency range to reduce the in-band noise level. Besides, a kind of noise shaping scheme is also used to change the distribution and the shape of the quantization noise, which can remove the noise out of the signal band. When an appropriate filter is applied to eliminate the out-of-band noise at the receiver side, the original signal could be restored smoothly

[21]. Figure 2-2 illustrates the basic principle of a DSM interface with 1-bit or 2-bit quantization bits [18].

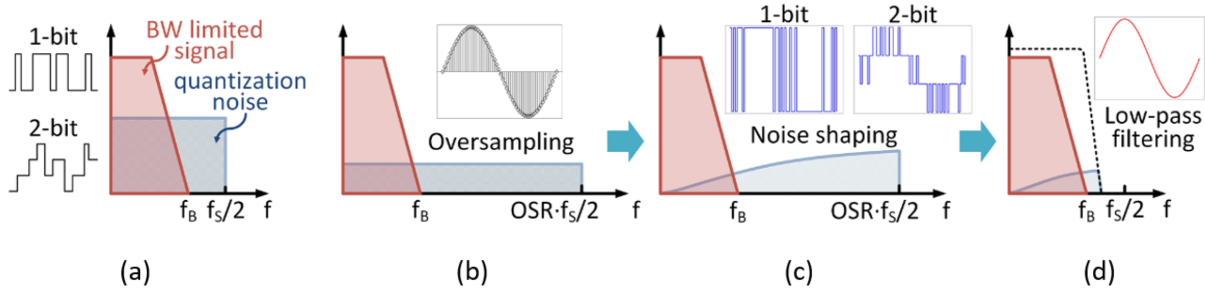

Figure 2- 2 Principle of basic DSM (a) Digital baseband signal if only one or two bits used at the Nyquist rate. (b) Oversampling extending the Nyquist zone. (c) Noise shaping pushing noise out of signal band. (d) Filter removing the out-of-band quantization noise [18]

2.1.2 Modulation methods and realization

In modern communication systems, the signal digital modulation is a crucial step, which specifically includes processes such as symbol mapping and signal up-conversion, etc. The common modulation methods include the amplitude shift keying (ASK), the frequency shift keying (FSK), the phase shift keying (PSK), and the quadrature amplitude modulation (QAM), etc. Among them, ASK and FSK generally modulate signals in a single carrier, so they are defined as non-orthogonal modulation methods. On the contrary, if signals are modulated by two orthogonal carriers like sin(x) and cos(x), the modulation is defined as an orthogonal modulation method, such as QAM and quadrature PSK (QPSK), which is also known as 4-QAM.

Compared to non-orthogonal modulation, orthogonal modulation has a higher modulation efficiency and is also more conducive to demodulation. With the development of communication technology, the demands for coding efficiency and spectrum utilization are becoming increasingly high. Orthogonal modulation techniques, represented by QAM, have also become the preferred choice. High-order QAM technology is gaining popularity due to its ability to carry more information per symbol. Therefore, orthogonal modulation is a necessary modulation method in 4G and 5G technologies [22]. Figure 2-3 shows a general orthogonal modulation [23].

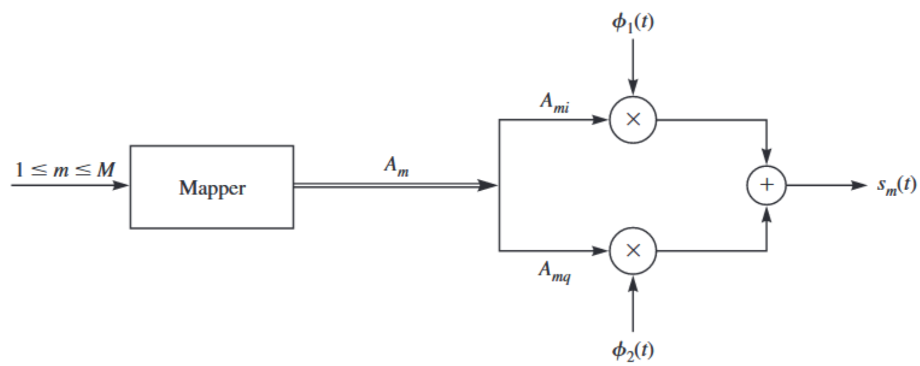

Figure 2- 3 A general orthogonal modulation

According to Figure 2-3, Am = Am_i + jAm_q, and Am_i and Am_q are the in-phase and quadrature components separately. The constellation diagram can represent a digital modulated signal by orthogonal modulation methods like QAM, and the error vector magnitude (EVM) is an effective index to measure the performance of a digital system. Generally, EVM is determined by identifying the optimal constellation position for every received symbol. The root mean square (RMS) of all error vector magnitudes between the received symbol sites and their nearest reference constellation locations defines the EVM of the transmission system [24].

After mapping the bit streams and before finally up-conversion, in order to further improve spectrum utilization efficiency, orthogonal frequency-division multiplexing (OFDM) is also a widely used modulation method. Similar to the frequency division multiple access (FDMA) or filtered multi-tone (FMT) scheme used in 3G, OFDM is also a medical multi-channel technology solution. The difference lies in that OFDM utilizes overlapping subcarrier spectra to enhance bandwidth efficiency without applying bandlimited filters and oscillators for every subchannel, while in FDMA or FMT, the subchannels are completely separated [25], [26].

Figure 2-4 illustrates the basic structure of a multicarrier system and the OFDM implementation of multicarrier modulation with IFFT/FFT. Figure 2-5 shows the spectral characteristics of FMT and OFDM separately [26], [27].

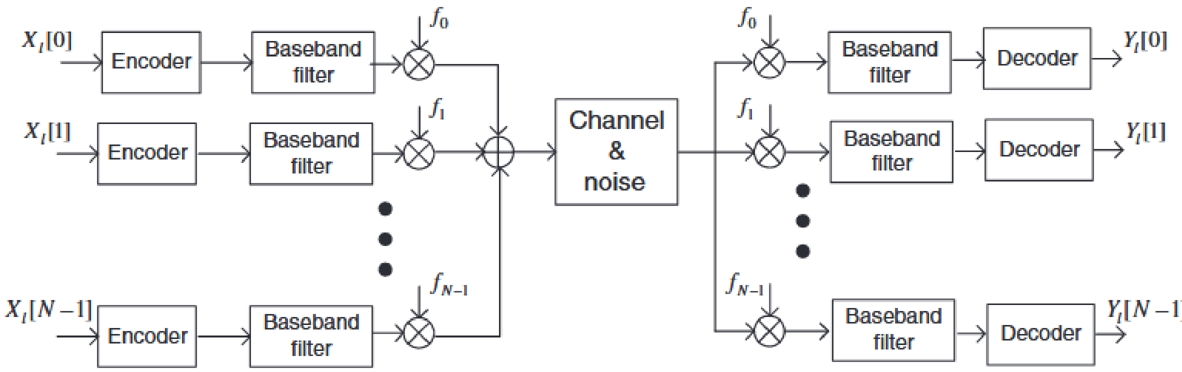

(a)

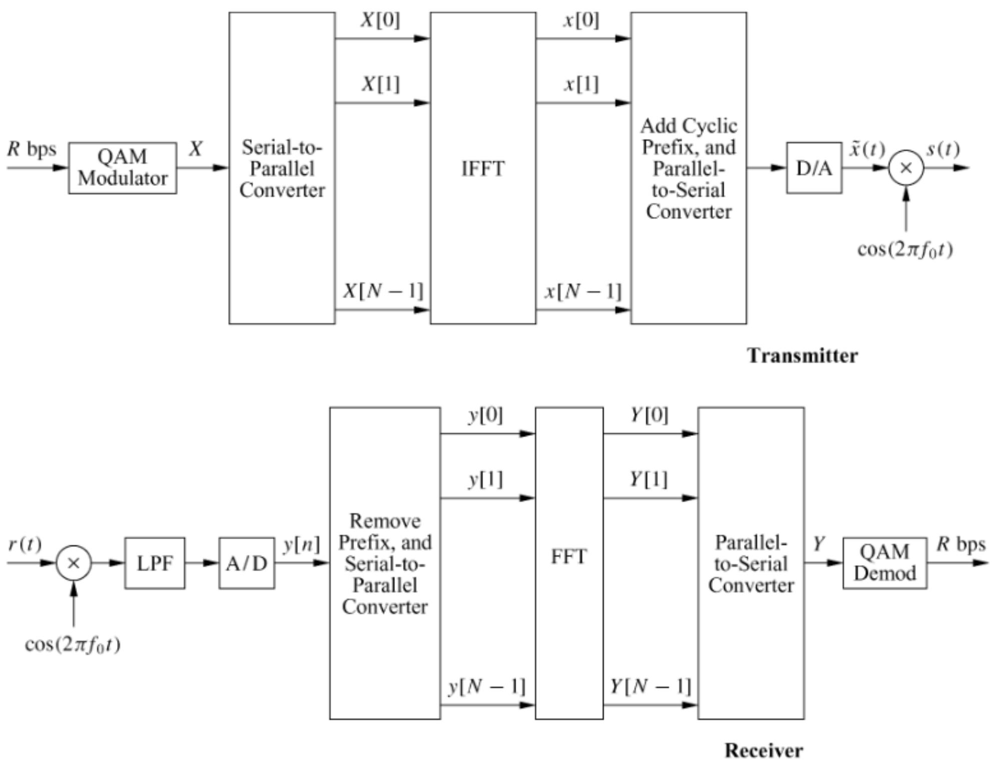

(b)

Figure 2- 4 (a) the basic structure of multicarrier system. (b) OFDM implementation with IFFT/FFT

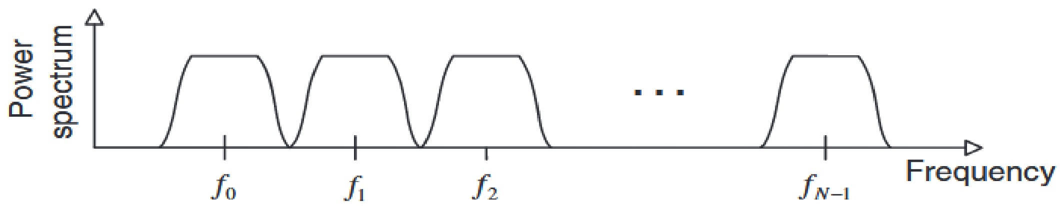

(a)

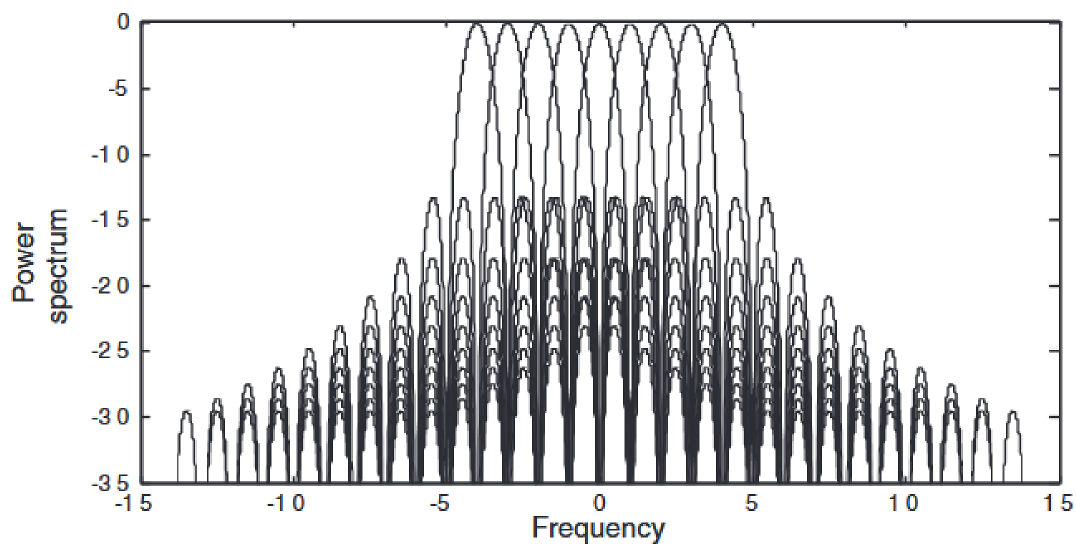

(b)

Figure 2- 5 (a) The spectrum of FMT. (b) The spectrum of OFDM signal (dB)

2.2 Delta-sigma modulation

Delta sigma modulators have emerged as a popular option for the realization of analog/digital interfaces in electronic systems. Relative to other types of ADCs, DSMs provide the most efficient method for digitizing a wide array of signals across an expanding range of applications, including high-resolution low-bandwidth data conversions for digital audio, sensor interfaces, instrumentation, ultra-low-power biomedical systems, and medium-resolution broadband wireless communications [28].

This section introduces the main principles of delta-sigma modulation, including oversampling and noise shaping and the current applications. Then, N-bit DSM and 1-bit DSM are discussed, as well as the principles, the realizations, and the typical blocks of lowpass and bandpass DSM.

2.2.1 Principles and applications of delta-sigma modulator

Data converters, including ADCs and DACs, are usually classified into two types: Nyquist-rate and oversampled converters, like DSMs. In the former group, a one-to-one relationship exists between the input and output samples. Each input sample is processed independently, without respect to previous samples [29]. For the Nyquist-rate converters, the sampling rate f_s can be just the Nyquist's criterion requirements: twice of the bandwidth of the input signal.

Figure 2-6 shows the operation process of basic analog to digital conversion [28]. An analog signal x(t) is sampled firstly by a sampling and holding circuit at a rate fs, which is slightly larger than the Nyquist rate. After that, a discrete-time and continuous-amplitude signal $x_s(n)$ is created. Then, the signal is quantized by an N-bit quantizer to be mapped as a discrete-valued signal $x_c(n)$ and finally becomes a digital output signal $y_d(n)$ after the digitization step [28].

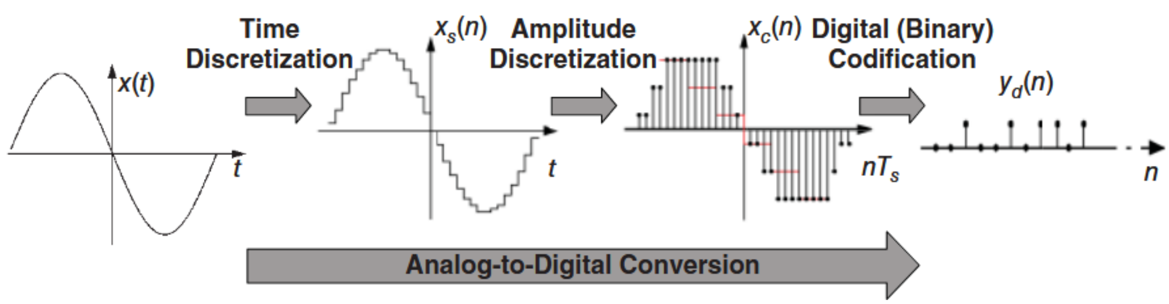

Figure 2- 6 The operation process of basic analog to digital conversion

Compared with the classic Nyquist-rate convertors, the oversampling convertors' precision is not only determined by the quantization bits and the matching accuracy of the analog components such as resistors and capacitors [29]. The oversampling data converters utilize the much higher sampling rate than the Nyquist rate to get the final output signal where many preceding input values are included. It is evident that the DSM converters' inputs and outputs are not a one-to-one relationship, thus the accuracy of the DSM converter can only be assessed by comparing the whole input and output waveforms.

The operation process of DSM conversion is illustrated in Figure 2-7 [29]. The oversampled signal is input to a loop filter that consists of integrators and then is quantized by a quantizer. Finally, the output are reinput to the filter with a feedback loop to realize the conversion process. After the moving average filter shown in Figure 2-7, the total output $\hat{u}$ is a digital representation of the input signal u [29].

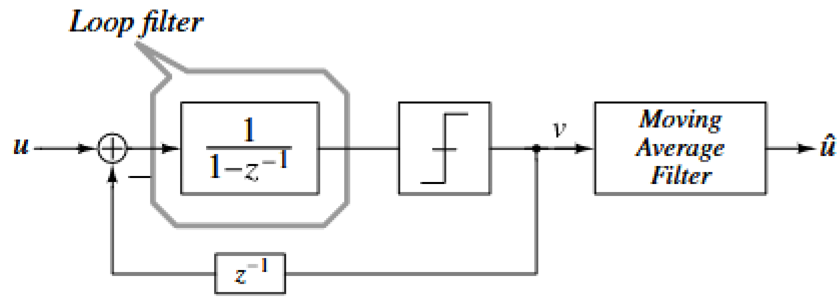

Figure 2- 7 The operation process of DSM conversion

Recent advancements in contemporary digital communication, along with the proliferation of portable devices, have heightened the demand for low-voltage, low-power ADCs. Among them, DSMs are an effective option for low-to-medium bandwidth high-resolution [30]. Contemporary design trends in DSMs focus on broadening the signal frequency range while maintaining SNR or increasing the SNR with a higher central frequency. A lot of research has been done to realize better performances of DSM to satisfy the requirements of the development of communication systems, such as the commercial continuous-time delta-sigma ADCs, which are integrated on CMOS chips [31], and the bandpass DSM that can support ultra-high-order QAM signals in fronthaul systems [32].

In this thesis, since the research is about the modulation and transmission of digital signals in RoF systems, the focus below is on discrete-time DSM and the related transmission system.

2.2.2 Over-sampling and noise shaping

In the delta sigma modulation process, over-sampling is the first step before the signal goes into the loop filter. If a signal is sampled at a sampling frequency f_s that is much higher than the

Nyquist rate, the ratio that compares the sampling rate to the Nyquist rate is the over-sampling ratio (OSR).

$$\mathrm{OSR} = \frac{f_s}{2 \cdot B} = \frac{f_s}{BW} \qquad (2.1)$$

where f_s is the sampling frequency, B is the maximum frequency of the baseband input signal, and the BW is the whole bandwidth of the input signal.

The above OSR is the definition of a baseband signal. For a bandpass input, for example, an intermediate frequency (IF) signal or a radio frequency (RF) signal, the OSR is

$$OSR_{bp} = \frac{f_s}{2 \cdot BW} \qquad (2.2)$$

where f_s is the sampling frequency and the BW is the bandwidth of the bandpass input signal.

Figure 2-8 illustrates the effect of oversampling. It is clear to notice that when the OSR is doubled, the quantization noise power is reduced to half (3 dB). Therefore, in the signal band, the signal-to-quantization noise ratio (SQNR) is improved by reducing the noise spectral density [33].

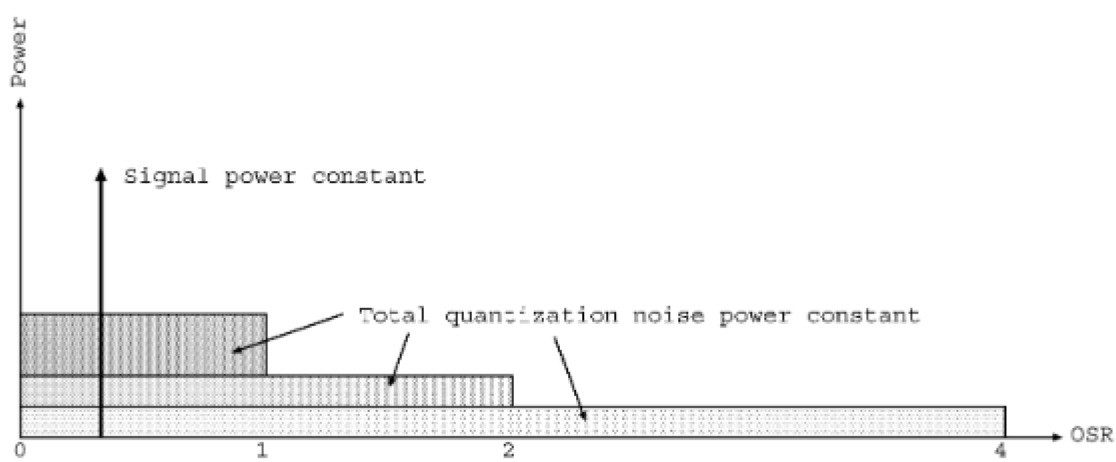

Figure 2- 8 The effect for the OSR of 1, 2, and 4 times [33]

Noise shaping is the second step to improve the SQNR. In this process, the quantization noise is altered and moved out of the signal band, which reduces the in-band quantization noise density. If an appropriate filter is applied at the receiver side, the out-of-band noise can be removed, so the quantization noise that is moved out is less harmful for the whole DSM process [33], [34].

Figure 2-9 shows the generic block diagram of a delta-sigma modulator [29]. The loop filter is responsible for noise shaping, which has two inputs: one is the digitized input signal u, and the other is the output v of the modulator from the feedback loop.

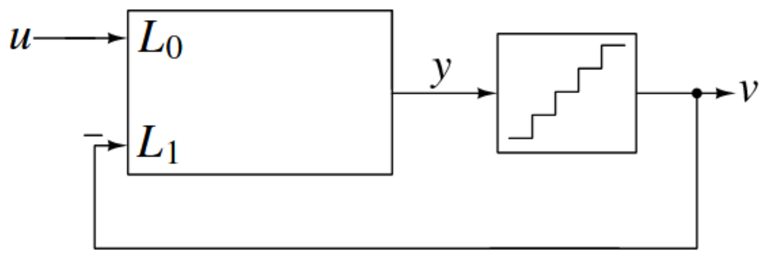

Figure 2- 9 The generic block diagram of a delta-sigma modulator [29]

According to the diagram above, in terms of z-transforms, the systems transfer functions are described as:

$$\mathrm{Y(z)} = L_0(z)U(z) - L_1(z)V(z) \tag{2.3}$$

$$\mathrm{V(z)} = Y(z) + E(z) \tag{2.4}$$

where E(z) is the quantization noise. For the system, if the signal transfer function and the noise transfer function are defined as STF and NTF, respectively, the output V(z) can be expressed as:

$$\mathrm{V(z)} = STF(z)U(z) + NTF(z)E(z) \tag{2.5}$$

Based on the above functions, it is clear that

$$\mathrm{STF(z)} = \frac{L_0(z)}{1+L_1(z)} \tag{2.6}$$

$$\mathrm{NTF(z)} = \frac{L_1(z)}{1+L_1(z)} \tag{2.7}$$

Usually, the loop filter consists of integrators, which commonly has the form $(1-z^{-1})^L$ in the z-domain. From the NTF expression, it is easy to see that NTF will be close to 0 when the $L_1(z)$ is infinite, showing that the poles of the loop filter are the zeros of the NTF. The loop filter with an L^{th} order NTF of the form $(1-z^{-1})^L$ should have L poles at the position z = 1 [29]. This indicates that there must be L integrators in the loop, which means that the number of integrators decides the order of the DSM or that of the loop filter. Typically, the result of the noise shaping of DSM can be presented like Figure 2-10 [33].

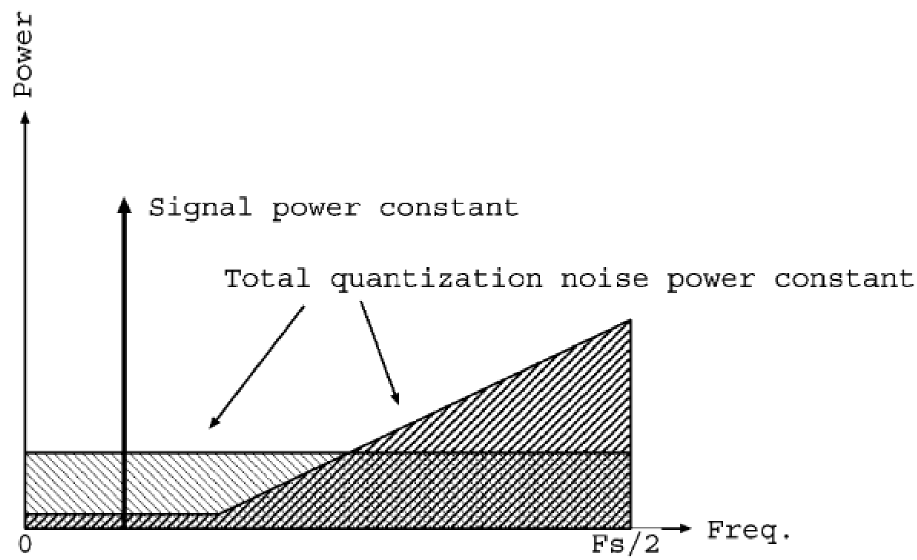

Figure 2- 10 Low frequency noise pushed to higher frequencies by noise shaping

2.2.3 1-bit and N-bit DSM

The number of bits in the quantizer determines whether the delta sigma modulator is a 1-bit DSM or a N-bit DSM. When applying the quantizer in the DSM, they each have their own advantages and disadvantages.

Nowadays, single-bit ADC is the most popular quantization method in the DSM. One of the most important advantages of 1-bit quantization is that the associated 1-bit DAC in the feedback is intrinsically linear. This linearity arises from the characteristic that a single-bit DAC possesses merely two output signal levels. The displacement of the DAC output levels only results in DC offset or linear gain error, which have a minimal impact on the overall performance of the delta sigma modulator [35], [36]. Additionally, the 1-bit quantizer makes the quantizer design simple and decreases the strain on the outputs of circuits that drive the quantizer [36], [37].

Meanwhile, the drawbacks also exist in the 1-bit modulator. For example, because the ADC only has 2 levels, the quantization step size becomes large, leading to a large integrator output swing. The op amp's restricted slew rate in the integrator of the loop may result in nonlinearity

[38]. In order to guarantee the fast settling of the ADC, more power consumption introduced by op amps may be needed [36].

As for the N-bit delta sigma modulator, like the traditional ADC's strategy, increasing the number of quantization bits is an effective way to decrease the quantization noise. Theoretically, it can be reduced by 6 dB for adding 1 bit to the quantizer. Because the quantization noise is reduced, the quantization noise dynamic range is enhanced, and the integrator swings within the loop filter are also decreased. Furthermore, multi-bit quantization can enhance modulator stability, facilitating the implementation of more aggressive high-order noise shaping to get high resolution, even at low oversampling ratios [37]-[41].

However, because the output of N-bit feedback DAC is directly pushed into the first integrator of the loop filter, any error produced by the DAC, commonly arising from mismatches among the components of the multi-bit DAC, emerges at the modulator output without noise shaping. What is more, another flaw of the N-bit quantization is the augmented power consumption and spatial requirements of the quantizer [36], [41].

In this thesis, the IM-DD modulation method is used in the following simulation and experiment. Considering the power limitation of the optical laser, the loss and distortion in the fiber transmission, and all the conditions discussed above, the 1-bit modulator is applied in the DSM design.

2.2.4 Lowpass and bandpass DSM

As discussed in section 2.1, the loop filter, primarily composed of integrators, mainly performs the noise shaping function in DSM. From equation (2.5), NTF and the STF determine the functionality and characteristics of the loop filter.

If the NTF behaves like a high-pass filter in the frequency domain, while the STF does not suppress the signal in low frequencies, it means that noise in the low-frequency range is suppressed while high-frequency noise can pass through the loop filter. Functionally, this DSM can be used as a lowpass DSM. Similarly, if the NTF is set as a band-stop filter, while the STF shows pass-through characteristics in the signal band, thus this DSM can be regarded as a bandpass DSM.

Following, a 2nd order DSM is as an example to illustrate the frequency response and the distribution of zeros and poles of the NTF in lowpass and bandpass DSM.

Figure 2-11 shows a 2nd order DSM with a cascade of integrators with feedback (CIFB) structure [29]. And the loop filter consists of a cascade of two delaying integrators, with the quantizer output fed back into each of the integrators with different weight factors. In this way, when different factors are designed, the different type of NTF can be obtained.

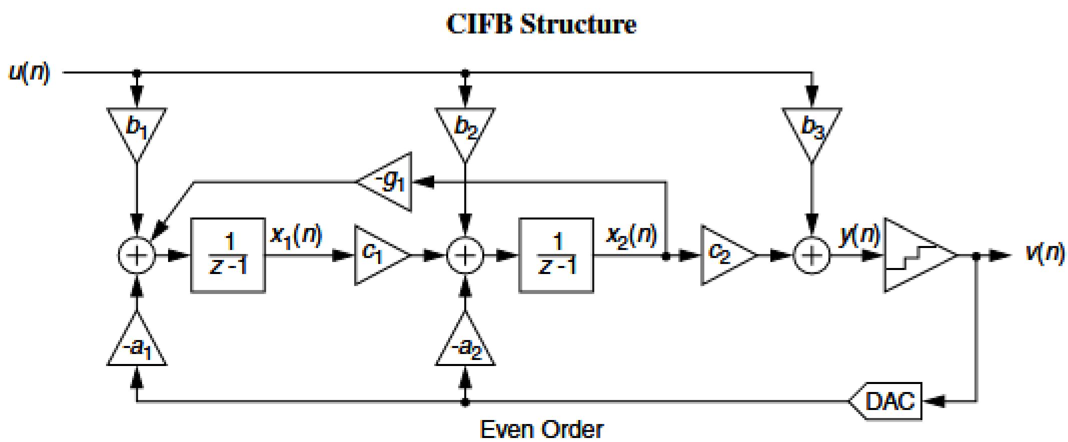

Figure 2- 11 A 2nd order DSM with CIFB structure

According to the block diagram above, the NTF and STF are able to calculated:

$$\mathrm{NTF(z)} = \frac{(1-z^{-1})^2-(1-c_1g_1)z^{-1}+1}{(1-z^{-1})^2+((a_1c_1-g_1)c_2)z^{-2}+a_2c_2z^{-1}(1-z^{-1})} \tag{2.8}$$

$$\mathrm{STF(z)} = \frac{(1-z^{-1})^2+(b_1c_1-g_1)c_2z^{-2}+b_2c_2z^{-1}(1-z^{-1})+b3}{(1-z^{-1})^2+((a_1c_1-g_1)c_2)z^{-2}+a_2c_2z^{-1}(1-z^{-1})} \tag{2.9}$$

Based on the calculated NTF and STF, modifying the weight factors can realize different functions according to the needs. And correspondingly, the NTF also has different responses in the frequency domain.

For example, if designing the CIFB DSM as a lowpass structure, the NTF should be like a high-pass filter. That means when z is close to infinite, the NTF = 1, which indicates that the position of zeros is close to 1 on the unit circle. In the same time, because it is a 2nd order structure, the NTF should have 2 poles that are located inside the unit circle to ensure the stability of the system. With the design methods of traditional filters and some tools, the noise transfer function of 2nd lowpass DSM can be obtained as

$$\mathrm{NTF} = \frac{z^2 - 1.999z + 1}{z^2 - 1.485z + 0.5906}$$

Figure 2-12 shows the frequency response and the zero-pole plot of the 2nd CIFB lowpass DSM

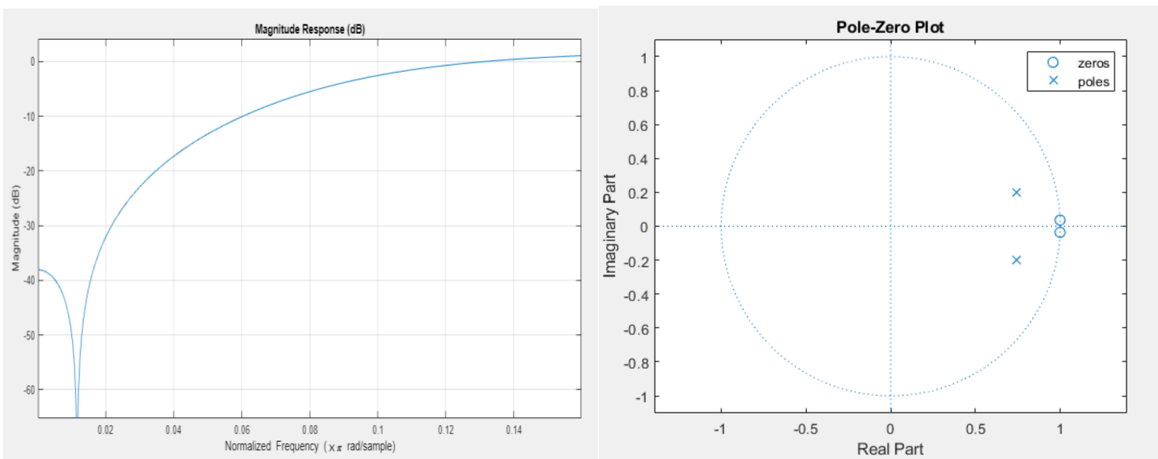

(a) (b)

Figure 2- 12 (a) Magnitude response of NTF of lowpass DSM in frequency domain. (b) the zero-pole plot

Similarly, if designing the CIFB DSM as a bandpass structure, the NTF should be like a band-stop filter and the stopband of the NTF should be located at the signal central frequency. N-path transformation is a good method to transfer a lowpass DSM to a bandpass one, where the transformation is realized by letting $z = -z^N$. In this way, a lowpass NTF (with n zeros near z = 1) into a bandpass NTF with n zeros near z = j and n zeros near z = j. The new NTF has an identical gain versus frequency profile as the original NTF, but the frequency axis is compressed by factor N [29]. The process of the N-path transformation is shown in Figure 2-13 [29].

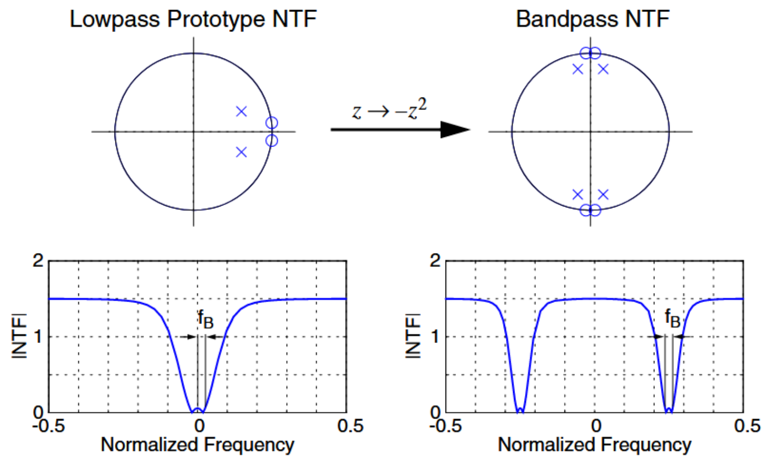

Figure 2- 13 A bandpass NTF from a lowpass NTF by applying a 2-path transformation

Typically, to make sure the input signal appears at the center of the spectrum, the passband is usually put at the center, which means that the sampling frequency is generally fixed at four times the center frequency of the bandpass signal, that is, f_s=4f_c, in order to ensure $\omega = 0.5\pi$.

Based on the N-path transformation method and the requirement of a bandpass DSM, the noise transfer function of 2nd bandpass DSM can be obtained as

$$\text{NTF} = \frac{(z^2 + 0.03627z + 1)(z^2 - 0.03627z + 1)}{(z^2 + 0.2275z + 0.7685)(z^2 - 0.2275z + 0.7685)}$$

Figure 2-14 shows the frequency response and the zero-pole plot of the 2nd CIFB bandpass DSM

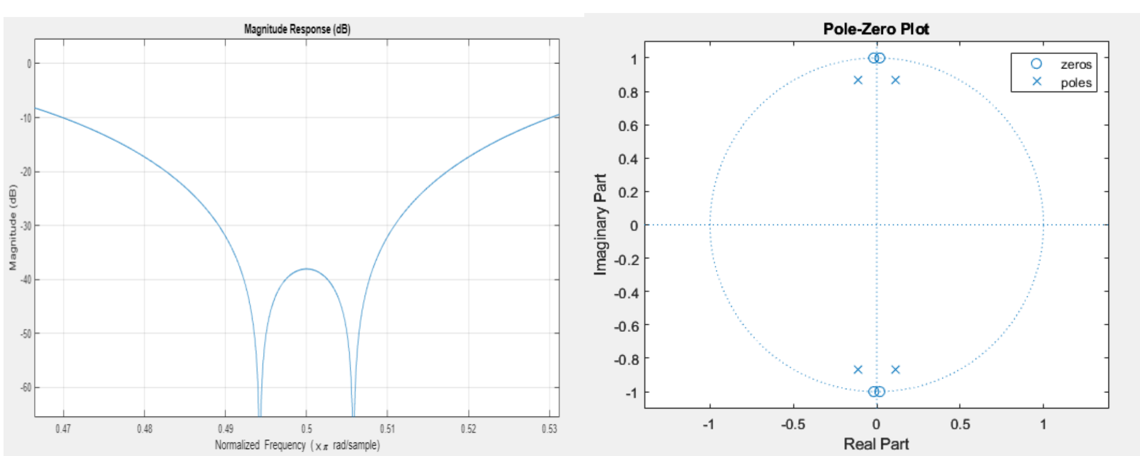

(a) (b)

Figure 2- 14 (a) Magnitude response of NTF of bandpass DSM in frequency domain. (b) the zero-pole plot

2.3 High order DSM

From the previous content, it is clear that through oversampling and noise shaping methods, DSM can significantly reduce quantization noise within the signal bandwidth. However, the 1st or 2nd order basic structures fall far short of the bandwidth requirements of current communication systems. According to the 5G NR standard, the channel bandwidth can be up to 100 MHz for the FR1 designation, whose frequency range is from 450 MHz to 6 GHz; meanwhile, for the FR2 designation, whose frequency range is between 24.25 GHz and 52.6 GHz, the maximum channel bandwidth is 400 MHz [42], [43]. The basic low order DSM cannot provide enough bandwidth, the required signal-to-noise ratio (SNR), and the corresponding stability. So, to enhance the SNR, the utilization of high-order DSM and novel feedback architectures such as the multi-stage DSM is recommended [32], [44], [45].

2.3.1 High order single-stage DSM

The simplest way to extend a low order DSM to L^{th}-order structure is applying L integrators before the quantizer. Figure 2-15 illustrates the topology of an L_{th}-order single-stage DSM with distributed feedback [28].

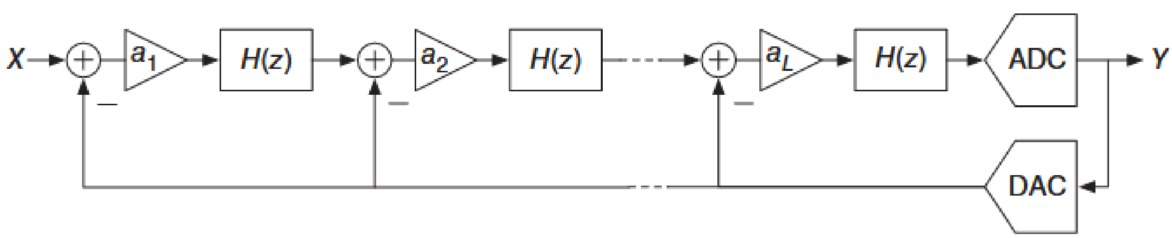

Figure 2- 15 L_{th}-order single-loop DSM

Next, considering the ideal condition of the loop filter, the NTF is easy to be obtained through the linear analysis and can be de expressed as

$$\mathrm{NTF(z)} = (1 - z^{-1})^L$$

Ideally, the in-band quantization (IBN) noise for a L_{th}-order NTF $(1 - z^{-1})^L$ is given by

$$\mathrm{IBN} \approx \frac{\Delta^2}{12\pi} \int_0^{\frac{\pi}{OSR}} \omega^{2L} d\omega = \frac{\Delta^2}{12\pi(2L+1)} \left(\frac{\pi}{OSR}\right)^{2L+1}$$

where Δ is the distance between the adjacent levels of the quantizer.

Nonetheless, the performance of this DSM cannot be realized in practice, as if the DSM utilizing pure-differentiator FIR NTFs are susceptible to instability when L > 2, resulting in unbounded states and inferior SNR relative to linear analysis predictions [28]. In fact, the primary source of instability is saturation of the quantizer rather than the quantization process, since if an infinite-level quantizer were applied, the modulator would be stable as the state variables would not get too large to handle [29].

From Figure 2-15, the input of the quantizer can be derived as

$$\mathrm{Q(z) = STF(z)X(z) + [NTF(z) - 1]E(z)}$$

the gain of the quantization noise [NTF(z)-1] should not be too large to avoid overloading the quantizer. Therefore, it is clear that the signal-dependent stability is expected, which is called the maximum stable amplitude (MSA) of a delta sigma modulator [29]. It is defined as the largest input for stable operation, normalized to the quantizer's full scale output M:

$$MSA \triangleq \frac{\max|u|}{M}$$

For the NTF itself, the scaling coefficients can be designed to limit the out-of-band gain to control the input value of the quantizer. In practice, the Butterworth or Chebyshev filter can be used as the reference to design the coefficients of NTF, ensuring the cut-off frequency beyond the signal band and the almost flat gain in the passband. A widely-used approximate criterion is the (modified) Lee's rule, which provides a practical optimal out-of-band gain (OBG) of the NTF [28], [29], [46]:

$$||\mathrm{NTF(z)}||_\infty = \max[NTF(z)] \cong 1.5$$

Considering the above limit and trade-off, various high order single loop DSM have been put forward. Some classic high order structures with feedforward or feedback loops have become the foundation for subsequent DSM designs, such as the cascade resonators with feedback (CRFB), the cascade integrators with feedforward (CIFF), the mentioned CIFB and so on. Figure 2-16 and Figure 2-17 show a 3rd order CIFF structure and a 3rd order CRFB structure [29].

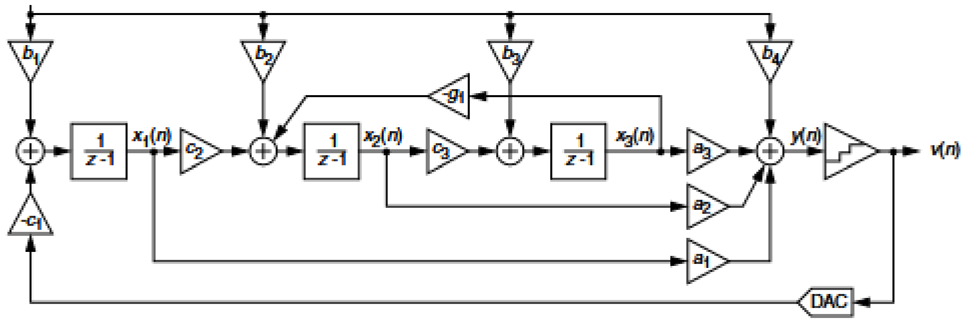

Figure 2- 16 A 3rd order CIFF structure DSM

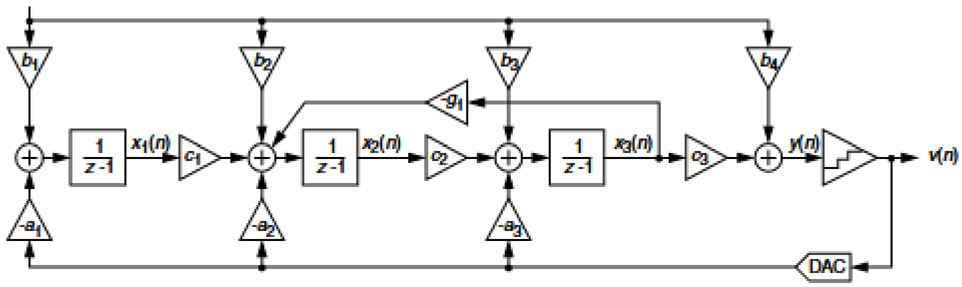

Figure 2- 17 A 3rd order CRFB structure DSM

2.3.2 Cascade multi-stage DSM

As discussed before, to improve the performance of the SQNR of a delta sigma modulator, many methods can be applied, such as increasing OSR, the order L of the loop filter, and even the quantization bit of the quantizer. However, these ways have their respective limitations. For example, higher OSR not only necessitates increased power but is also constrained by the operation speed of the existing integrated circuit (IC) technology [28], [29]. Increasing the order of the loop filter is contingent upon stability considerations, which restrict the highest allowable input signal amplitude for higher-order loops. As for the N-bit quantization, like we talked in the previous section, it causes the mismatch and more power consumption.

Apart from the methods above, cascade multi-stage structure as another extension topology of DSM is an effective strategy to help improve the performance. There are two main multi-stage structures: the multi-stage noise-shaping (MASH) and the sturdy multi-stage noise-shaping (SMASH).

Figure 2-18 illustrates the concept of MASH structure [29]. The MASH modulator is combined with 2 delta sigma modulators, which distribute in 2 stages. The output of the 1st stage is derived by

$$V_1(z) = STF_1(z)U(z) + NTF_1(z)E_1(z)$$

where U(z) is the total input signal, $E_1(z)$ is the quantization noise of the first stage, $NTF_1(z)$ and $STF_1(z)$ are the noise and signal transfer function of the 1st stage, respectively.

Then, according to Figure 2-18, $E_1(z)$ is fed into the second stage loop as the input and is modulated by the second DSM. The output is given by

$$V_2(z) = STF_2(z)E_1(z) + NTF_2(z)E_2(z)$$

where $E_2(z)$ is the quantization noise of the second stage, $NTF_2(z)$ and $STF_2(z)$ are the noise and signal transfer function of the 2nd stage, respectively.

The H_1 and H_2 at the output of the two stages are the digital filters, which are designed to cancel the 1st stage's quantization noise $E_1(z)$ at the final output V(z). It is clear that if

$$H_1 NTF_1 - H_2 STF_2 = 0$$

the target will be realized. So, the H_1 and H_2 can be designed as $H_1 = STF_2$ and $H_2 = NTF_1$. Finally, the overall output is derived as

$$V_{overall}(z) = H_1(z)V_1(z) - H_2(z)V_2(z) = STF_1 \cdot STF_2 \cdot \mathrm{U} - NTF_1 \cdot NTF_2 \cdot E_2$$

The remaining error in the output V is the shaped quantization error E_2, which is operated twice noise shaping. Besides, since the input to the 2nd stage is the quantization error E_1, which is itself noise-like, the overall quantization noise is suppressed further. What is more, based on the equation above, if the 2 stages both are 2nd order DSM, the overall noise shaping is like a 4th order DSM while maintaining the stability of a 2nd order structure.

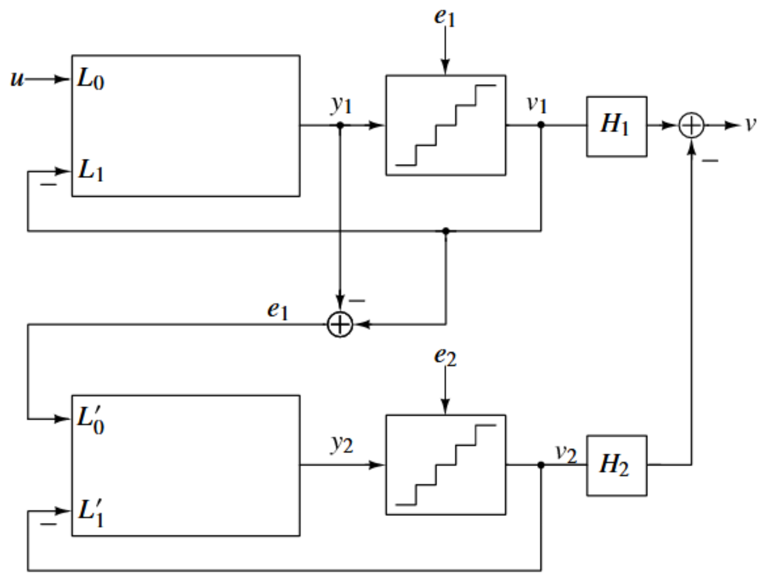

Figure 2- 18 A 2-stage MASH DSM structure

However, since the NTF and STF are analog transfer functions while the matching filters H_1 and H_2 are digital, the mismatch between them causes the leakage of the 1st stage's quantization noise, which is a critical issue to impact the performance of MASH [29], [40], [45], [47].

In order to decrease the influence of the high sensitivity of the cascade multi-stage structure to the analog circuit imperfections, the architecture of MASH can be modified to replace the noise cancellation with noise suppression, which generates the sturdy MASH (SMASH) structure.

Figure 2-19 illustrates the concept of SMASH structure [29]. As the figure shows, there are two differences between the MASH and SMASH structures: the first one, the output of the second stage is coupled back into the first loop; and the second one, the noise cancellation logic (H_1 and H_2) disappears in the SMASH. According to the changes, the output of the modulator is expressed as

$$V = STF_1 \cdot \mathrm{U} - NTF_1 \cdot NTF_2 \cdot E_2 + NTF_1 \cdot (1 - STF_2) \cdot E_1$$

Considering there is always delay in STF_2, the $STF_2 = 1$ cannot be realized. Thus, $STF_2 = 1 - NTF_2$ will be a good choice to reduce the error of $|1 - STF_2|$. Then, the overall output is given by

$$V = STF_1 \cdot \mathrm{U} - NTF_1 \cdot NTF_2 \cdot (E_1 + E_2)$$

From the equation above, we can notice that the high-sensitivity noise cancellation is replaced by low-sensitivity noise shaping while keeping the stability of the MASH structure [29].

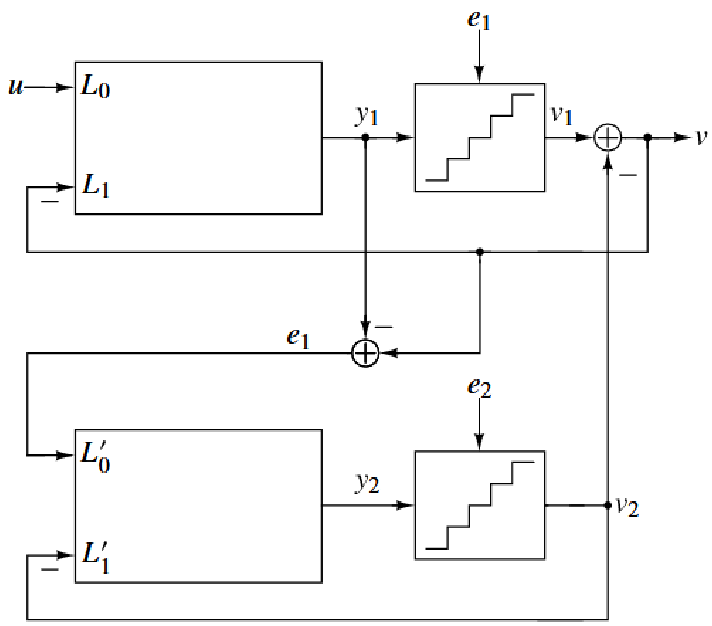

Figure 2- 19 A 2-stage SMASH DSM structure

2.4 Motivation and contributions

As a low-cost and efficient modulation method, DSM has garnered increasing attention in the development of 5G networks, especially in fronthaul systems. However, for the research about DSM in RoF systems, most focus on single-stage structures. Besides, for the research on MASH modulator structures, most studies focus on the ADC rather than considering its application in RoF transmission systems. At the same time, since traditional DSMs are often used for narrowband systems and baseband signal modulation as ADCs, their performance and stability have not been thoroughly studied and tested in broadband RF systems. There is also a lack of studies that involve the consideration and comparison of various nonlinear factors in RoF systems with multi-stage DSM structures. Therefore, considering the excellent performance and stability of the MASH structure as a type of DSM, it is necessary to discuss its application in RoF transmission systems.

In this thesis, a new SMASH delta sigma modulator for fronthaul systems is proposed based on the MASH structure, and a comprehensive comparison is made with traditional MASH and SMASH structures. The study includes simulations and experimental verification. One of the main contributions of this work is the design of a new SMASH DSM based on the traditional SMASH structure. By modifying and re-designing the structure of the two stages of the SMASH structure, the noise shaping capability of the proposed modulator has been enhanced while maintaining good stability. Furthermore, this work compared the proposed SMASH structure with the traditional MASH and SMASH structures under the 5G standard transmission: modulating RF signals with a bandwidth of 100 MHz at a sampling frequency of 10 Gbps and transmitting the modulated signal over 20-km SMF in the IM-DD RoF system. After the various nonlinear distortion effects during the transmission process, such as the Kerr effect and GVD introduced by fiber, the proposed new SMASH structures still demonstrated a better performance. Additionally, the design concepts and ideas from this process will also contribute to and provide help to our research team in the future.

Chapter 3 Theoretical analysis of multi-stage delta-sigma modulation

This chapter analyzes different types of multi-stage DSM, and proposes a new structure of multi-stage DSM, and discusses the principles and differences of them. Besides, the transmitter design based on these DSMs is also put here.

3.1 Transmitter structure design

The DSM is a process that modulates the baseband signal to RF signal, where the delta sigma modulators, up-convertors, and other signal processing units such as filters are included. In this section, the whole structure of transmitter part used is demonstrated, as well as the signal and basic modulation mode.

In this thesis, a bandpass type delta sigma modulation is used as a basic modulation structure, shown as Figure 3-1.

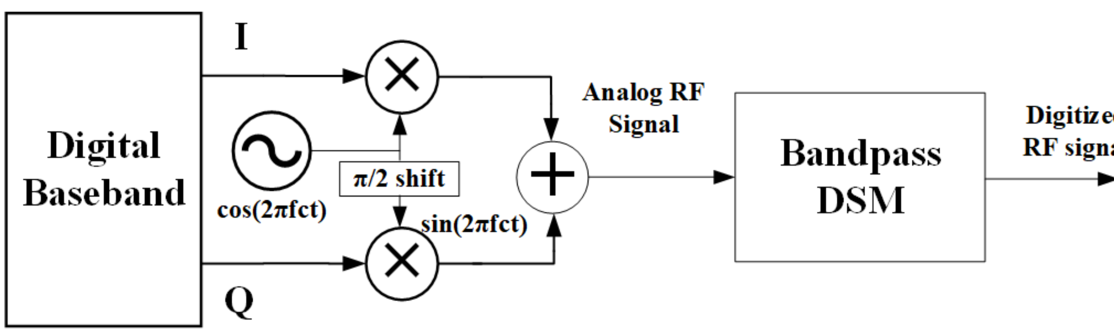

Figure 3- 1 The transmitter structure of a bandpass DSM system

The input signal is an equivalent digital baseband signal that has been mapped and modulated. The digital baseband signal is a 64-QAM OFDM digital signal with a bandwidth of 100-MHz. Firstly, the in-phase and quadrature (I/Q) modulation is implemented to up-convert the baseband signal to the band-limit RF signal with the high frequency sinusoid carrier. After that, before getting into the DSM, the signal has been modulated and up-converted to an analog RF signal, and the expression is given by

$$\mathrm{u(t)} = I \cdot \cos(2\pi f_c t) + Q \cdot \sin(2\pi f_c t) = A \cdot \cos(2\pi f_c t + \varphi)$$

where I and Q are the in-phase part and quadrature part of the digital baseband signal, and f_c is the carrier frequency, which is set 2.5 GHz in this thesis, also as the central frequency of the RF signal. A is the amplitude, and φ is the phase of the original equivalent digital baseband signal. Figure 3-2 shows the RF signal in the frequency domain.

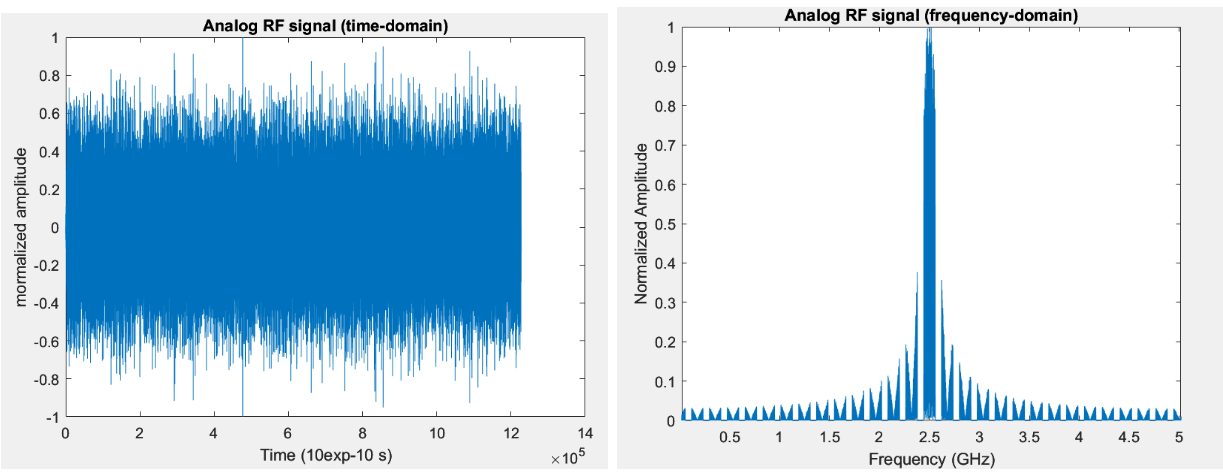

(a) (b)

Figure 3- 2 (a) The RF OFDM signal in time domain. (b) in frequency domain.

After the up-conversion, the analog RF signal is sent into the bandpass DSM to be modulated to the digital RF signal. In the following discussion, the delta sigma modulators involved are all bandpass structures.

3.2 Implemented SDSM, MASH and SMASH modulation

In this section, 3 types of DSM are demonstrated. One is a single-stage DSM (SDSM), the other two are multi-stage structures, i.e. MASH and SMASH structure.

3.2.1 SDSM structure and analysis

In chapter 2, the high order single-stage DSM has been discussed. In this section, a classic 4th order CRFB DSM structure is introduced and analyzed.

Figure 3-3 shows the topology of the 4th order SDSM structure with CRFB.

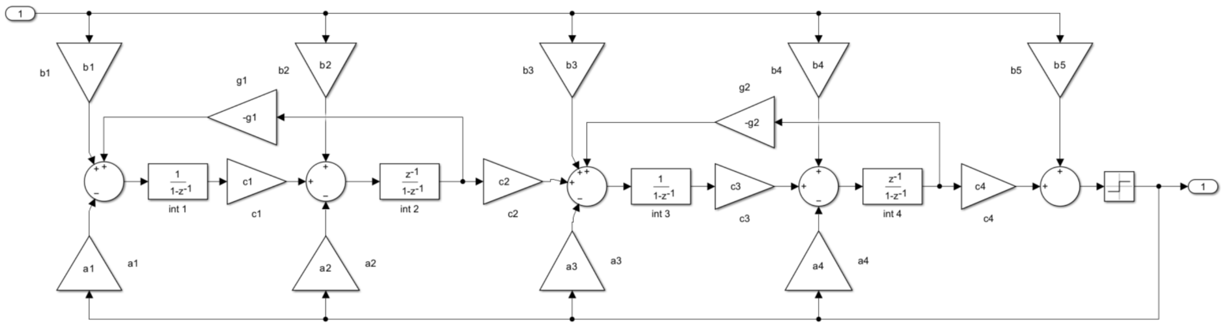

Figure 3- 3 A 4-th order SDSM structure with CRFB

The SDSM structure is a feedback loop including one quantizer and 4 integrators. The input signal and output feedback are fed into each integrator individually with weight factors a[k] and b[k]. From the figure, it is shown that the first and second integrators are combined with the feedback factor $-g_1$ to form one resonator, and the latter 2 integrators are combined with the feedback factor $-g_2$ to form the other resonator, which is one of the most typical structures of SDSM. Based on the structure, the NTF and STF is given as

$$\mathrm{NTF(z)} = \frac{[z^2-(2-g_1)z+1][z^2-(2-g_2)z+1]}{(a_1+a_2)z^2-a_2z+\{[z^2-(2-g_1)z+1]\cdot[z^2+(a_3+a_4-2+g_2)z+1-a_4]\}}$$

$$\mathrm{STF(z)} = \frac{(b_1+b_2)z^2-b_2z+\{[z^2-(2-g_1)z+1]\cdot[z^2+(b_3+b_4-2+g_2)z+1-b_4]\}}{(a_1+a_2)z^2-a_2z+\{[z^2-(2-g_1)z+1]\cdot[z^2+(a_3+a_4-2+g_2)z+1-a_4]\}}$$

Since in the CRFB SDSM structure, the weight factors c[k] are equal 1, which is not put into the NTF and STF.

For the bandpass input RF signal with the central frequency of 2.5 GHz and the bandwidth of 100 MHz and the sampling frequency $f_s = 4\times f_c = 10$ GHz, the oversampling rate $\mathrm{OSR} = \frac{f_s}{2BW} = 50$. When choosing the NTF as a band-stop filter, whose stop frequency is 2.5 GHz and the approximate range is a little more than 100 MHz, as well as taking the stability into consideration, the optimal weight factors and the NTF is shown below.

Table 3- 1 The weight factors of SDSM structure

	a_1	a_2	a_3	a_4	g_1	g_2
SDSM	-0.0891	-0.0148	-0.4094	0.4094	2.0363	1.9637
	b_1	b_2	b_3	b_4	b_5	c_k
	1	-3.8858×10^{-16}	1.9987	-3.2613×10^{-16}	1.	1

$$\mathrm{NTF(z)} = \frac{(z^2 + 0.03627z + 1)(z^2 - \ 0.03627z + 1)}{(z^2 + 0.2275z + 0.7685)(z^2 - \ 0.02275z + 0.7685)}$$

3.2.2 SMASH structure and analysis

In chapter 2, the SMASH DSM has been discussed. In this section, a classic SMASH structure with CRFB and a SMASH structure with CRFF are introduced and compared. Both of them are very popular SMASH structures in the current research.

Figure 3-4 shows the topology of the SMASH structure with CRFB structure in each stage.

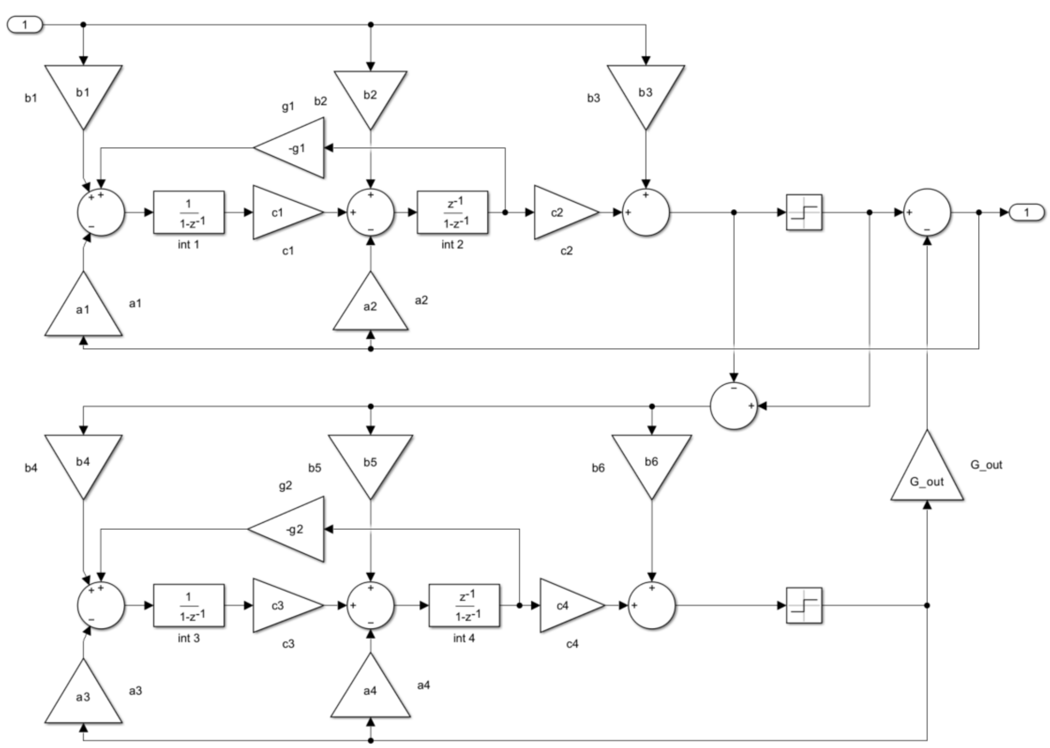

Figure 3- 4 A SMASH with CRFB structure in each stage

In the SMASH structure, each stage of the SMASH is a second order SDSM. The quantization noise of the first stage E_1 is fed into the second stage as the input. And in the 2^{nd} stage, the internal quantization noise E_2, smaller than E_1, is fed back into the 1^{st} stage to re-participate in the noise shaping of E_1. Because the loop in every stage is a 2^{nd} order SDSM, the overall structure is the 4^{th} order structure, which realizes the high order noise shaping with a better stability performance.

Considering every stage is a loop filter with input path L_0 and the feedback path L_1. Then, based on the structure shown in Figure 3-4, for the second stage, the loop filter is derived as

$$L_1 = -\frac{(a_3 + a_4)z - a_4}{1 - (2 - g_2)z + z^2}$$

$$L_0 = \frac{(b_3 + b_4)z - b_4}{1 - (2 - g_2)z + z^2} + 1$$

and then the output of the 2^{nd} stage is given by

$$Y_2 = L_0 \cdot E_1 + L_1 \cdot Y_2 + E_2$$

at the same time, we already know that

$$Y_2 = \frac{L_0}{1 - L_1} \cdot E_1 + \frac{1}{1 - L_1} \cdot E_2$$

According to the equations above, it is easy to derive that the 2^{nd} stage's NTF is expressed as

$$NTF_2 = \frac{1}{1 - L_1} = \frac{1 - (2 - g_2)z + z^2}{1 - a_4 - (2 - g_2 - a_3 - a_4)z + z^2}$$

Similarly, the NTF of the 1^{st} stage can be given by

$$NTF_1 = \frac{1}{1 - L_1} = \frac{1 - (2 - g_1)z + z^2}{1 - a_2 - (2 - g_1 - a_1 - a_2)z + z^2}$$

Finally, the overall output of the SMASH DSM is given by

$$V = STF_1 \cdot U + NTF_1 \cdot (-Y_2 + E_1) = STF_1 \cdot U + NTF_1 \cdot (-STF_2 \cdot E_1 - NTF_2 \cdot E_2 + E_1)$$

So, the total output is shown as

$$V = STF_1 \cdot U - NTF_1 \cdot NTF_2 \cdot (E_1 + E_2)$$

It is worth mentioning that, in the signal band, the magnitude of the error $|1 - STF_2|$ can be reduced by choosing it with properties similar to those of the NTFs. For example, in this CRFB structure, we choose $STF_2 = 1 - NTF_2$

The overall NTF is derived:

$$NTF_{overall} = NTF_1 \cdot NTF_2$$

$$NTF_{overall} = \frac{1-(2-g_1)z+z^2}{1-a_2-(2-g_1-a_1-a_2)z+z^2} \cdot \frac{1-(2-g_2)z+z^2}{1-a_4-(2-g_2-a_3-a_4)z+z^2}$$

Since in the CRFB structure of each stage, the weight factor c[k] equals 1, which is not put into the NTF and STF. And then, after selecting the optimal NTF in both stages according to the zero-optimization theory and the signal transmission requirement, the specific weight factors of SMSAH CRFB structure are calculated and shown below, as well as the NTF.

Table 3- 2 The weight factors of SMASH structure with CRFB

	a_1	a_2	a_3	a_4	g_1	g_2	Total order
SMASH CRFB	-0.6711	1.2743	-0.4745	0.9011	1.0533	1.0533	4
	b_1	b_2	b_3	b_4	b_5	b_6	OSR
	-0.6711	1.2743	1.0000	-0.4745	0.9011	1.0000	50

$$NTF_{\text{smash\_CRFB}}(z) = \frac{1-0.9467z+z^2}{-0.2743-0.0.3435z+z^2} \cdot \frac{1-0.9467z+z^2}{0.0989-0.5201z+z^2}$$

Compared with the CRFB structure, the CRFF structure has some key differences. The topology of a SMASH structure with CRFF is shown in Figure 3-5.

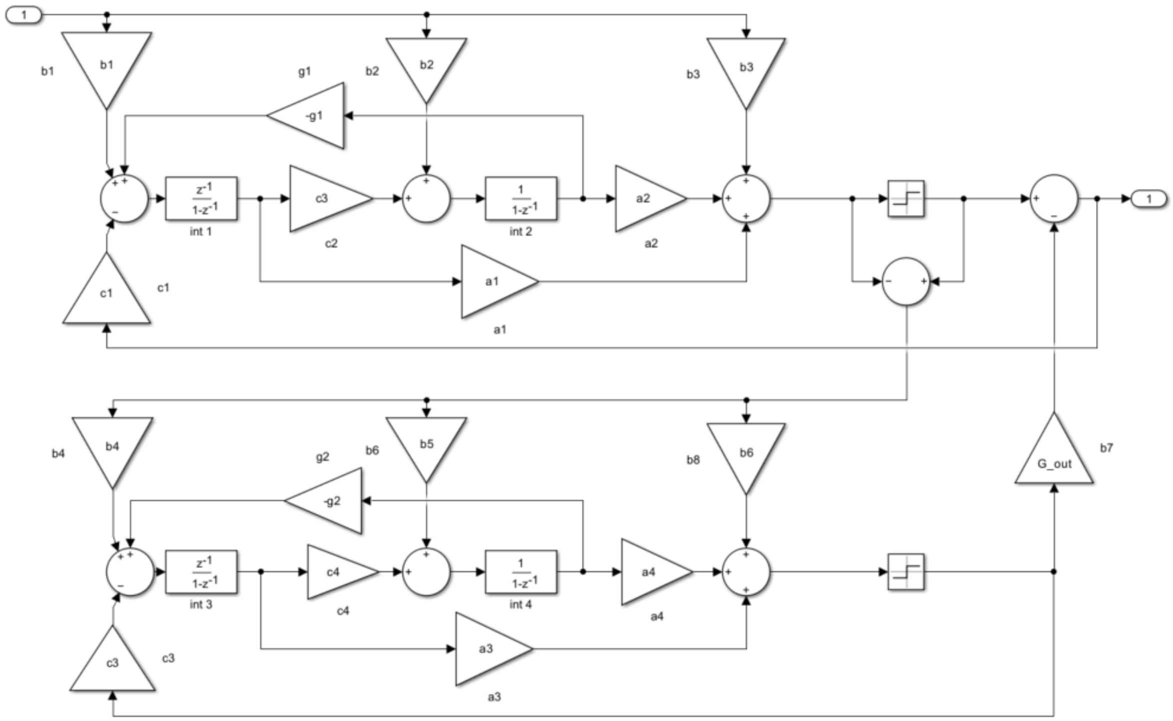

Figure 3- 5 A SMASH structure with CRFF in each stage

Firstly, for the loop filter in each stage, the feedback paths between output and quantizers are replaced by feedforward paths. Thus, the modulator only needs one DAC from the output to the input of the first integrator, simplifying the design.

Furthermore, if the weight factor of the path from the input to the quantizer directly is set to 1, as well as that between the input and the second integrator is set to 0, which means the input signal is directly fed into the output. In this way, all the integrators of the loop filter only deal with the shaped quantization noise components but do not process the input signal, reducing the harmonic distortion effectively. Therefore, the feedforward structure is one of the low-distortion structures [29].

In addition, it is precisely because the integrator does not process the signal components that its output is independent of the input signal of the modulator. Therefore, increasing the amplitude of the input signal will not cause the integrator to overload, thereby enhancing the dynamic range of the modulator. At the same time, due to the small output amplitude of the integrator, the requirements for the DC gain and the settling time of the op amp are reduced.

Based on the CRFF structure shown in Figure 3-5, and considering the common settings mentioned above, the loop filter of each stage is derived as

$$LF_1 = \frac{(a_2c_2 - a_1)z^{-2} + a_1z^{-1}}{(1-z^{-1})^2 + c_2g_1z^{-2}}$$

$$LF_2 = \frac{(a_4c_4 - a_3)z^{-2} + a_3z^{-1}}{(1-z^{-1})^2 + c_4g_2z^{-2}}$$

From the equation of the loop filter, the NTF of each stage is given by

$$NTF_1 = \frac{1}{1+LF_1} = \frac{(1-z^{-1})^2 + c_2g_1z^{-2}}{1-(2-a_1)z^{-1} + (1+c_2g_1 + a_2c_2 - a_1)z^{-2}}$$

$$NTF_2 = \frac{1}{1+LF_2} = \frac{(1-z^{-1})^2 + c_4g_2z^{-2}}{1-(2-a_3)z^{-1} + (1+c_4g_2 + a_4c_4 - a_3)z^{-2}}$$

Similar with the CRFB, the total output is shown as

$$V = STF_1 \cdot U - NTF_1 \cdot NTF_2 \cdot (E_1 + E_2)$$

where the $STF_1 = STF_2 = 1$, and the overall NTF is derived:

$$NTF_{overall} = NTF_1 \cdot NTF_2$$

$$NTF_{overall} = \frac{(1-z^{-1})^2 + c_2g_1z^{-2}}{1-(2-a_1)z^{-1} + (1+c_2g_1 + a_2c_2 - a_1)z^{-2}} \cdot \frac{(1-z^{-1})^2 + c_4g_2z^{-2}}{1-(2-a_3)z^{-1} + (1+c_4g_2 + a_4c_4 - a_3)z^{-2}}$$

After selecting the optimal NTF in both stages according to the to the zero-optimization theory and the signal transmission requirement, the specific weight factors of CRFF SMSAH structure are calculated and shown below, as well as the NTF

Table 3- 3 The weight factors of SMASH structure with CRFF

	a_1	a_2	a_3	a_4	c_1	c_2	c_3	c_4	Total order
SMASH	0.5659	-0.3622	0.8003	-0.5122	0.8156	1.5625	0.5767	1.5625	4
CRFF	b_1	b_2	b_3	b_4/G_in	b_5	b_6	g_1	g_2	OSR

	-0.6711	1.2743	1.0000	-0.4745	0.9011	1.0000	1.2800	1.2800	50

$$NTF_{smash\_CRFF}(z) = \frac{1 - 0.9467z + z^2}{-0.2743 - 0.3435z + z^2} \cdot \frac{1 - 0.9467z + z^2}{0.0989 - 0.5201z + z^2}$$

3.2.3 MASH structure and analysis

In this section a classic MASH structure with CRFF is introduced.

For SMASH structures, both the feedforward structures such as CIFF and CRFF and the feedback structures such as CIFB and CRFB can do the modulation work at each stage. But for MASH structures, feedback structures are quite rare.

As we discussed in Chapter 2, the principle of reducing quantization noise in the MASH structure is to eliminate quantization noise through digital filters. However, due to the impossibility of achieving a perfect match between the analog circuit part (the noise shaping unit such as NTF and STF) and the digital circuit part (such as the digital filter), it is not realistic to completely eliminate the quantization noise. Therefore, the noise leakage due to the mismatch is a very challenging issue that affects the performance of MASH structures.

For a MASH structure modulator, a large SQNR requires more precise elimination of quantization noise. A high specified SQNR must be achieved through a high-gain op amp with fast settling time, which has the ability to reduce the unfiltered leakage to a sufficiently low level [29].

Based on the above discussion, if a DSM modulator needs to have a fast settling time, the amplitude of the output from its internal integrator should be small. Therefore, the low-distortion modulator structure, such as CRFF and other feedforward structures, are more suitable choices for designing MASH DSM structures.

Figure 3-6 shows the topology of a MASH structure with CRFF in each stage.

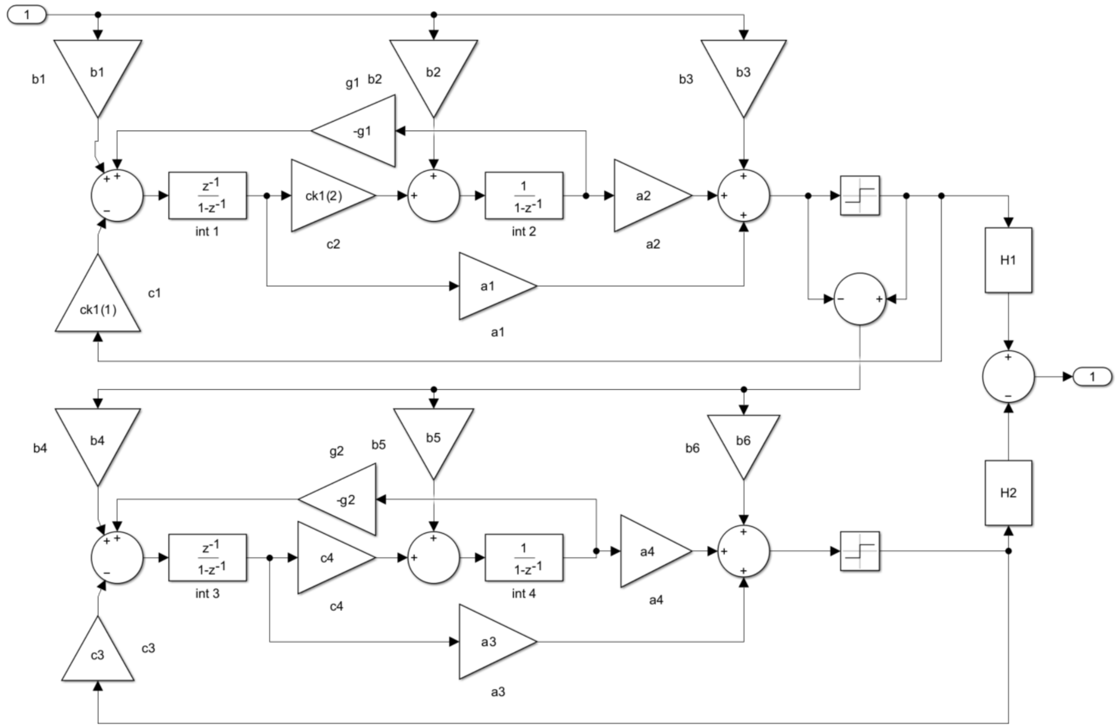

Figure 3- 6 A MASH structure with CRFF

Like the SMASH DSM, each stage of the MASH is a second order SDSM. The quantization noise of the first stage E_1 is fed into the second stage as the input. And the 2nd stage also does the noise shaping work generating the internal quantization noise E_2, smaller than E_1. Then the 1st stage output, including E_1 and the 2nd stage output, including E_2 are sent to the digital filters H_1 and H_2, respectively, to cancel the quantization noise.

Similar to the CRFF SMASH, according to the structure shown in Figure 3-6, the loop filter and NTF of each stage is derived as

$$LF_1 = \frac{(a_2c_2 - a_1)z^{-2} + a_1z^{-1}}{(1 - z^{-1})^2 + c_2g_1z^{-2}} \qquad LF_2 = \frac{(a_4c_4 - a_3)z^{-2} + a_3z^{-1}}{(1 - z^{-1})^2 + c_4g_2z^{-2}}$$

$$NTF_1 = \frac{1}{1 + LF_1} = \frac{(1 - z^{-1})^2 + c_2g_1z^{-2}}{1 - (2 - a_1)z^{-1} + (1 + c_2g_1 + a_2c_2 - a_1)z^{-2}}$$

$$NTF_2 = \frac{1}{1 + LF_2} = \frac{(1 - z^{-1})^2 + c_4g_2z^{-2}}{1 - (2 - a_3)z^{-1} + (1 + c_4g_2 + a_4c_4 - a_3)z^{-2}}$$

And the overall output is given by

$$V = STF_1 \cdot U \cdot H_1 + (NTF_1 \cdot E_1 \cdot H_1 - STF_2 \cdot E_1 \cdot H_2) - NTF_2 \cdot E_2 \cdot H_2$$

to satisfy the logic of noise cancelation, removing E_1, the function below should be satisfied as

$$NTF_1 \cdot H_1 = STF_2 \cdot H_2$$

thus, the digital filter, H_1 and H_2, is given by

$$H_1 = STF_2 = 1, \quad H_2 = NTF_1 = \frac{(1 - z^{-1})^2 + c_2 g_1 z^{-2}}{1 - (2 - a_1)z^{-1} + (1 + c_2 g_1 + a_2 c_2 - a_1)z^{-2}}$$

and considering the noise leakage from the quantization noise of the first stage E_1, the overall output and NTF of the CRFF MASH is derived as

$$V = STF_1 \cdot U - NTF_1 \cdot NTF_2 \cdot E_2 + noise\_leakage$$

$$NTF_{overall} = NTF_2 \cdot H_2 = NTF_2 \cdot NTF_1$$

After selecting the optimal NTF in both stages according to the to the zero-optimization theory and the signal transmission requirement, the specific weight factors of CRFF MSAH structure are calculated as the same with the CRFF SMASH before

$$NTF_{\text{mash\_CRFF}}(z) = \frac{1 - 0.9467z + z^2}{-0.2743 - 0.3435z + z^2} \cdot \frac{1 - 0.9467z + z^2}{0.0989 - 0.5201z + z^2}$$

However, due to the different processing logic for reducing quantization noise, SMASH for suppressing noise while MASH for cancelling it, the same form of NTF processes noise from both stages $E_1 + E_2$ in SMASH, but in MASH it only processes the noise only from the second stage E_2 while sustaining a certain amount of noise leakage from E_1.

3.3 Proposed sturdy multi-stage delta-sigma modulator

In this thesis, based on the multi-stage DSM and taking a lot of influence factors into consideration, a bandpass delta sigma modulator for the RoF system is proposed.

Figure 3-7 illustrates the topology of the proposed SMASH structure. Unlike the existing SMASH structures, the proposed new SMASH structure has some differences from the classical structures in terms of the signal and noise transmission between 2 stages and the optimization choices of the structure.

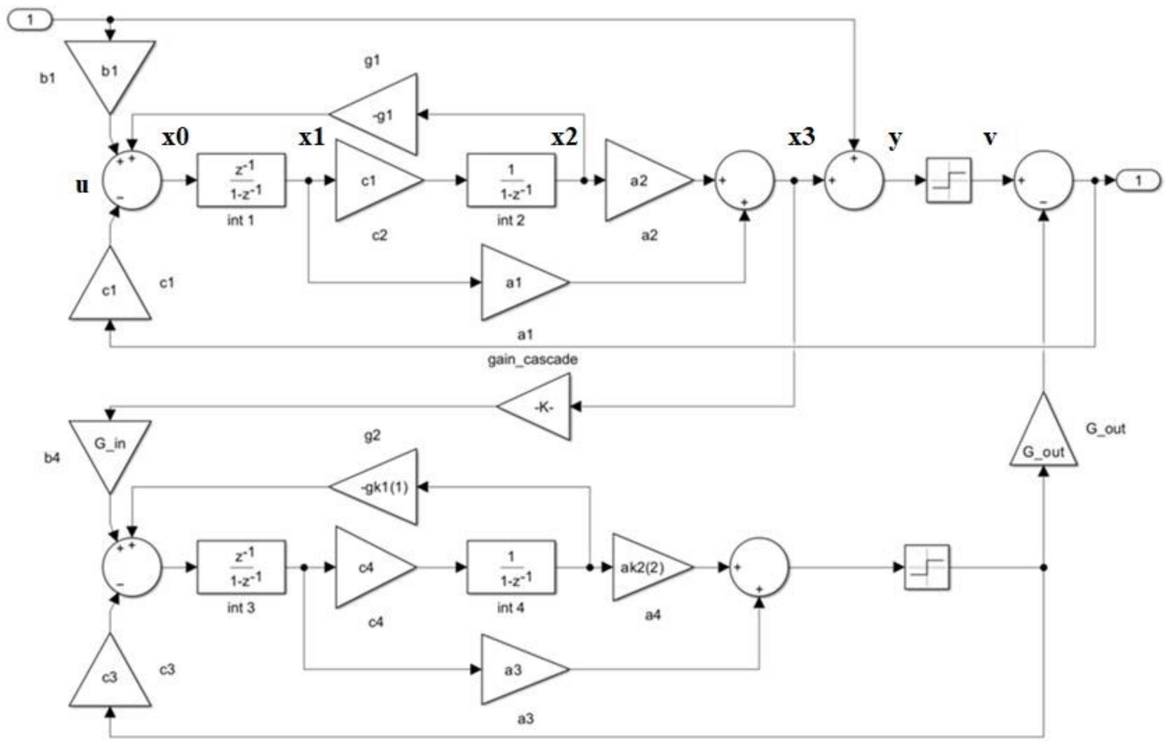

Figure 3- 7 The structure of the proposed SMASH

First of all, similar to the SMASH and MASH structures mentioned above, due to the significant advantages in low-distortion, low latency, larger input dynamic range, and low design complexity, a 2nd order CRFF structure is still chosen to be the delta sigma modulator at the first stage in the proposed structure. And since a path is set from input directly to the quantizer, the signal transfer function of the first stage, $STF_1 = 1$.

The type of topology, whose $STF_1 = 1$, is also called unity signal transfer function (USTF), which is often reported and used to design multi-stage DSMs [48]. The simplest USTF architecture would be the quantizer itself, and the 2nd CIFF structure we talked about in the previous section is the common 2nd order structure with simplest structure.

Then, in contrast to the existing SMASH or MASH structure, the proposed structure doesn't transmit the 1st stage's quantization noise between the two stages. According to Figure 3-7, another adder is set before the quantizer to receive the original signal from the direct path, while the previous one only receives the partial quantized noise from the feedforward path of the loop filter. Because of the separation, the signal at the point between the 2 adders, x_3 shown on Figure 3-7, can be exported.

In the traditional structure, the quantization noise of the 1st stage E_1 is obtained by subtraction operation. However, there is always a delay in the quantization process, so it is impossible to perform the subtraction without any delay. Considering this, the proposed SMASH obtains E_1 without subtraction, avoiding the consequent delay, which allows the entire system to have a faster response and lower complexity.

The signal before quantizer is given by

$$\mathrm{Y(z)} = \mathrm{U(z)} + X_3(z)$$

and the output of the 1st stage is shown as

$$V(z) = STF_1(z) \cdot U(z) + NTF_1(z) \cdot E_1(z)$$

where $STF_1(z) = 1$. Because the CRFF is a low-distortion structure, the output amplitude of integrators could be small, which could be considered that $y[n] - \mathrm{u[n]} \approx \mathrm{e}[n]$ in time domain. Based on this, the signal at the x_3 point can be derived as

$$X_3(z) = NTF_1'(z)E_1(z)$$

Besides, from the figure, the output also given by

$$\mathrm{V(z)} = \mathrm{Y(z)} + E_1(z) = \mathrm{U(z)} + (NTF_1'(z) + 1)E_1(z)$$

It is clearly to obtain the expression of $NTF_1'(z)$ and the $X_3(z)$ as shown below:

$$NTF_1'(z) = NTF_1(z) - 1$$

$$X_3(z) = (NTF_1(z) - 1)E_1(z)$$

Therefore, $X_3(z)$ is considered as the shaped quantization noise, which can be the input of the second stage fed into the loop filter. However, such an operation means that the signal $X_3(z)$ is not the original quantization noise, but rather the shaped noise, which tends to be a litter larger than $E_1(z)$ in the whole frequency spectrum. As a result, the modulator in the second stage must be capable of handling larger input signals with low distortion to avoid generating harmonics of the input signal, such as the feedforward structure mentioned before. Considering all the conditions above, the low distortion structure, CRFF, is chosen as the modulator of the second stage to reduce the input swing of the integrators.

At this point, we can summarize why the proposed structure chooses CRFF at both stages. The first discussion is why the cascade resonator (CR) structure is chosen instead of the cascade integrator (CI) structure. Because the CR structure contains an integrator without delay, with a transfer function of $\frac{1}{1-z^{-1}}$, the advantage is that the zeros of NTF will be exactly distributed on the unit circle. In contrast, the CI structure with all delayed integrators will cause the zeros to be approximately on the unit circle (actually located outside the unit circle). It is concluded that the CR structure is inherently more stable than the CI structure. Then the discussion is the reason to choose feedforward (FF) rather than feedback (FB) structure in each stage. As mentioned in the previous subchapter, in the FF structure, the integrators of the loop filter only deal with the shaped quantization noise without input signal components, which leads to the output of the loop filter being independent of the input signal of the modulator. In this way, increasing the amplitude of the input signal will not cause the integrator to overload, thereby enhancing the dynamic range of the modulator. At the same time, due to the small output amplitude of the integrator, the requirements for the op amp are reduced. Taking the above discussion into consideration, the CRFF is chosen as the base structure of the proposed SMASH DSM.

Additionally, because the $X_3(z)$ is the shaped noise, becoming larger than $E_1(z)$ due to the out-of-band gain, the signal $X_3(z)$ fed into the second stage should be scaled to ensure that the second stage does not overload.

Even so, due to the first stage being a low-distortion structure, the output of the last integrator is still controlled within a very small range, and the signal fed into the second stage does not contain the original signal. Therefore, the second stage, also being a low-distortion structure, still has an excellent input signal range for further processing of quantization noise. Thus, in the new proposed structure, the path for the input signal to directly enter the quantizer and the second integrator has been removed, allowing the input signal of the second stage to be reshaped again. This is equivalent to performing a 4$^{\text{th}}$ order noise shaping on the quantization noise of the 1$^{\text{st}}$ stage $E_1(z)$, which not only better suppresses out-of-band noise but also further reduces the use of amplifiers, greatly simplifying the complexity of the structure and reducing power consumption.

Based on the proposed SMASH structure shown in Figure 3-7, and considering the common settings mentioned above, the loop filter of each stage is derived as

$$LF_1 = \frac{(a_2c_2 - a_1)z^{-2} + a_1z^{-1}}{(1 - z^{-1})^2 + c_2g_1z^{-2}}$$

$$LF_2 = \frac{(a_4c_4 - a_3)z^{-2} + a_3z^{-1}}{(1 - z^{-1})^2 + c_4g_2z^{-2}}$$

From the equation of the loop filter, the NTF of each stage is given by

$$NTF_1 = \frac{1}{1 + LF_1} = \frac{(1 - z^{-1})^2 + c_2g_1z^{-2}}{1 - (2 - a_1)z^{-1} + (1 + c_2g_1 + a_2c_2 - a_1)z^{-2}}$$

$$NTF_2 = \frac{1}{1 + LF_2} = \frac{(1 - z^{-1})^2 + c_4g_2z^{-2}}{1 - (2 - a_3)z^{-1} + (1 + c_4g_2 + a_4c_4 - a_3)z^{-2}}$$

Contrast to the traditional SMASH structure, because the signal fed into the second stage is $X_3(z) = (NTF_1(z) - 1)E_1(z)$, not $E_1(z)$, so the total output is given by

$$V = STF_1 \cdot U + NTF_1 \cdot E_1 - [STF_2 \cdot (NTF_1 - 1) \cdot E_1 + NTF_2 \cdot E_2] \cdot NTF_1$$

Since $STF_1 = 1$, and $STF_2 = 1 - NTF_2 \neq 1$,

$$V_{proposed\_SMASH} = U + NTF_1 \cdot [STF_2 \cdot (NTF_1 - 1)] \cdot E_1 + NTF_1 \cdot NTF_2 \cdot E_2$$

Here, compared to the traditional SMASH discussed before, whose total output is given as

$$V_{traditional\_SMASH} = STF_1 \cdot U - NTF_1 \cdot NTF_2 \cdot E_1 - NTF_1 \cdot NTF_2 \cdot E_2$$

It is found that the proposed SMASH structure has a higher order noise-shaping to E_1. Because in the multi-stage DSMs, the quantization noise of the first stage E_1 significantly influences the system's performance, it is reasonable that the proposed SMASH DSM has a better noise shaping ability.

Furthermore, if scaling the amplitude of the 2nd stage's input to the same level of total input signal, quantization noise in the two stages can be considered as the same level because they are additional noise; that is considered $E_1 = E_2 = E$. In this way, the output and the overall NTF of the proposed one is given by

$$V_{proposed\_SMASH} = STF_1 \cdot U + NTF_1 \cdot [STF_2 \cdot (NTF_1 - 1) + NTF_2] \cdot E$$
$$NTF_{proposed\_SMASH} = NTF_1 \cdot [STF_2 \cdot (NTF_1 - 1) + NTF_2]$$

If substitute the loop filters' equation, LF_1 and LF_2, the NTF is expressed by

$$NTF_{proposed\_SMASH} = \frac{1 + LF_1 - LF_1 \cdot LF_2}{(1 + LF_1)(1 + LF_1)}$$

It is obvious that when the input of the 2 stages in the same level, because the loop filters are of 2nd order structure, the order of NTF of this structure is at least four, which leads the better performance.

The calculated weight factors and the NTFs in each stage of the proposed SMASH structure with CRFF are shown below, which are optimized according to the zero-optimizing technique and the specific signal bandwidth requirements.

Table 3- 4 The weight factors of proposed SMASH structure with CRFF

	a_1	a_2	a_3	a_4	c_1	c_2	c_3	c_4	Total order
SMASH CRFF	0.5659	-0.3622	0.8003	-0.5122	0.8156	1.5625	0.5767	1.5625	4
	b_1	b_3	b_4/G_in	G_out	$gain_{cascade}$		g_1	g_2	OSR
	0.8156	1.	2.	0.5	-0.5		1.28	1.28	50

$$NTF_{proposed\_SMASH} = \frac{1 - 6.8682z^{-1} + 12.1516z^{-2} - 6.2770z^{-3} + 3.7929z^{-4}}{1 - 2.6336z^{-1} + 4.9880z^{-2} - 4.2481z^{-3} + 2.6143z^{-4}}$$

Chapter 4 Simulation results and discussions

This chapter demonstrates the simulation results and comparison of different structures in electric domain and fiber transmission. The simulation work is mainly proceeded in MATLAB, including Simulink, and the VPI Photonics Transmission System (VPI).

4.1 Simulation system design

The overall simulation process and schematic diagram are shown in Figure 4-1

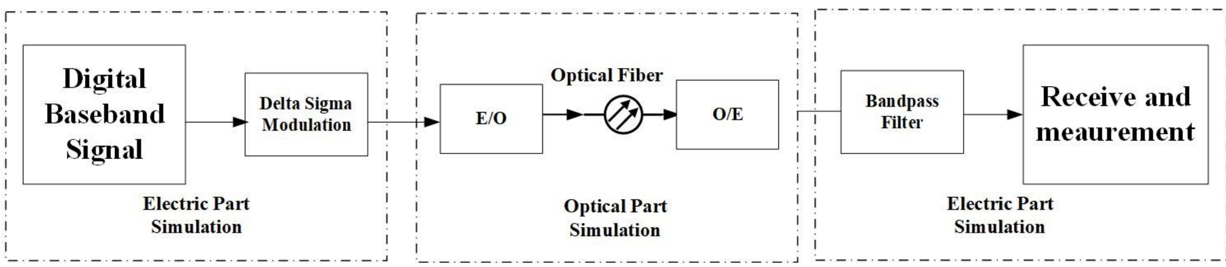

Figure 4- 1 Simulation process setup

From the beginning, the digital baseband signal is generated on MATLAB. To meet the 5G NR standard, the OFDM signal is adopted at the baseband with the bandwidth of 100 MHz and the subcarrier spacing of 30 kHz. Before the OFDM modulation, the bitstreams are first mapped to a 64-QAM signal. Then, they are modulated to subcarriers with certain bits of cyclic prefix (CP) to generate the baseband OFDM signal, showing in Figure 4-1 as a digital baseband signal.

Next, the OFDM signal is up-converted to radio frequency as shown in Figure 3-1. RF sinusoid signal is adopted as carrier with the central frequency 2.5 GHz, and the I/Q modulation is applied when two sinusoid signals are set quadrature. Having completed the up-conversion, we obtain the RF OFDM signal at 2.5 GHz with a 100-MHz bandwidth. Up to this point, the above work is implemented on MATLAB.

After that, it is the delta sigma modulation operation to the OFDM signal. Since the input is an RF signal, in the simulation, all the delta sigma modulators are bandpass structures. The DSM transfers the analog OFDM signal to the digitized signal at a sampling rate of 10 Gbps. Considering the bandwidth of the RF OFDM signal is 100 MHz, the oversampling rate of the DSM is 50. The DSM process is implemented on Simulink of MATLAB.

For the fiber transmission system, VPI undertakes the optical part simulation. The digitized RF signal from DSM in MATLAB is transferred to VPI by co-simulation function. An IM-DD optical system is set up on VPI, including the optical modulation by lasers, demodulation by photodiodes, and the signal transmission on the fiber link. Completing the whole optical signal transmission, VPI samples and transfers the electric signal that outputs from the photodiode to MATLAB form.

In the end, the received signal is back to MATLAB and implemented down-conversion, signal processing, demodulation, and measurements.

Since the original digital baseband signal is mapped to 64-QAM, the EVM is applied to as a measurement index to evaluate the performance of different structures in the constellation diagram.

4.2 Directly received signal comparison

The directly received signal comparison is for evaluating the performance of DSM structures. In this step, the receiver side receives signal directly from the output of DSM without fiber transmission, which can directly reflect the DSM structures' performances of quantization noise suppression, as the received signal has been implemented down-conversion and demodulation without being attenuated and distorted by channels.

4.2.1 Input dynamic range comparison for DSM structures

In Chapter 3, one single-stage DSM, two SMASH DSMs, one MASH DSM, and the proposed SMASH DSM are introduced. Among them, because the two classic SMASH structures have similar performance, to maintain the consistency with the MASH structure between the two SMASH structures, the CRFF is chosen to do simulation here.

As we discussed earlier, the stability of the DSM is a very important indicator. Large inputs may lead to quantizer overload, resulting in instability of the modulator. Therefore, the input dynamic range (DR) and the maximum stable amplitude (MSA) reflect the stability and robustness of a delta sigma modulator.

Figure 4-2 illustrates the impact of input signal level on the SNR performance of DSMs. The input level of 0 dB represents the input signal peak-to-peak amplitude equals the output range of the modulator. It can be seen that small input levels lead to low SNR, and SNR increases continuously with the rise in input levels until the input reaches the DSMs' output range. When inputs exceed the proper levels, the instability such as overload of quantizers happens. Therefore, the input signal of DSMs needs to be adjusted to a suitable amplitude level to optimize the SNR of the digitized signal.

Figure 4-2 (a) shows the input dynamic range of different DSMs. It can be roughly noticed that at the same SNR level, the proposed SMASH structure has the widest input dynamic range, followed by traditional SMASH and MASH, while SDSM performs the worst in terms of input DR.

For the traditional SMASH and MASH structure, the SMASH is closer to the large input level compared with the MASH, which means the traditional SMASH structure has a better performance on the relevant large input. The cause of this situation may be related to the noise leakage of the first-stage of MASH structure, which makes the MASH structure more sensitive to larger input signals, affecting its stability.

Additionally, it is obvious that for the same input level, the proposed SMASH structure almost has the best performance on SNR. On the contrary, the single-stage DSM performs worst on it.

Figure 4-2 (b) gives the clearer and more detailed information of the delta sigma modulators. It can be seen that at the same SNR, 50 dB, for example, the proposed SMASH structure has the largest relevant input dynamic range, around 6.5 dB. Then the traditional SMASH and MASH have around 5 dB and 4.5 dB input DR at 50 dB SNR level, respectively. The SDSM performs worst, having about 3.6 dB input range.

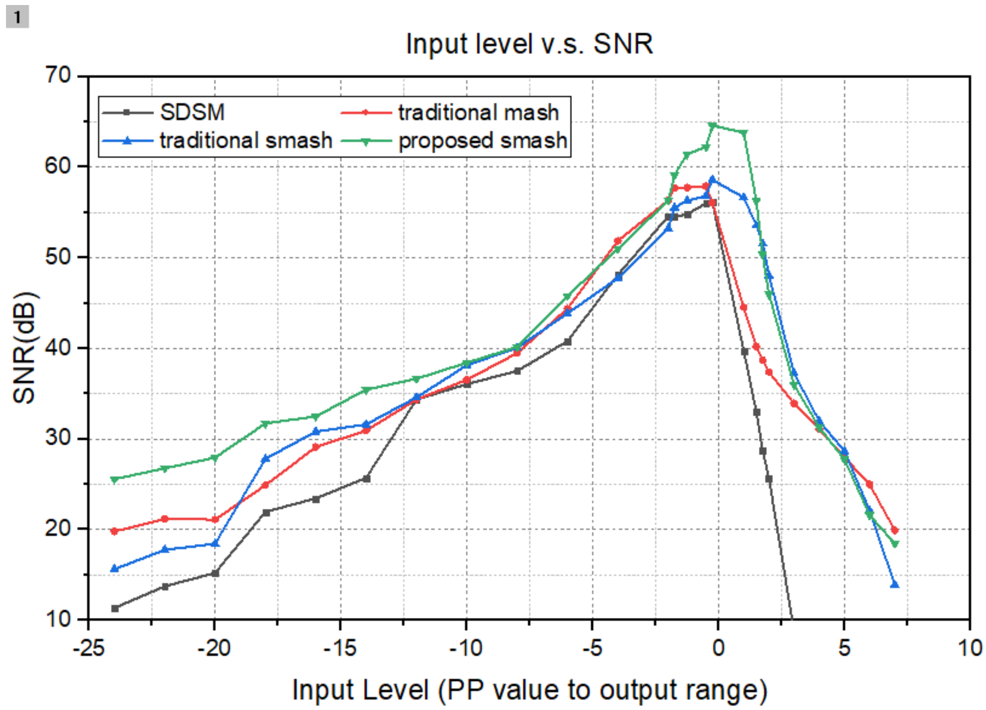

(a)

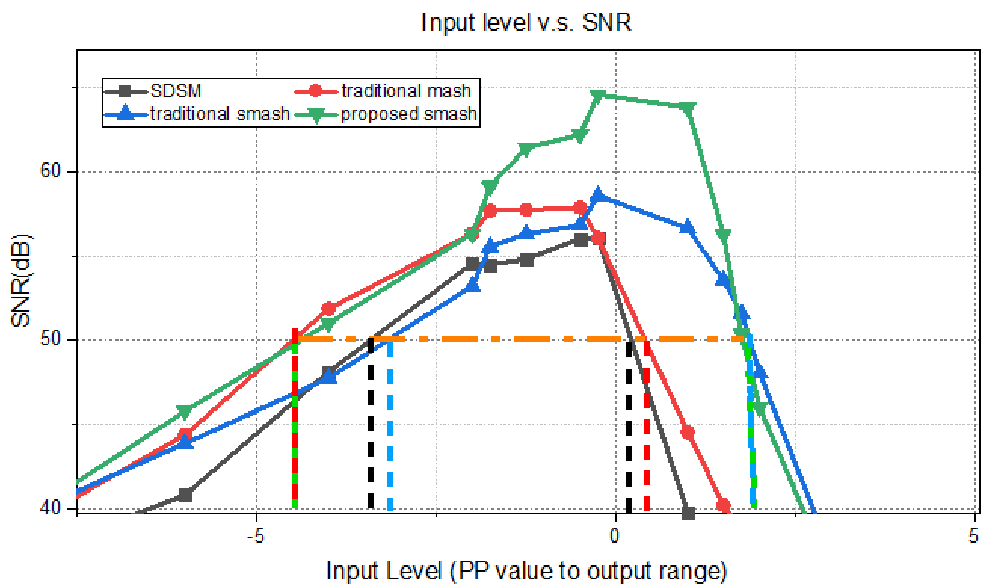

(b)

Figure 4- 2 (a) The impact of input level (normalized peak-to-peak value to output range) on the SNR of DSMs. (b) At the same SNR level, 50 dB, the input range of DSMs shown.

4.2.2 Comparison of DSM modulation process and output results

Because all four structures use 1-bit quantizer to complete the analog to digital conversion, the output waveform of each quantizer is an NRZ signal. Thus, since SDSM only has one quantizer, its output is NRZ form, which is different from the other multi-stage structures due to the multi-stage DSMs having two quantizers at least.

In the following, the detailed modulation process and results of these DSM structures are provided. The input amplitudes of them have been adjusted to the optimal level. Figure 4-3 shows the analog RF signal before DSM.

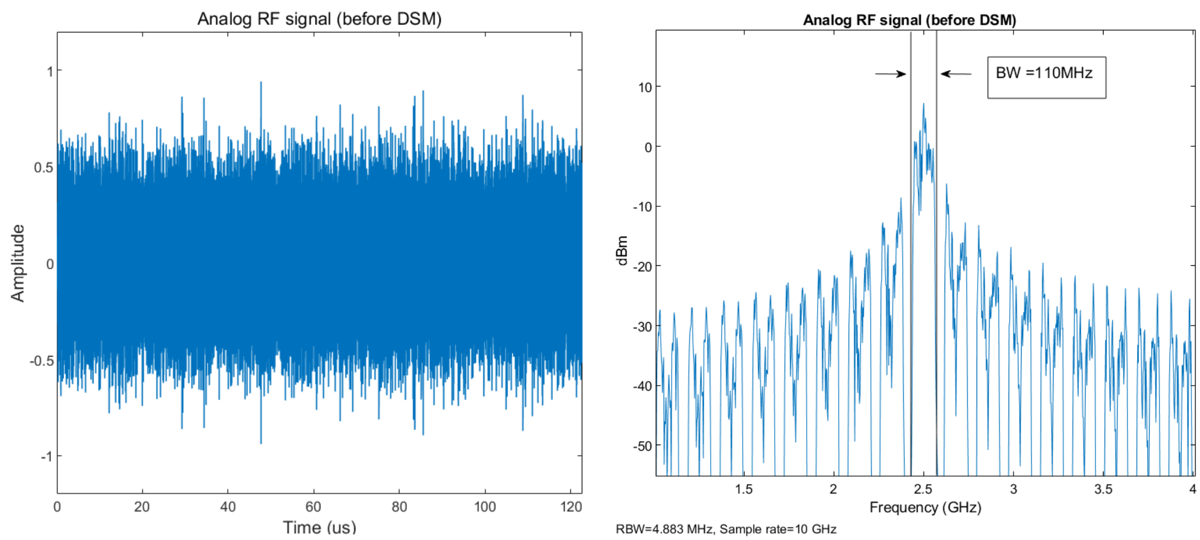

(a) (b)

Figure 4- 3 (a) The analog RF signal before DSM in time domain. (b) The RF signal before DSM in frequency domain.

The modulation of the SDSM structure is shown in Figure 4-4. Figure 4-4 (a) and (b) shows the digitized RF signal after the DSM in the time domain and the frequency domain, respectively. From Figure 4-4 (a), it is seen that the output of SDSM is an NRZ stream form, which is a pulse density modulation (PDM) signal. In terms of DSM, the pulse density of PDM reflects the changes in signal amplitude to some extent. For example, during a certain period, if the average amplitude of the input signal is relatively high, the quantizer of DSM is mostly keeping in a high quantization position. This is reflected in the output of the DSM, where the PDM consistently maintains a high amplitude level, resulting in a relatively sparse pulse density.

In addition, from Figure 4-4 (b), it is clear to see the noise shaping process of a delta sigma modulator. Referring to Figure 4-3 (b), we can find that the quantization noise in the signal band is moved out and amplified out of band, which is where the integrators in the loop filter are functioning in the modulator.

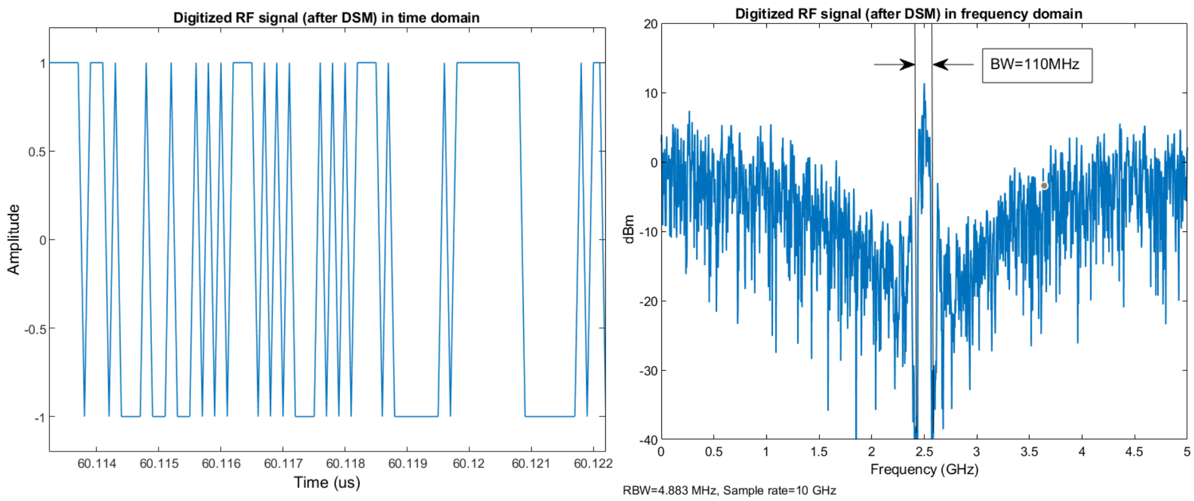

(a) (b)

Figure 4- 4 (a) The digitized RF signal after SDSM in the time domain. (b) The digitized RF signal after SDSM in the frequency domain.

The modulation of the traditional SMASH structure is illustrated in Figure 4-5. Figure 4-5 (a) and (b) show the digitized RF signal after the DSM in the time domain and the frequency domain, respectively. As shown in Figure 4-5 (a), the output of SMASH is in PAM4 form, and the density distribution of the signal spectrum does not directly reflect the amplitude changes of the input signal because, in the SMASH structure, the overall output is also affected by the noise shaping process of the second stage. As discussed in Chapter 2, the quantization noise from the first stage is fed into the second stage, and after being shaped by the second loop, it not only exports from the system's output but also enters the first loop again with the quantization noise from the second stage. Since the overall output is a combination of the outputs from two stages, when appropriate quantizers and cross-stage gain factors are selected, PAM4 is generated as the overall output with a good performance.

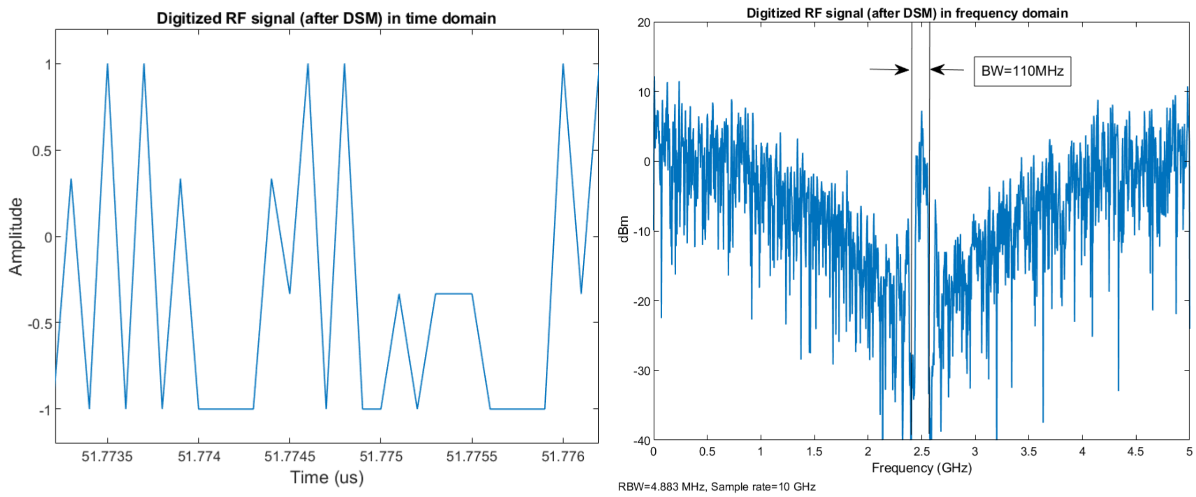

(a) (b)

Figure 4- 5 (a) The digitized RF signal after traditional SMASH DSM in the time domain. (b) The digitized RF signal after traditional SMASH DSM in the frequency domain.

The modulation of the traditional MASH structure is shown in Figure 4-6. Figure 4-6 (a) and (b) show the digitized RF signal after the DSM in the time domain and the frequency domain, respectively. It can be found that the output of MASH is not a pure digital signal because, in order to cancel the quantization noise of each stage, the matched digital filters are set at the output of quantizers, which introduce analog elements to the digital signal. Although CRFF structure is applied in each stage, making $STF_1 = STF_2 = 1$, it only leads the digital filter at the first stage $H_1 = 1$, while the second filter $H_2 = NTF_1$. As known, the NTF_1 implements the noise shaping, where the output is kind of an analog signal. Therefore, although the output signal has a general shape of PAM4, it is not strictly a digital signal; rather, it belongs to a type of analog signal. The details can be seen from Figure 4-6 (a). As for Figure 4-6 (b), in the frequency domain, the output signal from MASH is similar to that from SMASH, quantization noise is shaped out from the signal band.

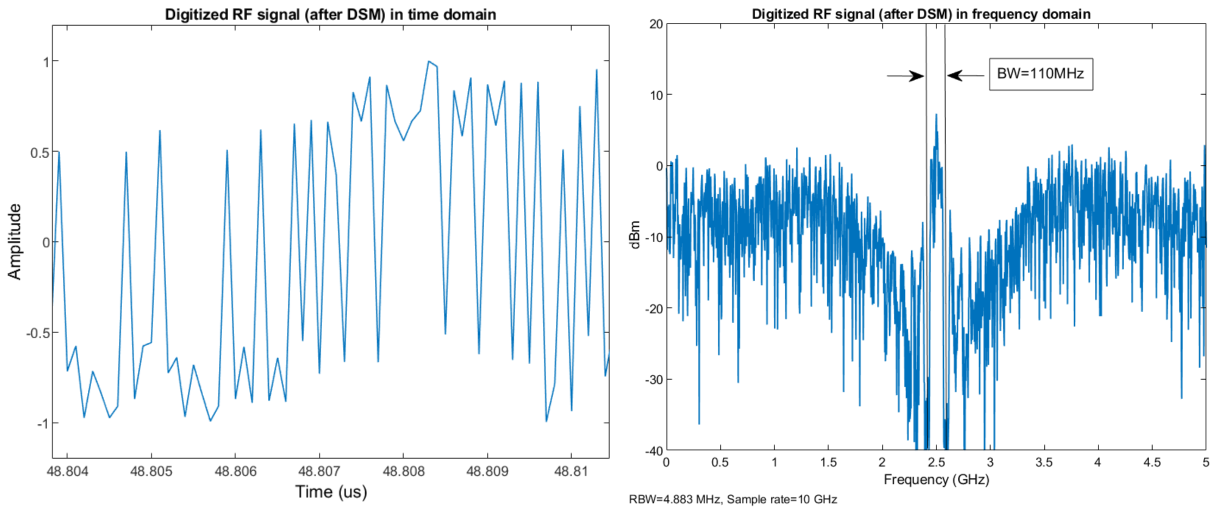

(a) (b)

Figure 4- 6 (a) The digitized RF signal after traditional MASH DSM in the time domain. (b) The digitized RF signal after traditional MASH DSM in the frequency domain.

The modulation of the proposed SMASH structure is illustrated in Figure 4-7. Figure 4-7 (a) and (b) show the digitized RF signal after the DSM in the time domain and the frequency domain, respectively. As shown in Figure 4-7 (a), because the proposed SMASH DSM structure is also of SMASH structure, the output of the modulator is also the PAM4, which is combined with outputs of the quantizers in two stages. Besides, from Figure 4-7 (b), it is roughly seen that the in-band noise is suppressed at a lower level compared to the traditional ones, which means the proposed SMASH structure has a better performance on noise shaping. The detailed comparison about the performance of noise suppression among these DSM structures is demonstrated in the following session.

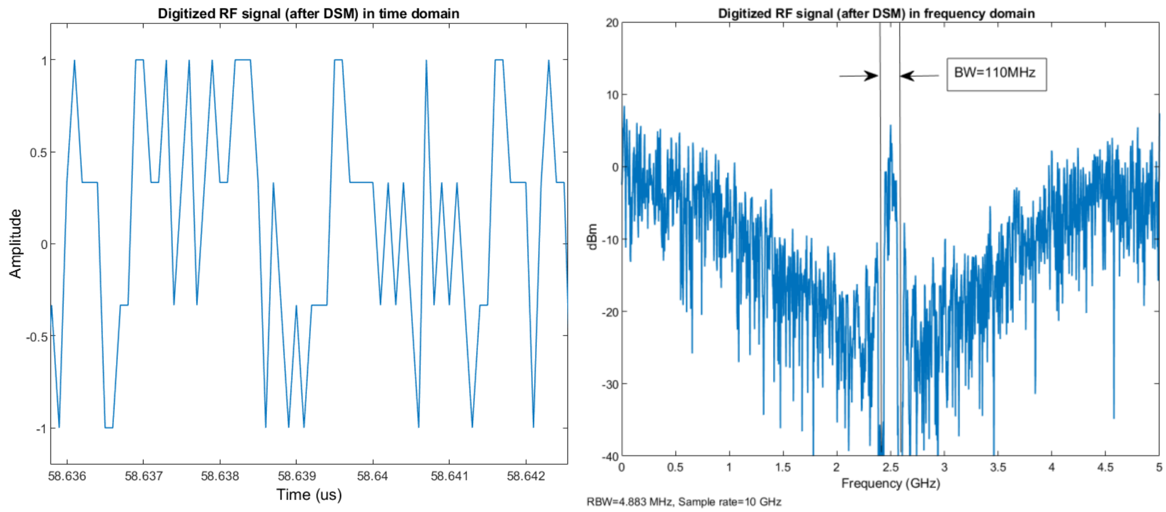

(a) (b)

Figure 4- 7 (a) The digitized RF signal after proposed SMASH DSM in the time domain. (b) The digitized RF signal after proposed SMASH DSM in the frequency domain.

As discussed earlier, for the DSMs, due to their noise shaping function, they effectively modulate the signal to the carrier frequency while modulating the noise outside the signal band. Therefore, the demodulation can be realized by applying a filter that matches the signal. For example, in the case of a bandpass DSM, the NTF is equivalent to a band-stop filter. If a bandpass filter with the same passband as the signal is applied at the receiver side, the out-of-band noise will be filtered out while also the extraction and demodulation of the signal are achieved.

It is known that SNR is the most core index to evaluate a system. And in delta sigma modulation, the filter, being of the same bandwidth with the signal, is applied to complete the demodulation, the SNR is equaled to the directly demodulated SNR measured from the constellation diagram, which means the EVM completely reflects the SNR. The relationship between them is given by

$$\mathrm{SNR(dB)} = 20 \cdot \lg\left(\frac{1}{EVM^2}\right)$$

Figure 4-8 shows the constellation diagram and the EVM of the above DSM structures after demodulation. Based on the results, at the same situation, including the input signal, the carriers, OSR, the sampling frequency, etc., the proposed SMASH DSM structure has the best performance on noise suppression ability, with the EVM equal to -32.56 dB, followed by traditional SMASH (EVM at -29.30 dB) and MASH (EVM at -29.04 dB), while the SDSM at the last position, whose EVM is -28.05 dB. So, that means the proposed SMASH structure has around 3.3 dB improvement over the other two multi-stage structures and around 4.5 dB improvement over the single stage structure on EVM.

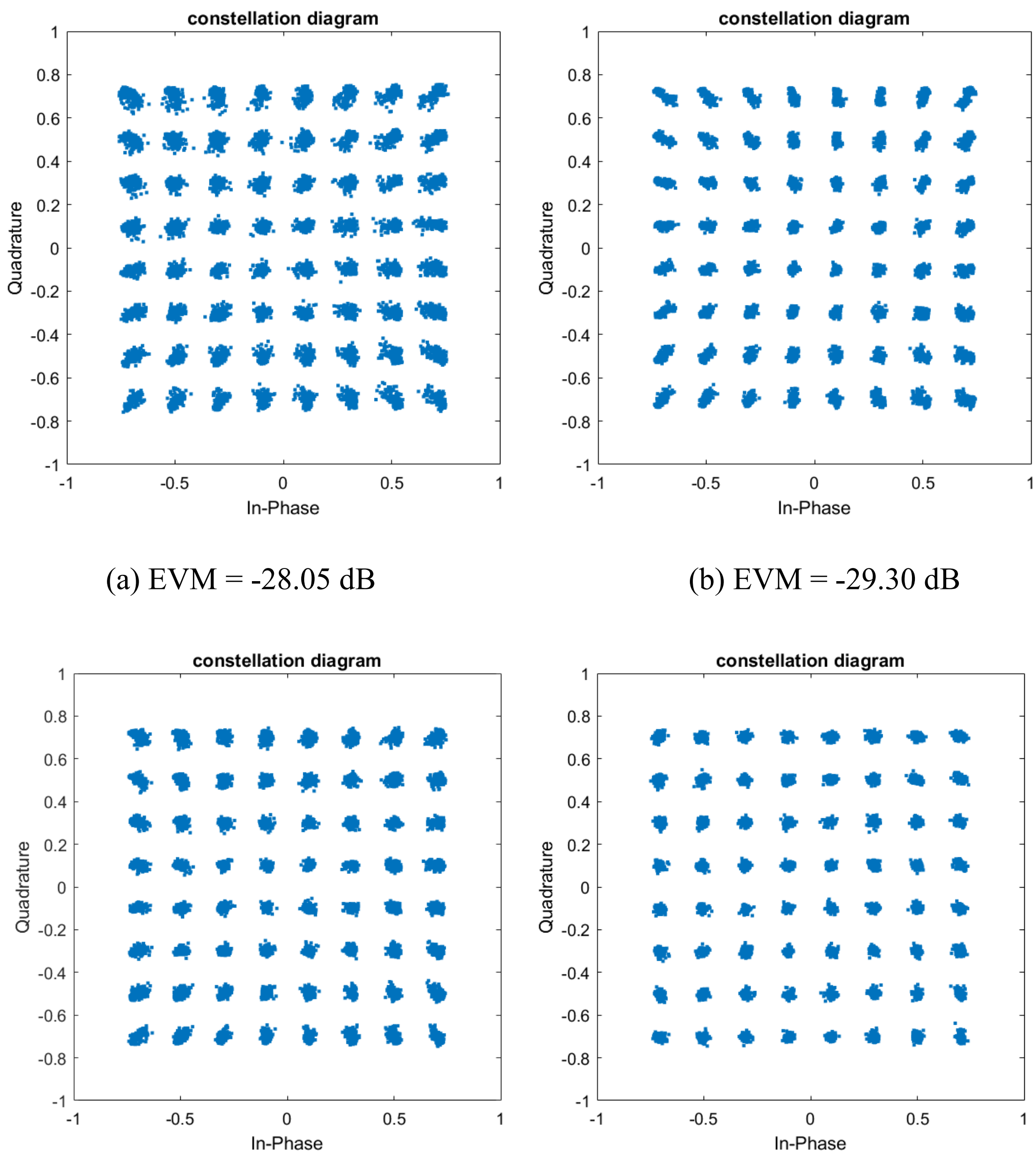

(a) EVM = -28.05 dB

(b) EVM = -29.30 dB

(c) EVM = -29.04 dB

(d) EVM = -32.56 dB

Figure 4- 8 Constellation diagram and EVM of (a) SDSM, (b) traditional SMASH, (c) traditional MASH, (d) proposed SMASH

Figure 4-9 shows the signal spectrum of outputs from different DSM structures. From Figure 4-9 (a), it is clear that the four types of DSM have different abilities to suppress the quantization noise in the signal band. Overall, the multi-stage structure performs better in terms of in-band noise suppression compared with the single-stage structure SDSM, which also means that they often have a better SNR within the signal bandwidth. Figure 4-9 (b) is an enlargement of the black rectangular area in Figure 4-9 (a), showcasing more details on noise suppression within the signal band. It can be seen that the proposed SMASH, represented by the red line, has the best noise suppression ability among these modulators, while SDSM (the blue line) is the worst. SMASH (the yellow line) and MASH (the green line) exhibit similar performances. The above result is also consistent with their performance on EVM.

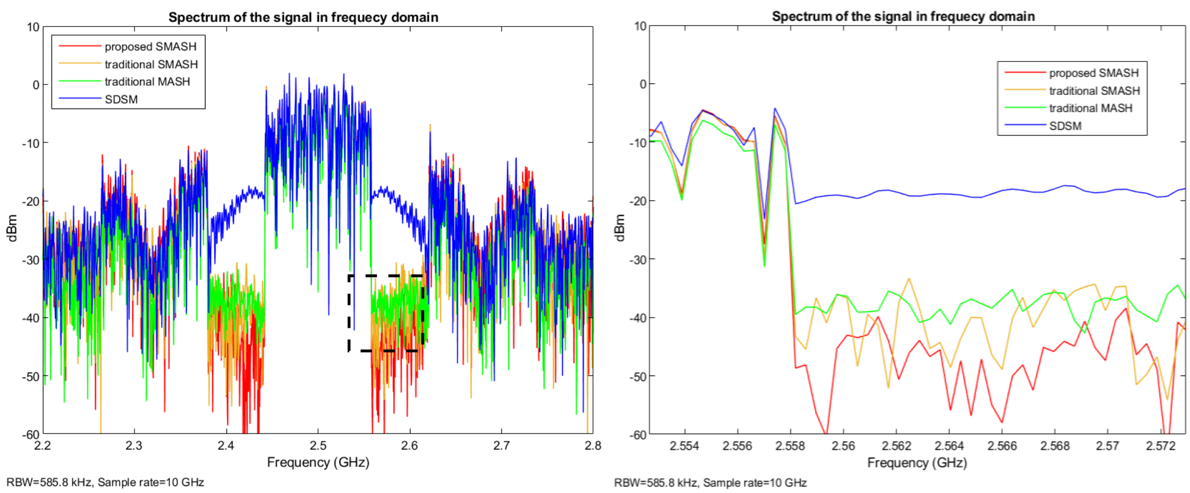

(a) (b)

Figure 4- 9 (a) The signal frequency spectrum of outputs from different DSM structures. (b) Zoon-in of the circle area of (a).

4.3 Simulation with fiber transmission

This section presents the simulation results of these DSM structures for transmission over fiber. The simulation is completed through the co-simulation of MATLAB and VPI. The DSM modulated signals are generated by Simulink, and VPI takes the optical simulation work, including the optical modulation, fiber transmission, and the optical demodulation, as the optical part in the middle of Figure 4-1 shows.

The detailed parameters of the fiber transmission system on VPI are shown from Table 4-1 to Table 4-2. It is an IM-DD system, the direct modulation laser at 1550 nm with the relative intensity noise (RIN) of -130 dB/Hz is adopted, which is an analog laser. The optical fiber is the standard single mode fiber with the attenuation of 0.2 dB/km and group velocity dispersion (GVD) of 17×10^{-6} ps/m^2. At the optical receiver side, a PIN photodiode (PD) is chosen to do the optical demodulation, and before that, an attenuator is applied to control and change the optical power that gets into the PD.

Table 4- 1 The core parameters of laser

	Emission Frequency	Relative Intensity Noise (RIN)	Linewidth
Values	1550 nm	-130 dB/Hz	10^6 Hz
	RIN Measurement Power	Threshold Current	Slope Efficiency
Values	0.05 W	0.02 A	0.3 W/A

Table 4- 2 The core parameters of fiber

	Emission Frequency	Attenuation	Dispersion (GVD)
Values	1550 nm	0.2 dB/km	17×10^{-6} ps/m^2
	Dispersion slope	Nonlinear Index (Kerr effect)	Core Area
Values	0.08×10^3 ps/m^3	$2.6 \times 10^{-20}\ m^3/W$	$80 \times 10^{-12}\ m^2$

4.3.1 Loss and nonlinearity effects of fiber

Considering the characteristics of the output signals from the above DSM structures and their performance of them in directly transmission in electric field, also called electric back to back (EBTB) in previous section, the three multi-stage DSMs, traditional MASH, traditional SMASH and the proposed SMASH, are simulated and compared over the fiber transmission system. Especially, due to being of the same output form, the two SMASH structures are given more attention.

For a fiber transmission system, the fiber loss and the main nonlinearity, such as the Kerr effect and GVD, are the most important factors affecting transmission quality. Considering the above factors, the fiber transmission simulation of these three DSM structures are shown in Table 4-3 and Figure 4-10, where the optical power to fiber is set at around 4 dBm.

Table 4- 3 The received EVM (dB) after fiber in different lengths of 3 multi-stage DSM structures

Fiber length / DSM structures	*2 km*	*4 km*	*6 km*	*8 km*	*10 km*
Traditional MASH	-28.94	-28.53	-28.16	-27.69	-27.18
Traditional SAMSH	-29.22	-28.86	-28.25	-27.47	-26.61
Proposed SMASH	-32.30	-31.67	-30.80	-29.84	-28.87
Fiber length / DSM structures	*12 km*	*14 km*	*16 km*	*18 km*	*20 km*
Traditional MASH	-26.60	-26.01	-25.30	-24.58	-23.93
Traditional SAMSH	-25.72	-24.85	-24.01	-23.22	-22.36
Proposed SMASH	-27.93	-27.04	-26.20	-25.43	-24.71

From Table 4-3, it is seen that after fiber transmission, the proposed SMASH structure still has the best performance on EVM. When the fiber length is 8 km, the EVMs of the 3 structures are -29.84 dB for the proposed SMASH, -27.47 dB for the traditional SMASH, and -27.69 dB for the traditional MASH. So, the proposed SMASH has the 2.37 dB and 2.15 dB improvements compared with the traditional SMASH and MASH, respectively. And on the 20-km fiber link, the proposed SMASH has the 2.35 dB and 0.78 dB improvements, respectively.

The three structures' frequency spectra are illustrated in Figure 4-10, and the EVMs on different fiber lengths are shown in Figure 4-11. Based on Figure 4-10 (a) to (d), it is seen that the proposed SMASH structure has the best noise shaping ability compared with the 2 tradition structures after 8-km and 20-km fiber transmission. After normalizing the received signal, the noise suppression capability within the signal band can be clearly compared from Figure 4-10 (b) and (d). However, according to Figure 4-10 (a) and (c), for the traditional MASH structure, after 8-km and 20-km of fiber, the attenuation is not as much as in the two SMASH structures.

Besides, from the relationship between EVM and fiber length in Figure 4-11, it can also be seen that the SMASH structure is more sensitive to changes in fiber length. It is because the signal modulated by MASH DSM is more like an analog signal, shown in Figure 4-6 (a), which means that in the same time interval, the rate of frequency change of the analog signal is not as dramatic as that of the digital signal, so there are fewer frequency components in the analog signal during that time interval. Also, since the optical power at the receiver side is only 0 dBm, it can be considered that the nonlinearity brought about by the Kerr effect is very small, leading GVD as the main factor in introducing nonlinear distortion. Compared to the MASH structure, whose output signal is similar to an analog signal, the two SMASH structures have more frequency components within a certain time slot, and as a result, they suffer more GVD penalties.

However, as can be seen from Figure 4-11, even though the proposed SMASH is affected more by the nonlinear distortion introduced by GVD, it still exhibits the best performance on EVM after 20 km of fiber transmission. Here, the optical power to fiber is set at 4 dBm.

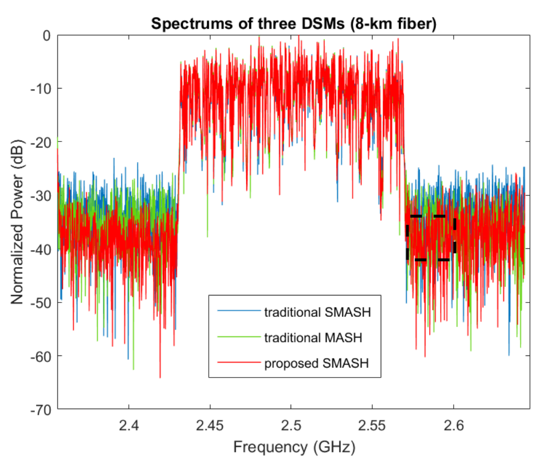

(a)

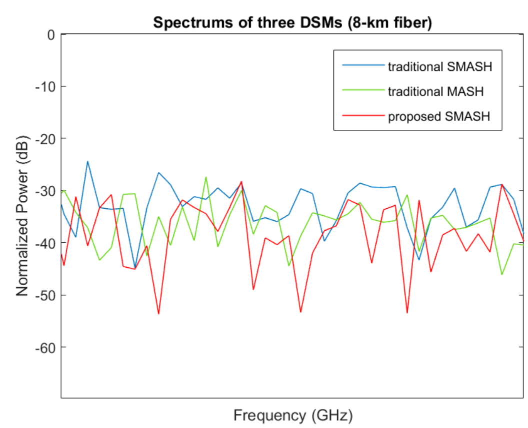

(b)

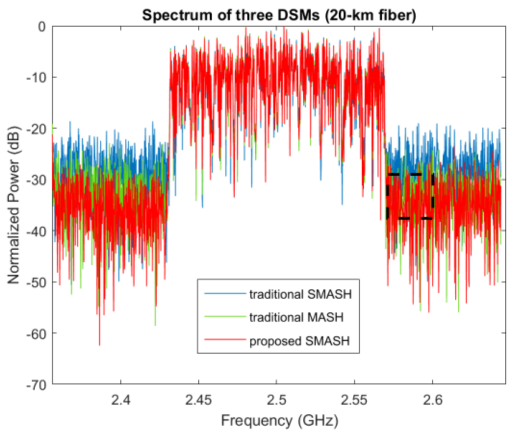

(c)

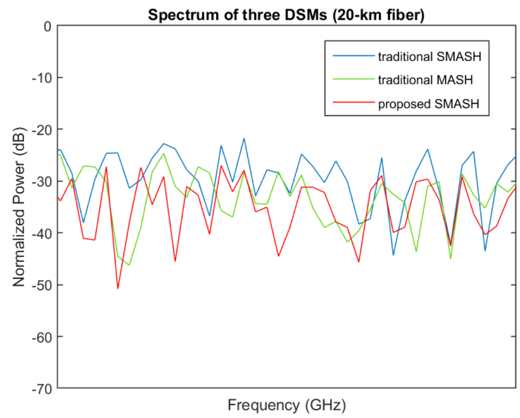

(d)

Figure 4- 10 (a) The spectrum of 3 DSMs after 8-km fiber, (b) The enlarged spectrum at noise suppression band after 8-km fiber, (c) The spectrum of 3 DSMs after 20-km fiber, (d) The enlarged spectrum at noise suppression band after 20-km fiber.

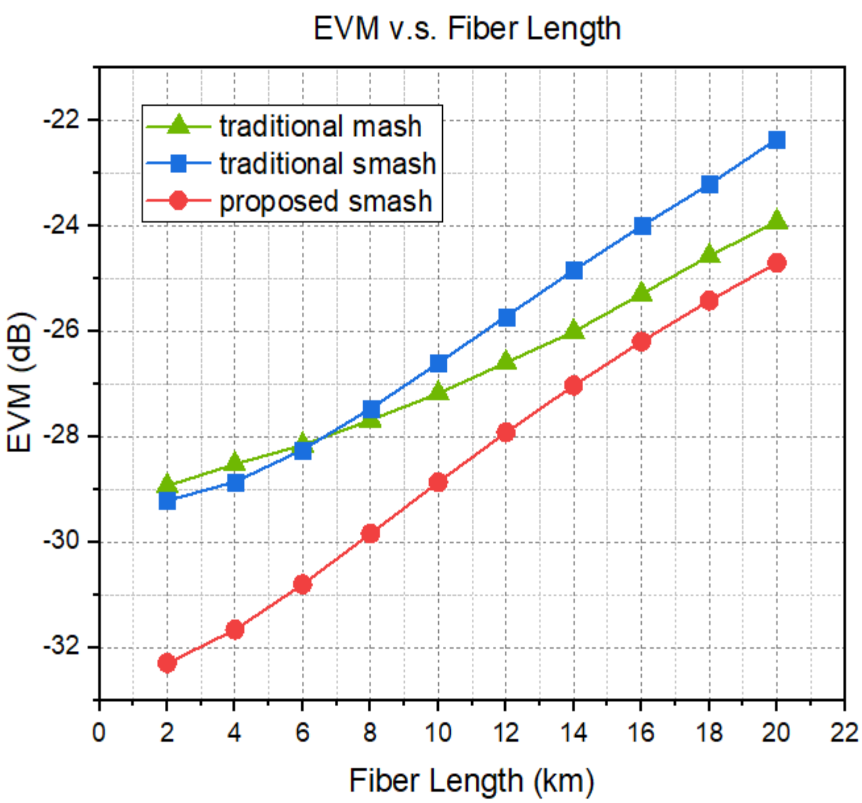

Figure 4- 11 EVM vs. fiber length of 3 structures

4.3.2 Optical power effect

Apart from the fiber loss and the nonlinear distortion, the signal transmission over the fiber is also affected by the optical power. In the fiber transmission system set up on VPI, attenuators are added to control the optical power getting into fiber and received by the photodiode.

Figure 4-12 illustrates the EVM performance of three DSM structures versus the optical power to fiber after 8-km and 20-km fiber transmission. It is clear that when the optical power to fiber is less than -10 dBm, for all the structures, the EVM performances have a significant improvement with the increase in the optical power, which is because the thermal noise effect decreases with the rise of power. According to the requirement about the 64-QAM signal transmission in the standards IEEE 802.11, the EVM should be larger than -21.93 dB to ensure the quality of the system [49]. From Figure 4-12, if the fiber length is equal to or over 20 km, the optical power to fiber is at least -10 dBm to satisfy the requirement.

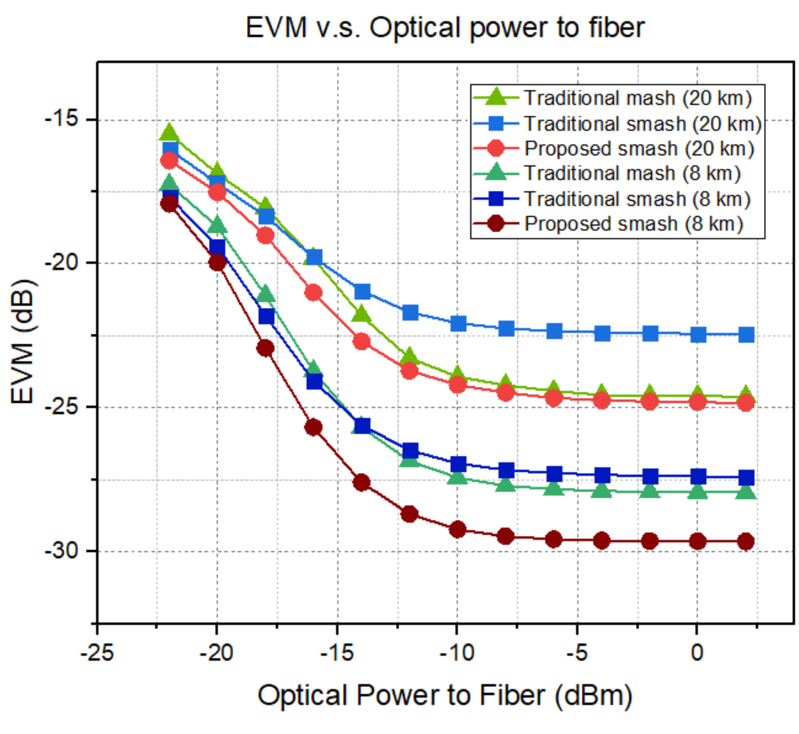

Figure 4- 12 EVM versus the optical power to fiber for 3 DSM structures

Figure 4-13 (a) shows that, after the optical power increased over -8 dBm, the improvements of EVM become very slow and limited, and it can be considered that at this point, the EVM no longer increases a lot with the enlargement of optical power. From Figure 4-13 (b), it can be seen that for the main nonlinear distortions in fiber, the Kerr effect and GVD, if the impact of the Kerr effect is not considered, the curve of EVM versus optical power to fiber is very close to the curve when both the Kerr effect and GVD are considered; however, if the influence of GVD is removed, the relationship between EVM and optical power changes a lot. From Figure 4-13 (c), it can be seen that as the power increases, the EVM after 8-km and 20-km fiber transmission has significantly improved, and the values far exceed that when taking GVD impact into consideration. Moreover, when the optical power is greater than 0 dBm, the curves after 8-km and 20-km transmission overlap. This indicates that GVD dominates among the nonlinear factors in the fiber, and the optical power to fiber more significantly affects fiber loss and the Kerr effect than GVD. Plus, to some extent, increasing the optical power to the fiber can compensate for the fiber's inherent loss.

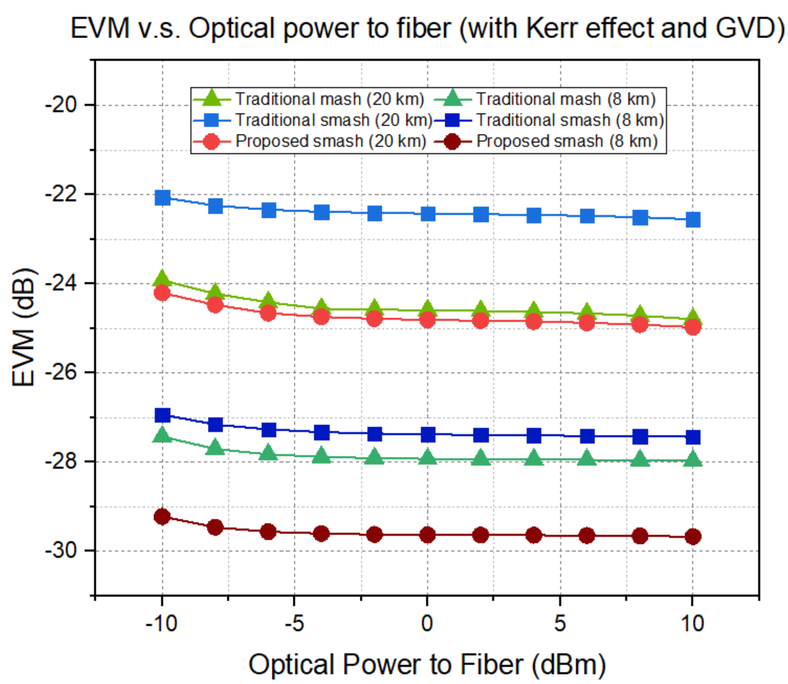

(a)

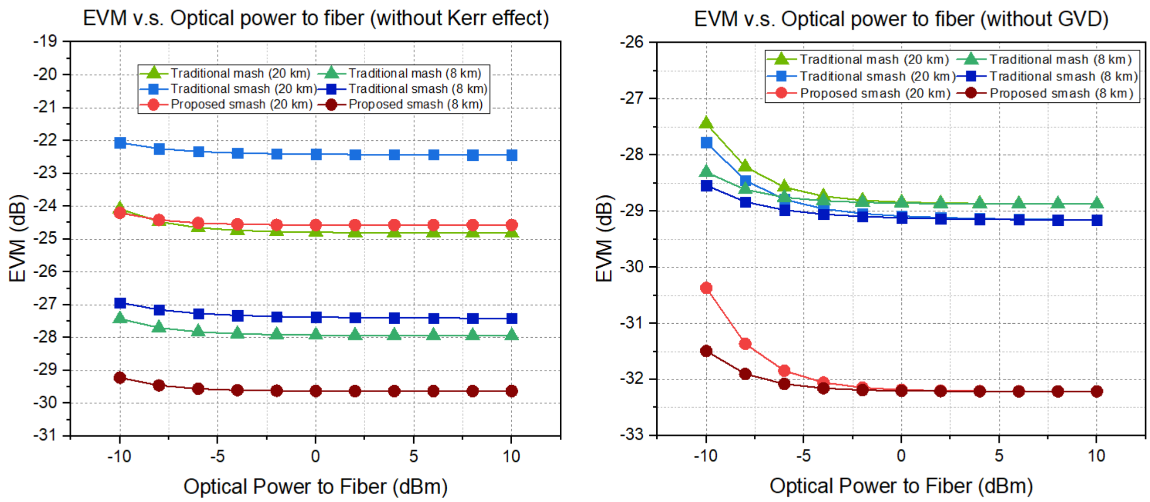

(b) (c)

Figure 4- 13 (a) EVM versus the optical power to fiber for 3 DSM structures (with Kerr effect and GVD), (b) EVM versus the optical power to fiber without Kerr effect, and (c) EVM versus the optical power to fiber without GVD.

4.4 Simulation Summary

In this simulation part, firstly, the structures, relevant input characters, and the directly received results of four types of DSM are illustrated. SDSM is the single-stage structure, while the other three structures, traditional MASH, traditional SMASH, and the proposed SMASH, are the multi-stage structures. Among them, the proposed SMASH is a new designed structure based on the traditional SMASH DSM, having better performance on the input dynamic range and the ability of in-band noise suppression. Besides, due to the poor performance on stability and worse noise shaping compared to the multi-stage DSM, the SDSM is not discussed in the fiber transmission system modulation.

Furthermore, by comparing the transmission performance of the three multi-stage DSMs over fiber, they all suffer from fiber loss and nonlinear distortion such as the Kerr effect and GVD. Although the traditional MASH structure gets the least nonlinear effect introduced by GVD among them because of its analog output, it sacrifices the merit of a digital RoF system, which brings more difficulties and distortions when doing the demodulation. Therefore, the main comparison focuses on the traditional SMASH and the proposed SMASH. Being of the similar stability and noise shaping logic, the proposed SMASH has a better performance on the in-band noise shaping, improving 3.3 dB on the EBTB system and 2.37 dB after the 20-km fiber transmission, respectively. Following, the two multi-stage DSMs are discussed in the experiment parts.

Chapter 5 Experiment results and discussions

5.1 Experiment system setup

Figure 5-1 and Figure 5-2 show the experiment set up. The DSM modulated signal is generated in MATAB and sent to the waveform generator to create the real RF signal. The PAM4 signal (the SMASH DSM output) is sampled at 10.32192 Gbps in the AWG7122B arbitrary waveform generator and then modulated to fiber link by direct laser modulation, where a VCSEL laser (DBL-VI) from PONEX company is used, with the 7 GHz modulation bandwidth at 1550 nm wavelength. After modulated, the optical signal is amplified by a C-band Erbium Doped Fiber Amplifier (EDFA) and filtered by an XTM-50 optical filter. Then the signal gets through 8 km or 20 km single mode fiber with the attenuation of 0.21 dB/km at 1550 nm wavelength, which is standard single mode fiber with total loss around 1.68 dB and 4.2 dB for the 8 km and 20 km fiber, respectively. Then, the signal is received by a photodiode, MITEQ SCMT-100M6G-28-20-M14, whose bandwidth is 6 GHz. After that, a low-noise electric amplifier with the model HMC659LC5 is applied to amplify the small signal, which is sent to the real-time oscilloscope to be detected and analyzed. Besides, an attenuator is set before the PD to control the received optical power.

The optical power from the VCSEL laser is around 0.8 dBm with the drive current at 12 mA. Then, the optical power is amplified by the EDFA with the bias of 81 mA and 120 mA to get the optical power to fiber at 1.98 dBm and 4.13 dBm, which are used for 8-km and 20-km of fiber transmission, respectively.

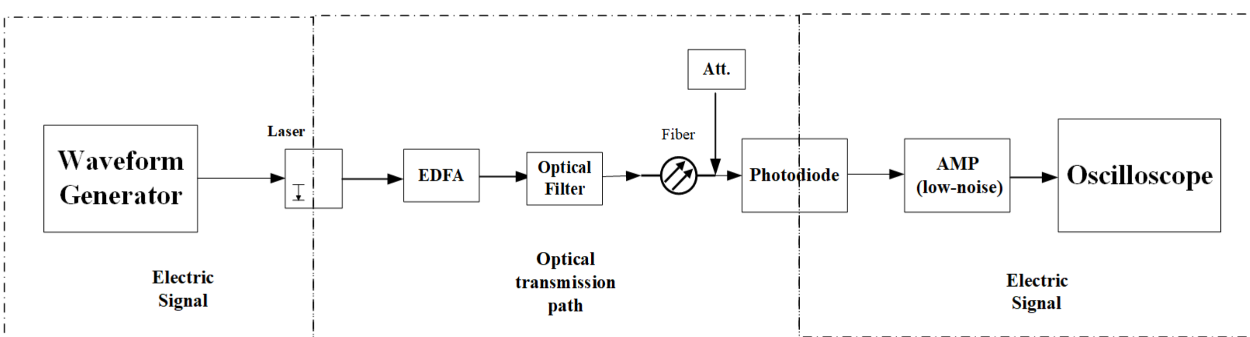

Figure 5- 1 Block diagram of the experiment setup

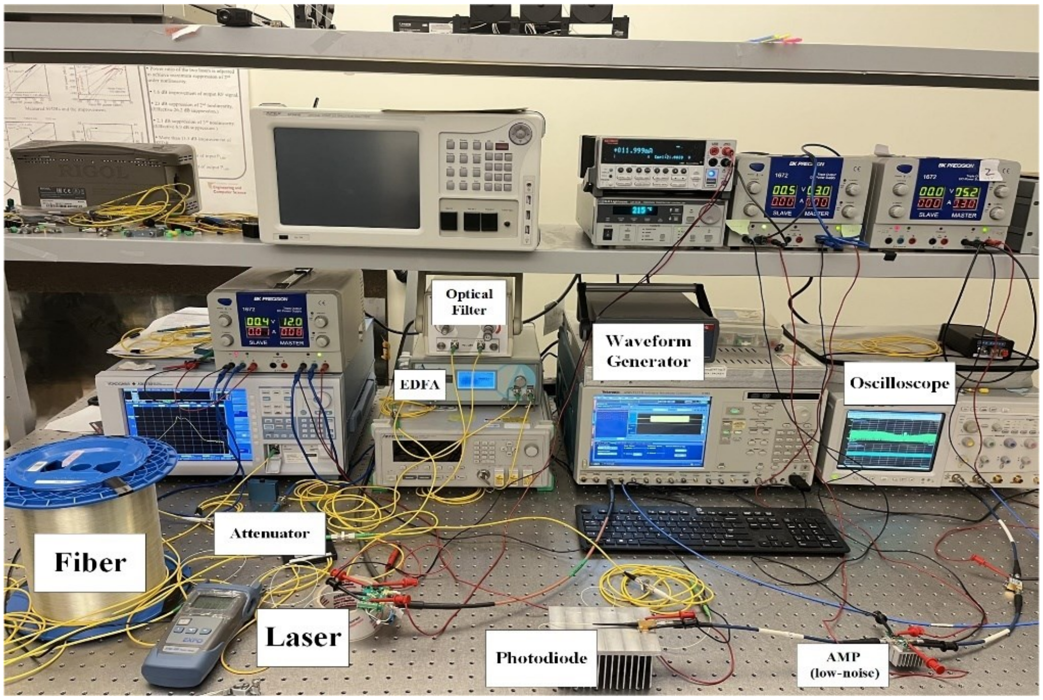

Figure 5- 2 The equipment setup for the experiment

5.2 Directly received performance for two SMASH structures

As mentioned in Chapter 4, considering the signal form and stability, in the experiment part, the two SMASH DSM structures are mainly discussed. Due to the high OSR of DSM, the RF signal has too many digital points for the AWG and the oscilloscope. Separating the whole signal into several frames in the time domain doesn't change the characteristic of the RF signal, which can be recombined after being received by the oscilloscope. In this way, the DSM modulated signal can be transmitted and received over the fiber system with satisfying the equipment limits.

Firstly, to evaluate the DSMs' transmission performance over fiber, it is necessary to test the direct transmission without fiber. Here, the EBTB transmission is implemented, where the signal generated from AWG is directly received by the oscilloscope. Besides, the optical back-to-back (OBTB) link is also tested, which means that after optical modulation by laser, the signal is directly transmitted to the photodiode. The result is shown in Table 5-1. And the direct waveform received (the traditional SMASH structure as the example) in the oscilloscope is shown in Figure 5-3. Besides, Figure 5-4 illustrates the EVM of the two SMASH structures after the OBTB transmission.

According to Table 5-1, it is seen that the EVM of OBTB is worse than EBTB in both structures. The reason includes that the optical modulation and demodulation introduce extra noise, as well as the amplifier after the photodiode also introduces noise.

From Figure 5-3, it is seen the noise shaping process: the in-band noise is removed out from the signal band and amplified in the out-of-band around the carrier central frequency.

Table 5- 1 The measured EVM of EBTB and OBTB of two DSM structures

	EVM of EBTB	EVM of OBTB
Traditional SMASH	-29.30 dB	-22.92 dB
Proposed SMASH	-32.56 dB	-26.65 dB
Improvement	3.26 dB	3.73 dB

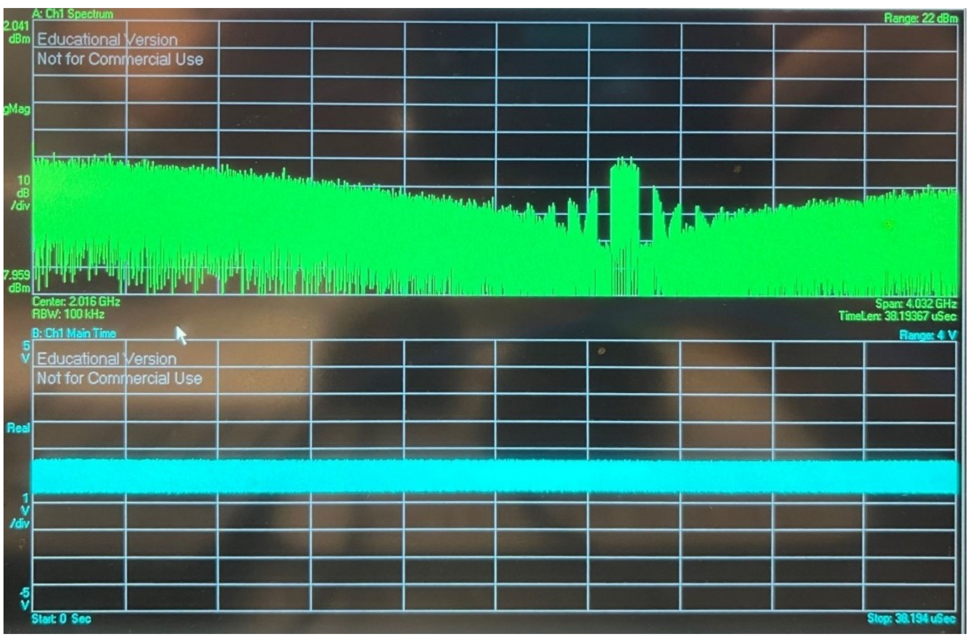

Figure 5- 3 The received signal spectrum of EBTB (from traditional SMASH)

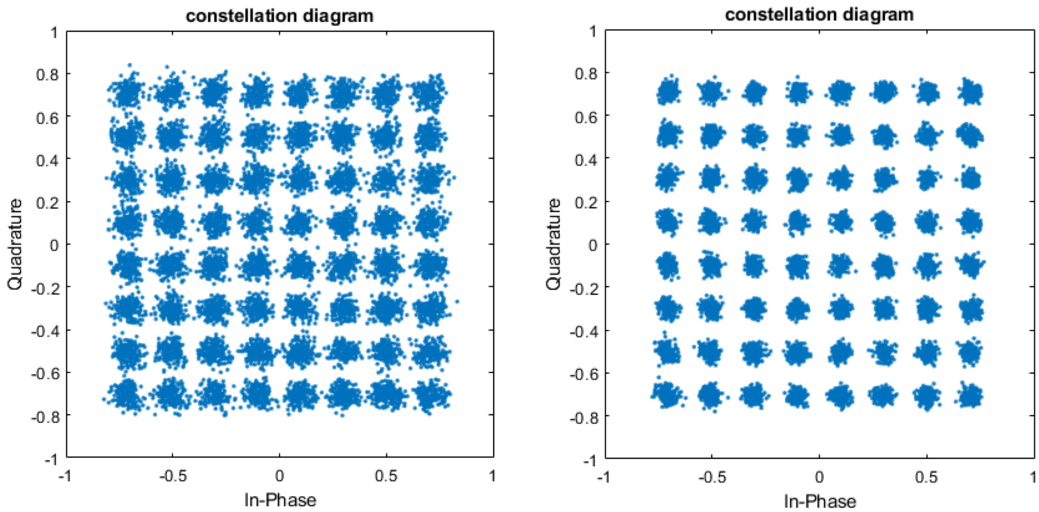

(a) (b)

Figure 5- 4 EVM of the (a) Traditional SMASH (- 22.92 dB) and (b) Proposed SMASH (-26.65 dB) after OBTB transmission.

5.3 Transmission over fiber and demodulation for two SMASH structures

In this section, the transmission performances over fiber of the two SMASH structures are discussed. In the experiment, since there are only two fibers with lengths of 8 km and 20 km, the distances of fiber transmission are set at 8 km and 20 km separately, which are enough to reflect the influence of fiber on the SMASH structures. When the fiber length is 8 km, the optical power into fiber is 1.98 dBm. And when the length is 20 km, the optical power into fiber is 4.13 dBm.

Table 5-2 illustrates the measured EVM of the two structures at the fiber length of 8 km and 20 km. It is proved that the proposed DSM has better EVM performance over fiber, both with 8 km (2.76 dB improved) and 20 km (2.94 dB improved). Based on that, there are reasons to believe that within the 20-km distance of the fiber link, the proposed SMASH always performs better than the traditional DSM.

Besides, the measured EVMs of the two DSMs are also shown in Figure 5-5 and Figure 5-6. It is clear to see from Figure 5-5 (a) to (d) that the EVM comparison of the two modulators at the fiber distance of 8 km and 20 km, respectively. Figure 5-6 and Figure 5.6 show that the performances of the two SMASH structures are both dependent on fiber length, where fiber loss and nonlinearity, mainly GVD, play the leading roles.

It has to be noticed that the EVM performance in the experiment is typically worse than that in the simulation. The reasons may exist in several parts, such as the imperfection of the devices, including the AWG and the oscilloscope, and the noise introduced by the process of optical modulation and demodulation. For example, because the sampling rate of AWG is set at 10.32192 Gbps, where the signal bandwidth is around 5 GHz, while the maximum work frequency of the direct modulation laser used (VCSEL) is around 7 GHz, less than the signal's sampling rate. This may cause the nonlinear distortion for the RF signal. What is more, the amplifier used after the PD also introduces plenty of noise while increasing the amplitude of the signal, which commonly happens when the amplitude of the signal has a significant rise or fall with a very high frequency. Due to the amplifier's inability to respond in time in that situation, the delay is easy to cause the signal's amplitude distortion.

Table 5- 2 The measured EVM of two DSM structures in different length of fiber transmission

	EVM with 8-km fiber	EVM with 20-km fiber
Traditional SMASH	-21.42 dB	-18.94 dB
Proposed SMASH	-24.49 dB	-21.88 dB

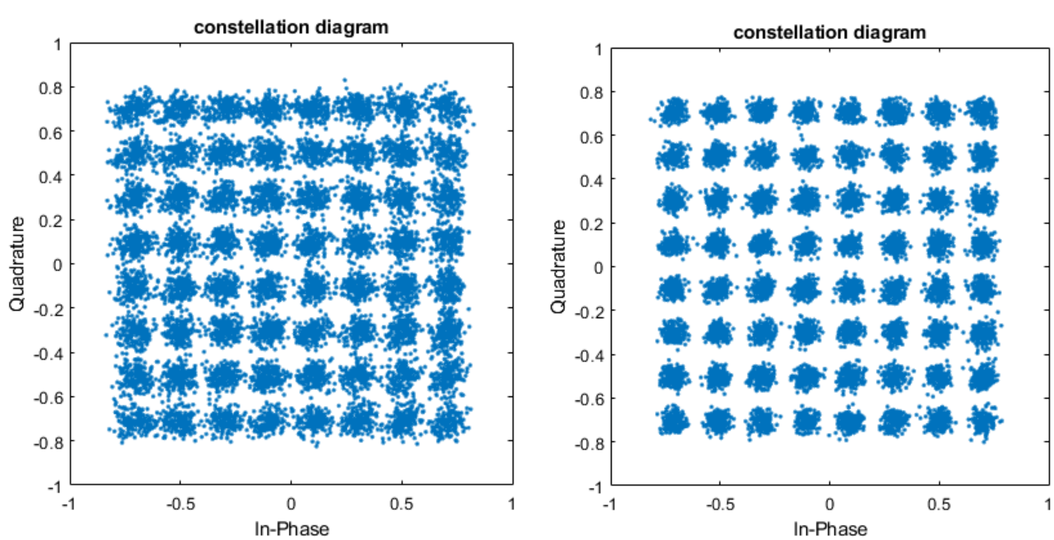

(a) (b)

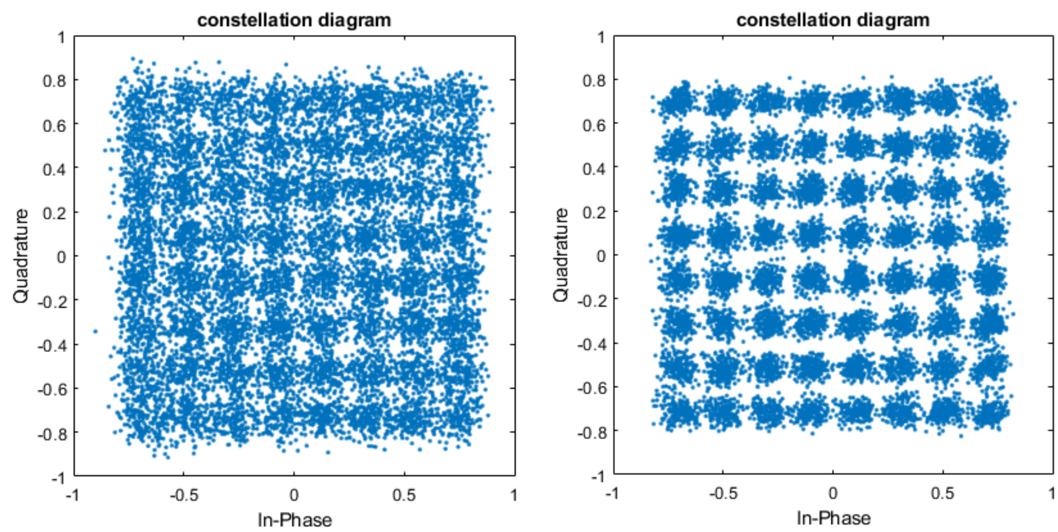

(c) (d)

Figure 5- 5(a) Measured EVM of traditional SMASH at 8 km with -21.42 dB. (b) Measured EVM of proposed SMASH at 8 km with -24.49 dB. (c) Measured EVM of traditional SMASH at 20 km with -18.94 dB. (d) Measured EVM of proposed SMASH at 20 km with -21.89 dB.

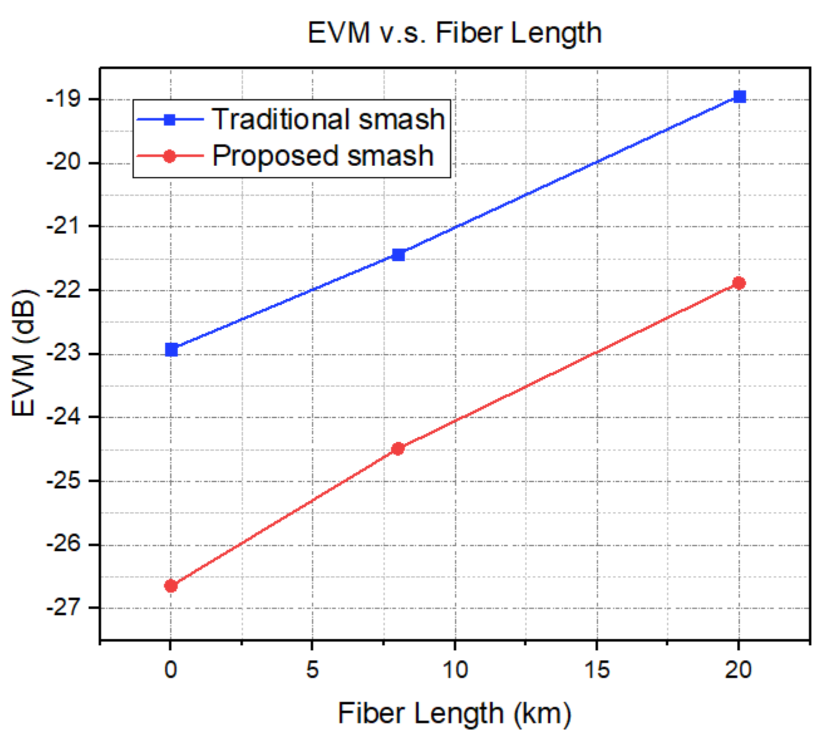

Figure 5- 6 Measured EVM versus fiber length for the traditional SMASH (blue line) and the proposed SMASH (red line).

5.4 Experiment summary

The experiment compares the transmission performance of two multi-stage DSM structures over the optical fiber. Overall, although there is some discrepancy between the experimental results and the simulation results, the general trend is consistent with the simulation results. In the transmission of OBTB, the proposed SMASH structure improves EVM by about 3.7 dB compared to the traditional SMASH structure. Meanwhile, the experiment results show that the EVM for the proposed structure is increased by 2.76 dB and 2.94 dB over the 8 km and 20 km fiber, respectively. The performance increase is similar to the simulation results.

Chapter 6 Conclusions and future work

6.1 Thesis conclusion

Due to the widespread application of 5G, the demands for communication systems are becoming higher, such as more efficient transmission rates and larger channel bandwidth, etc. This requires modulators to have better performance, for instance, they are expected to have high SNR, high stability, and modulation efficiency. The digital RoF system is one of the optimal solutions for RF signal transmission; meanwhile, the low-cost modulation method, DSM, has also become a popular scheme. How to combine them together has received more and more attention, especially in fronthaul transmission systems. However, in the current research on DSM, there is relatively little focus on RF signals and bandpass systems. Most studies concentrate on the characteristics of DSM as an ADC itself and its role in narrowband signal modulation. With the current significant increase in the demand for broadband RF signal modulation, the research on bandpass DSM holds certain importance. Especially in fronthaul systems, designing an appropriate DSM can enhance the transmission efficiency and performance, as well as reduce the complexity of the structure design. Besides, when it comes to improving the performance of the modulator, a lot of research focuses on increasing the order of the DSM. However, high-order single-stage DSMs easily encounter stability issues, and as each integrator is connected in cascade, the output swing caused by noise shaping becomes increasingly larger, which makes the integrator prone to overload and instability, limiting the signal range in the system's input.

This study proposes a new multi-stage DSM structure based on the current traditional SMASH structure, with some improvements made. A comprehensive comparison with the traditional DSM structure was conducted through simulations in MATLAB and VPI, and finally verified in the experiment. In this thesis, a 64-QAM OFDM signal with a bandwidth of 100 MHz, which is satisfied with the 5G RF1 standard (the maximum design bandwidth of RF1 is 100 MHz), is used as a digital baseband signal for modulation, and then it is upconverted to a carrier with a frequency of 2.5 GHz, followed by DSM modulation at an OSR of 50.

In the simulation work, it can be seen that, with the order of the whole system remaining unchanged, reducing the order for each stage results in higher stability and a larger dynamic range for the DSM modulation system. The results show that the proposed SMASH structure has an improvement in SNR compared to existing structures. For example, in the directly received signal reception system (EBTB), its EVM is improved by 4.5 dB compared to SDSM and by 3.3 dB compared to the two multi-stage structures. In the RoF system, after fiber transmission of 8 km and 20 km, the proposed SMASH shows improvements in EVM of 2.37 dB and 2.15 dB compared with traditional SMASH and MASH at 8 km, and 2.35 dB and 0.78 dB at 20 km, respectively.

In the experiment, the proposed SMASH structure is compared with the traditional SMASH structure. Similar to the simulation, the experimental results show the same trend, indicating that the proposed structure performs better than the traditional SMASH DSM across different lengths of optical fibers, with 20 km of fiber also being one of the design standards for the fronthaul system. Therefore, from the experimental results, the newly designed SMASH structure has achieved performance improvements over the existing multi-stage structures. To be precise, it has been verified that the proposed SMASH structure improves the EVM by 3.26 dB and 3.73 dB in the EBTB and OBTB systems, respectively, compared with the traditional SMASH structure. And in the RoF systems with fiber lengths of 8 km and 20 km, the improvements are 2.76 dB and 2.94 dB, respectively.

6.2 Future work

Due to limitations in design and production processes, the DSM modulator cannot be designed with great flexibility. Some NTF in modulators theoretically have good performance, but their designs are not practical, and sometimes compromises and trade-offs need to be made. Besides, as a DSP structure, DSM is not a linear system and can also suffer from some nonlinear distortions due to nonlinear components, such as integrators, power amplifiers, and so on. In the electrical domain, it may be worth considering methods like predistortion to compensate for the potential nonlinear distortions. Additionally, in the optical domain, it may be possible to adopt more efficient transmission methods with higher SNR performance for modulation and transmission along optical paths by integrating external modulators, such as mode-locked lasers and wavelength division multiplexing (WDM) modulation, etc.

References

[1] A. Dogra, R. K. Jha, and S. Jain, “A Survey on Beyond 5G Network With the Advent of 6G: Architecture and Emerging Technologies,” *IEEE Access*, vol. 9, pp. 67512–67547, 2021, doi: 10.1109/ACCESS.2020.3031234.

[2] A. Leon-Garcia and I. Widjaja, *Communication networks : fundamental concepts and key architectures*. McGraw-Hill, 2004. Accessed: Jun. 20, 2024. [Online]. Available: https://thuvienso.hoasen.edu.vn/handle/123456789/9679

[3] A. F. M. Shahen Shah, “A Survey From 1G to 5G Including the Advent of 6G: Architectures, Multiple Access Techniques, and Emerging Technologies,” in *2022 IEEE 12th Annual Computing and Communication Workshop and Conference (CCWC)*, Las Vegas, NV, USA: IEEE, Jan. 2022, pp. 1117–1123. doi: 10.1109/CCWC54503.2022.9720781.

[4] B. B.s and S. Azeem, “A survey on increasing the capacity of 5G Fronthaul systems using RoF,” *Optical Fiber Technology*, vol. 74, p. 103078, Dec. 2022, doi: 10.1016/j.yofte.2022.103078.

[5] P. Rani, “Comparative Study of Different Generations of Mobile Network,” in *Cybersecurity and Evolutionary Data Engineering*, R. Jain, C. M. Travieso, and S. Kumar, Eds., Singapore: Springer Nature, 2023, pp. 171–177. doi: 10.1007/978-981-99-5080-5_15.

[6] R. Muthalagu, “Literature Survey for Transceiver Design in MIMO and OFDM Systems.,” *J. Commun.*, vol. 13, no. 2, pp. 45–59, 2018.

[7] C. Xing, Z. Fei, Y. Zhou, and Z. Pan, “Matrix-field water-filling architecture for MIMO transceiver designs with mixed power constraints,” in *2015 IEEE 26th Annual International Symposium on Personal, Indoor, and Mobile Radio Communications (PIMRC)*, Aug. 2015, pp. 392–396. doi: 10.1109/PIMRC.2015.7343330.

[8] M. Jaber, M. A. Imran, R. Tafazolli, and A. Tukmanov, “5G Backhaul Challenges and Emerging Research Directions: A Survey,” *IEEE Access*, vol. 4, pp. 1743–1766, 2016, doi: 10.1109/ACCESS.2016.2556011.

[9] B. M. Shah, M. Murtaza, and M. Raza, “Comparison of 4G and 5G Cellular Network Architecture and Proposing of 6G, a new era of AI,” in *2020 5th International Conference on Innovative Technologies in Intelligent Systems and Industrial Applications (CITISIA)*, Sydney, Australia: IEEE, Nov. 2020, pp. 1–10. doi: 10.1109/CITISIA50690.2020.9371846.

[10] M. Peng, Y. Sun, X. Li, Z. Mao, and C. Wang, “Recent Advances in Cloud Radio Access Networks: System Architectures, Key Techniques, and Open Issues,” *IEEE Commun. Surv. Tutorials*, vol. 18, no. 3, pp. 2282–2308, 2016, doi: 10.1109/COMST.2016.2548658.

[11] K. Zeb, X. Zhang, and Z. Lu, “High Capacity Mode Division Multiplexing Based MIMO Enabled All-Optical Analog Millimeter-Wave Over Fiber Fronthaul Architecture for 5G and Beyond,” *IEEE Access*, vol. 7, pp. 89522–89533, 2019, doi: 10.1109/ACCESS.2019.2926276.

[12] D. H. Hailu, B. G. Gebrehaweria, S. H. Kebede, G. G. Lema, and G. T. Tesfamariam, “Mobile fronthaul transport options in C-RAN and emerging research directions: A comprehensive study,” *Optical Switching and Networking*, vol. 30, pp. 40–52, Nov. 2018, doi: 10.1016/j.osn.2018.06.003.

[13] M. Peng, C. Wang, V. Lau, and H. V. Poor, “Fronthaul-constrained cloud radio access networks: insights and challenges,” *IEEE Wireless Commun.*, vol. 22, no. 2, pp. 152–160, Apr. 2015, doi: 10.1109/MWC.2015.7096298.

[14] S. R. Abdollahi, H. S. Al-Raweshidy, S. M. Fakhraie, and R. Nilavalan, “Digital Radio over Fibre for Future Broadband Wireless Access Network Solution,” in *2010 6th International Conference on Wireless and Mobile Communications*, Sep. 2010, pp. 504–508. doi: 10.1109/ICWMC.2010.32.

[15] S. Hori *et al.*, “A digital radio-over-fiber downlink system based on envelope delta-sigma modulation for multi-band/mode operation,” in *2016 IEEE MTT-S International Microwave Symposium (IMS)*, San Francisco, CA: IEEE, May 2016, pp. 1–4. doi: 10.1109/MWSYM.2016.7539965.

[16] A. Checko *et al.*, “Cloud RAN for Mobile Networks—A Technology Overview,” *IEEE Communications Surveys & Tutorials*, vol. 17, no. 1, pp. 405–426, 2015, doi: 10.1109/COMST.2014.2355255.

[17] A. Pizzinat, P. Chanclou, F. Saliou, and T. Diallo, “Things You Should Know About Fronthaul,” *Journal of Lightwave Technology*, vol. 33, no. 5, pp. 1077–1083, Mar. 2015, doi: 10.1109/JLT.2014.2382872.

[18] J. Wang *et al.*, “Digital Mobile Fronthaul Based on Delta–Sigma Modulation for 32 LTE Carrier Aggregation and FBMC Signals,” *J. Opt. Commun. Netw., JOCN*, vol. 9, no. 2, pp. A233–A244, Feb. 2017, doi: 10.1364/JOCN.9.00A233.

[19] T. Pfeiffer, “Next generation mobile fronthaul and midhaul architectures [Invited],” *Journal of Optical Communications and Networking*, vol. 7, no. 11, pp. B38–B45, Nov. 2015, doi: 10.1364/JOCN.7.000B38.

[20] J. Shi, J. Liu, L. Zhang, L. Zhao, W. Zhou, and J. Yu, “Digital Mobile Fronthaul Based on Delta-Sigma Modulation and Chirp-Managed Signal Transmission,” *Journal of Lightwave Technology*, vol. 41, no. 20, pp. 6521–6532, Oct. 2023, doi: 10.1109/JLT.2023.3289528.

[21] W. Tan, A. Xu, Z. Luo, X. Wang, and F. Li, “Digital mobile fronthaul based on noise-coupling sturdy-multistage noise-shaping modulator,” *Optics & Laser Technology*, vol. 168, p. 109999, Jan. 2024, doi: 10.1016/j.optlastec.2023.109999.

[22] X. Yang *et al.*, “NTF-Improved Delta-Sigma Modulation Supported 65536 QAM Signal for Mobile Fronthaul,” *Journal of Lightwave Technology*, vol. 42, no. 2, pp. 513–522, Jan. 2024, doi: 10.1109/JLT.2023.3319691.

[23] J. G. Proakis and M. Salehi, *Digital communications*. McGraw-Hill, 2008. Accessed: Sep. 09, 2024. [Online]. Available: https://thuvienso.hoasen.edu.vn/handle/123456789/10005

[24] “How Error Vector Magnitude (EVM) Measurement Improves Your System-Level Performance | Analog Devices.” Accessed: Sep. 09, 2024. [Online]. Available: https://www.analog.com/en/resources/technical-articles/how-evm-measurement-improves-system-level-performance.html

[25] J. Speidel, “Multicarrier Modulation and OFDM,” in *Introduction to Digital Communications*, J. Speidel, Ed., Cham: Springer International Publishing, 2021, pp. 103–117. doi: 10.1007/978-3-030-67357-4_7.

[26] Y. S. Cho, J. Kim, W. Y. Yang, and C. G. Kang, *MIMO-OFDM Wireless Communications with MATLAB*. John Wiley & Sons, 2010.

[27] A. F. Molisch, *Wireless Communications*. John Wiley & Sons, 2012.

[28] J. M. de la Rosa, *Sigma-Delta Converters: Practical Design Guide*. John Wiley & Sons, 2018.

[29] S. Pavan, R. Schreier, and G. C. Temes, *Understanding Delta-Sigma Data Converters*. John Wiley & Sons, 2017.

[30] N. Maghari, S. Kwon, and U.-K. Moon, "74 dB SNDR Multi-Loop Sturdy-MASH Delta-Sigma Modulator Using 35 dB Open-Loop Opamp Gain," *IEEE Journal of Solid-State Circuits*, vol. 44, no. 8, pp. 2212–2221, Aug. 2009, doi: 10.1109/JSSC.2009.2022302.

[31] B. Park, C. Han, and N. Maghari, "Correlated Dual-Loop Sturdy MASH Continuous-Time Delta-Sigma Modulators," *IEEE Journal of Solid-State Circuits*, vol. 57, no. 10, pp. 2934–2943, Oct. 2022, doi: 10.1109/JSSC.2022.3186079.

[32] L. Zhong *et al.*, "An SNR-improved Transmitter of Delta-sigma Modulation Supported Ultra-High-Order QAM Signal for Fronthaul/WiFi Applications," *Journal of Lightwave Technology*, vol. 40, no. 9, pp. 2780–2790, May 2022, doi: 10.1109/JLT.2022.3147059.

[33] E. Janssen and A. van Roermund, "Basics of Sigma-Delta Modulation," in *Look-Ahead Based Sigma-Delta Modulation*, E. Janssen and A. van Roermund, Eds., Dordrecht: Springer Netherlands, 2011, pp. 5–28. doi: 10.1007/978-94-007-1387-1_2.

[34] M. Nagahara and Y. Yamamoto, "Frequency Domain Min-Max Optimization of Noise-Shaping Delta-Sigma Modulators," *IEEE Trans. Signal Process.*, vol. 60, no. 6, pp. 2828–2839, Jun. 2012, doi: 10.1109/TSP.2012.2188522.

[35] B. E. Boser and B. A. Wooley, "The design of sigma-delta modulation analog-to-digital converters," *IEEE Journal of Solid-State Circuits*, vol. 23, no. 6, pp. 1298–1308, Dec. 1988, doi: 10.1109/4.90025.

[36] J.-K. Cho, "Low-Voltage, Low-Power, High-Resolution, Broadband Oversampling Analog-To-Digital Conversion," Ph.D., Stanford University, United States -- California, 2012. Accessed: Sep. 10, 2024. [Online]. Available: https://www.proquest.com/docview/2460651427/abstract/64F0F76DE09B447BPQ/1

[37] S. M. Moussavi and B. H. Leung, "High-order single-stage single-bit oversampling A/D converter stabilized with local feedback loops," *IEEE Transactions on Circuits and Systems II: Analog and Digital Signal Processing*, vol. 41, no. 1, pp. 19–25, Jan. 1994, doi: 10.1109/82.275665.

[38] L. Qi, "Low-Power Cascaded Delta-Sigma Modulator for Wideband Telecommunication Applications," Ph.D., University of Macau, Peoples Rep. of China, 2019. Accessed: Sep. 10, 2024. [Online]. Available: https://www.proquest.com/docview/2390593929/abstract/D6110F3A94B84380PQ/1

[39] Y. Fujimoto, Y. Kanazawa, P. Lo Re, and K. Iizuka, "A 100 MS/s 4 MHz Bandwidth 70 dB SNR \Delta \Sigma ADC in 90 nm CMOS," *IEEE Journal of Solid-State Circuits*, vol. 44, no. 6, pp. 1697–1708, Jun. 2009, doi: 10.1109/JSSC.2009.2020458.

[40] C. Jing, T. Li, B. Gao, and M. Gong, "A MASH2-2 Sigma Delta Modulator with NTF Zero Optimization Technique," in *2022 5th International Conference on Communication Engineering and Technology (ICCET)*, Feb. 2022, pp. 68–72. doi: 10.1109/ICCET55794.2022.00021.

[41] D. Li, C. Fei, Q. Zhang, Y. Li, and Y.-T. Yang, “Mismatch errors randomization for multi-bit DAC in sigma-delta modulators based on butterfly-type network,” *Microelectronics Journal*, vol. 94, p. 104651, Dec. 2019, doi: 10.1016/j.mejo.2019.104651.

[42] “5G System Overview.” Accessed: Sep. 11, 2024. [Online]. Available: https://www.3gpp.org/technologies/5g-system-overview

[43] “5G | ShareTechnote.” Accessed: Sep. 11, 2024. [Online]. Available: https://www.sharetechnote.com/html/5G/5G_FR_Bandwidth.html#38_101_1_Table_5_1_1

[44] N. Maghari and U.-K. Moon, “Multi-loop efficient sturdy MASH delta-sigma modulators,” in *2008 IEEE International Symposium on Circuits and Systems (ISCAS)*, May 2008, pp. 1216–1219. doi: 10.1109/ISCAS.2008.4541643.

[45] L. Qi, S.-W. Sin, S.-P. U, and R. P. Martins, “Resolution-enhanced sturdy MASH delta–sigma modulator for wideband low-voltage applications,” *Electronics Letters*, vol. 51, no. 14, pp. 1061–1063, 2015, doi: 10.1049/el.2015.1655.

[46] J. Flemming, B. Wicht, and P. Witte, “Stability Analysis for Frequency Tunable Bandpass Delta-Sigma ADC Architectures,” in *2023 19th International Conference on Synthesis, Modeling, Analysis and Simulation Methods and Applications to Circuit Design (SMACD)*, Jul. 2023, pp. 1–4. doi: 10.1109/SMACD58065.2023.10192145.

[47] X. Qin, J. Zhang, L. Qi, S.-W. Sin, R. P. Martins, and G. Wang, “Discrete-Time MASH Delta-Sigma Modulator with Second-Order Digital Noise Coupling for Wideband High-Resolution Applications,” in *2021 IEEE International Symposium on Circuits and Systems (ISCAS)*, May 2021, pp. 1–5. doi: 10.1109/ISCAS51556.2021.9401651.

[48] A. O. Ucar and F. Gerfers, “Sturdy-MASH Delta-Sigma Modulator with Improved Resolution Using Noise-coupling Multi-bit Quantizer,” in *2022 IEEE 65th International Midwest Symposium on Circuits and Systems (MWSCAS)*, Aug. 2022, pp. 1–4. doi: 10.1109/MWSCAS54063.2022.9859279.

[49] “IEEE Standards Association,” IEEE Standards Association. Accessed: Sep. 16, 2024. [Online]. Available: https://standards.ieee.org/ieee/802.11/10548/